



**ADAPTIVE PN CODE SYNCHRONISATION IN
DS-CDMA SYSTEMS**

A Thesis

by

JOB AKPOFURE OBIEBI

**Submitted in partial fulfilment of the requirements of
Napier University for the degree of
DOCTOR OF PHILOSOPHY**

OCTOBER 2005

ABSTRACT

Spread Spectrum (SS) communication, initially designed for military applications, is now the basis for many of today's advanced communications systems such as Code Division Multiple Access (CDMA), Global Positioning System (GPS), Wireless Local Loop (WLL), etc. For effective communication to take place in systems using SS modulation, the Pseudo-random Noise (PN) code used at the receiver to despread the received signal must be identical and be synchronised with the PN code that was used to spread the signal at the transmitter. Synchronisation is done in two steps: *coarse synchronisation* or *acquisition*, and *fine synchronisation* or *tracking*. Acquisition involves obtaining a coarse estimate of the phase shift between the transmitted PN code and that at the receiver so that the received PN code will be aligned or synchronised with the locally generated PN code. After acquisition, tracking is now done which involves maintaining the alignment of the two PN codes.

This thesis presents results of the research carried out on a proposed adaptive PN code acquisition circuit designed to improve the synchronisation process in Direct Sequence CDMA (DS-CDMA) systems. The acquisition circuit is implemented using a Matched Filter (MF) for the correlation operation and the threshold setting device is an adaptive processor known as the Cell Averaging Constant False Alarm Rate (CA-CFAR) processor. It is a double dwell acquisition circuit where the second dwell is implemented by Post Detection Integration (PDI). Depending on the application, PDI can be used to mitigate the effect of frequency offset in non-coherent detectors and/or in the implementation of multiple dwell acquisition systems. Equations relating the performance measures – the probability of false alarm (P_{fa}), the probability of detection

(P_d) and the mean acquisition time ($E\{T_{acq}\}$) – of the circuit are derived. Monte Carlo simulation was used for the independent validation of the theoretical results obtained, and the strong agreement between these results shows the accuracy of the derived equations for the proposed circuit. Due to the combination of PDI and CA-CFAR processor in the implementation of the circuit, results obtained show that it can provide a good measure of robustness to frequency offset and noise power variations in mobile environment, consequently leading to improved acquisition time performance. The complete synchronisation circuit is realised by using this circuit in conjunction with a conventional code tracking circuit. Therefore, a study of a Non-coherent Delay-Locked Loop (NDLL) code tracking circuit is also carried out.

DECLARATION OF ORIGINALITY

I, Job Akpofure Obiebi, of the School of Engineering, Napier University, Edinburgh, hereby declare that the research work recorded in this thesis was originated and wholly carried out by me under the guidance of my Director of Studies.

DEDICATION

In Loving Memory of My Brother, Mr. Achoja V. Obiebi.

I wish you were here.

ACKNOWLEDGEMENT

First and foremost, I wish to give thanks to God Almighty for being the source of my strength and for seeing me through this research programme.

I also thank God for the life of my father Mr. James Obiebi and my mother Mrs. Lady Obiebi. With God helping them, they gave me the best upbringing I could ever wish for. I wish to thank them for their support, advice, inspiration and for teaching me the importance of obedience, honesty and hard work. You are the best. I also wish to thank my brothers and sisters for their continuous support and encouragement.

I would like to use this opportunity to thank my Director of Studies, Dr. Mohammad Y. Sharif for proposing this interesting area of research and for being there while it lasted. Thanks for your contributions, support and encouragement. I will also thank my second supervisor, Dr. John Sharp for his contributions and support. I am indeed very grateful.

This is also an opportunity for me to also acknowledge the help and support from staff of the university. Thanks to the staff of the School of Engineering, the Library and International Office.

For the past three years, I have had the opportunity to meet with great people in Edinburgh. I have had many friends but I must mention a very important family friend Mr. and Mrs. Mark Walker. You have been a great friend to me. Thanks.

Finally, thanks to my fellow researchers. We were able to do things together irrespective of our cultural differences. Of course there is unity in diversity.

Let me use this opportunity to acknowledge that this research programme was fully funded by Napier University, Edinburgh.

Job A. Obiebi
Napier University, Edinburgh.
October 2005.

LIST OF ABBREVIATIONS AND SYMBOLS

| | |
|-------------|---|
| A | Amplitude of transmitted signal |
| ACQ | Acquisition state |
| AMPS | Advanced Mobile Phone Systems |
| AWGN | Additive White Gaussian Noise |
| B_d | Doppler spread |
| BPSK | Binary Phase Shift Keying |
| B_s | Data signal bandwidth |
| BS | Base Station |
| CA-CFAR | Cell Average Constant False Alarm Rate |
| CCD | Charged Coupled Devices |
| CD | Coincidence Detector |
| CDMA | Code Division Multiple Access |
| CDMA2000 | 3G standard for North America |
| $c(t)$ | PN signal |
| CW | Continuous Wave |
| δ | Residual offset between the received and local PN codes |
| $\delta(.)$ | Dirac delta function |
| DCChs | Dedicated Control Channels |
| DLL | Delay-Locked Loop |
| DS-CDMA | Direct Sequence CDMA |
| DS-SS | Direct Sequence Spread Spectrum |
| $d(t)$ | Data signal |
| Δ | Incremental order |

| | |
|----------------|--|
| Δf | Frequency offset |
| E_b | Energy per bit |
| E_c | Energy per chip |
| EDGE | Enhanced Data rate for GSM Evolution |
| ϵ_r | Dielectric of free space |
| $e(t)$ | Error correcting signal |
| $E\{T_{acq}\}$ | Mean acquisition time |
| $E\{x\}$ | Expectation of x |
| f_a | False alarm state |
| f_c | Carrier frequency |
| FChs | Fundamental Channel |
| FDMA | Frequency Division Multiple Access |
| FH-CDMA | Frequency Hopping CDMA |
| FH-SS | Frequency Hopping Spread Spectrum |
| f_D | Doppler frequency |
| FPChs | Forward Paging Channels |
| FPiCh | Forward Pilot Channel |
| F_u | Frequency uncertainty |
| GSM | Global System for Mobile Communication |
| GPRS | General Packet Radio Service |
| GPS | Global Positioning System |
| 1G | First Generation |
| 2G | Second Generation |
| 3G | Third Generation |

| | |
|---------------------------|---|
| H_0 | Hypothesis region for no or false acquisition |
| H_1 | Hypothesis region for true or missed acquisition |
| $H(f)$ | Transfer function |
| $\tilde{h}(\tau)$ | Impulse response |
| $H_D(z)$ | Gain of the branch connecting the synchro cell to the acquisition state (ACQ) |
| $\tilde{h}_l(d, p(t))$ | Large-scale fading |
| $H_M(z)$ | Gain of the branch connecting the missed cell to the first non-synchro cell |
| $\tilde{h}_s(\tau, p(t))$ | Small-scale fading |
| $H_0(z)$ | Gain of the branch connecting one non-synchro cell to another (non-synchro or the synchro) cell |
| i.i.d. | Independent and identically distributed |
| I_{L-1} | ($L-1$)th-order modified Bessel function of the first kind |
| IMT | International Mobile Telecommunications |
| I_0 | Interference psd |
| I and Q | In-phase and Quadrature-phase |
| IS-95 | Interim Standard 95 (first CDMA standard) |
| ITU | International Telecommunications Union |
| J | Jammer power |
| J_0 | Zeroth-order Bessel function of the first kind |
| J / S | Jammer power to signal power ratio in dB |
| K | Number of users |

| | |
|----------|--|
| k_R | Ricean factor |
| L | Length of PDI |
| LFSR | Linear Feedback Shift Register |
| L_p | Total number of paths in a multipath channel |
| LOS | Line-Of-Sight |
| M | Length of PN code |
| MAI | Multiple Access Interference |
| MF | Matched Filter |
| MF-LL | MF Longer Length |
| MIP | Multipath Intensity profile |
| ML | Maximum Likelihood |
| MS | Mobile Station |
| N | Length of MF |
| η | Decaying rate of an exponential MIP |
| N_{AW} | Output of MF due to AWGN signal |
| NLOS | Non-Line-Of-Sight |
| N_0 | Noise psd |
| N_J | Jammer psd |
| P_d | Probability of detection |
| pdf | Probability density function |
| PDI | Post Detection Integration |
| P_{fa} | Probability of false alarm |
| P_G | Processing Gain |
| P_m | Probability of miss |

| | |
|--------------------------------------|---|
| PN | Pseudo-random Noise |
| ppm | Parts per millions |
| Pr | Probability |
| Psd | Power spectral density |
| $p_{T_c}(t)$ | Basic pulse shape of duration T_c |
| QoS | Quality of Service |
| QPChs | Quick Paging Channels |
| RF | Radio Frequency |
| $R_c(k)$ | Discrete autocorrelation function of $c(t)$ |
| $R(\tau_c)$ | Autocorrelation of $p_{T_c}(t)$ |
| $R_{\tilde{n}_i, \tilde{n}_s}(\tau)$ | Equation for MIP |
| R-MF | Reference MF |
| $r(t)$ | Received SS signal |
| S | SS signal power |
| SAW | Surface acoustic wave |
| SINR | Signal-to-interference-noise ratio |
| SNR | Signal-to-noise ratio |
| $S(\lambda)$ | Doppler power spectrum |
| SS | Spread Spectrum |
| $s(t)$ | Transmitted SS signal |
| $S(\tau, \lambda)$ | Channel scattering function |
| $S_x(f)$ | Psd of white noise before filtering |
| $S_y(f)$ | Psd of white noise after filtering |

| | |
|---------------------|--|
| σ_j^2 | Variance of jamming signal |
| σ_l^2 | Power per path in a multipath channel |
| σ_{ls}^2 | Variance of v_{ls} |
| σ_{ls-mai}^2 | Variance of v_{ls-mai} |
| σ_{AW}^2 | Variance of N_{AW} |
| σ_{nl}^2 | Variance of v_{nl} |
| σ_{nl-mai}^2 | Variance of v_{nl-mai} |
| τ | Delay in received signal |
| $\hat{\tau}$ | Estimate of τ |
| t' | Ratio of the power of the other users to the desired user |
| T_c | Chip duration |
| t_d | Dwell time |
| T_d | Amount by which the local PN signal is advanced or delayed |
| T_{fa} | False alarm penalty time |
| T_h | Threshold |
| TH-CDMA | Time Hopping CDMA |
| TH-SS | Time Hopping SS |
| T_m | Multipath spread |
| T_r | Threshold scaling factor |
| T_s | Symbol duration |
| T_u | Time uncertainty |
| μ | Degradation in SNR due to frequency offset |
| u | Output noise power from the CA-CFAR processor |

| | |
|--------------|---|
| μ_{ls} | Mean of v_{ls} |
| UHF | Ultra High Frequency |
| v | Total output signal value from the MF correlator |
| v_{ls} | Output of MF due to LOS signal of the desired user |
| v_{ls-mai} | Output of MF due to LOS signal of the other users |
| v_{nl} | Output of MF due to NLOS signal of the desired user |
| v_{nl-mai} | Output of MF due to NLOS signal of the other users |
| VCO | Voltage Controlled Oscillator |
| VHF | Very High Frequency |
| W | Number of cells in uncertainty region |
| W_s | Bandwidth of SS signal |
| W_j | Bandwidth of jammer signal |
| WLL | Wireless Local Loop |
| WSS | Wide Sense Stationary |
| WSSUS | WSS Uncorrelated Scatter |
| Z_+ | NDLL circuit output resulting from correlating the received PN signal with its locally generated delayed version |
| Z_- | NDLL circuit output resulting from correlating the received PN signal with its locally generated advanced version |

TABLE OF CONTENTS

| | |
|---|-----------|
| ABSTRACT | i |
| DECLARATION OF ORIGINALITY | iii |
| DEDICATION | iv |
| ACKNOWLEDGEMENT | v |
| LIST OF ABBREVIATIONS AND SYMBOLS | vii |
| LIST OF FIGURES | xvii |
| LIST OF TABLES | xx |
| 1. General Overview | 1 |
| 1.1. Introduction | 1 |
| 1.2. Synchronisation in Digital Communications Systems | 4 |
| 1.3. Motivation for this Thesis | 6 |
| 1.4. Contributions of this Thesis | 9 |
| 1.5. Layout of the Thesis | 10 |
| 2. Spread Spectrum and CDMA | 11 |
| 2.1. Introduction | 11 |
| 2.1.1. FH-SS | 15 |
| 2.1.2. TH-SS | 16 |
| 2.1.3. DS-SS | 17 |
| 2.2. Implementation of DS-SS System. | 19 |
| 2.3. Code Division Multiple Access | 21 |
| 2.3.1. Call Processing in DS-CDMA Systems | 24 |
| 2.3.1.1. MS Initialisation State | 25 |
| 2.4. Generation of PN codes | 26 |
| 2.4.1. PN Codes in CDMA Systems | 30 |
| 2.6. Summary | 34 |
| 3. Mobile Radio Channel and Interferences | 35 |
| 3.1. Introduction | 35 |
| 3.2. Characterisation of a Wireless Channel | 37 |
| 3.3. Classification of Fading | 38 |
| 3.3.1. Large-Scale Fading | 39 |
| 3.3.2. Small-Scale Fading | 40 |
| 3.3.2.1. Pdf of Ricean and Rayleigh Fading Channel | 43 |
| 3.3.2.2. Important parameters | 44 |
| 3.3.3. Computer Simulation of Rayleigh Fading Channel | 47 |
| 3.3.3.1. Gaussian Noise Filtering Method | 48 |
| 3.3.3.2. Summation of Sinusoids Method | 50 |
| 3.3.4. TDL Model of Frequency Selective Rayleigh Fading Channel | 53 |
| 3.4. Interference in Mobile Networks | 56 |
| 3.4.1. Definition of Interference | 56 |
| 3.4.2. Sources of Interference | 58 |
| 3.4.2.1. Unintentional Interferences | 58 |
| 3.4.2.2. Intentional Interferences | 60 |

| | |
|--|------------|
| 3.4.2.3. Multiple Access Interference | 61 |
| 3.5. Summary | 62 |
| 4. Introduction to PN Code Acquisition | 63 |
| 4.1. Introduction | 63 |
| 4.2. PN Code Acquisition Problem Definition | 65 |
| 4.2.1. Search Strategies | 68 |
| 4.2.1.1. Maximum-likelihood Search Strategy | 70 |
| 4.2.1.2. Serial Search Strategy | 71 |
| 4.2.1.3. Parallel Search Strategy | 72 |
| 4.2.1.4. Hybrid-Search Strategy | 73 |
| 4.2.1.5. Sequential Estimation Strategy | 73 |
| 4.2.2. Detector Structure | 73 |
| 4.2.2.1. Active Correlator | 76 |
| 4.2.2.2. Passive Correlator | 76 |
| 4.2.3. Dwell Time | 78 |
| 4.2.4. Threshold Setting | 80 |
| 4.2.5. Performance Measures | 81 |
| 4.3. Summary | 82 |
| 5. Adaptive PN Code Acquisition | 84 |
| 5.1. Introduction | 84 |
| 5.2. The Proposed Circuit | 84 |
| 5.3. Performance Analysis | 88 |
| 5.3.1. The Channel Model | 88 |
| 5.3.1.1. Rician Fading Channel | 89 |
| 5.3.1.2. Frequency Selective Rayleigh Fading Channel | 105 |
| 5.3.2. Mean Acquisition Time | 110 |
| 5.3.3. Numerical Results | 117 |
| A. Ricean Fading Channel | 118 |
| 5.3.3.1. Choice of P_{fa} | 118 |
| 5.3.3.2. Effect of Ricean Factor | 120 |
| B. Frequency Non-selective Rayleigh Fading Channel | 124 |
| 5.3.3.3. Effect of N and Doppler Shift on P_d | 124 |
| 5.3.3.4. Effect of N and PDI on $E\{T_{acq}\}$ | 127 |
| 5.3.3.5. Verification of P_{fa} , P_d and $E\{T_{acq}\}$ by Simulation | 129 |
| 5.3.3.6. Performance Comparison | 131 |
| C. Frequency Selective Rayleigh Fading Channel | 133 |
| 5.3.3.7. Exponential MIP | 135 |
| 5.3.3.8. Uniform MIP | 136 |
| D. Effect of MAI | 137 |
| E. Effect of CW Jammer | 139 |
| F. Effect of Frequency Offset | 143 |
| 5.4. Summary | 146 |
| 6. PN Code Tracking | 148 |
| 6.1. Introduction | 148 |
| 6.2. The Non-Coherent Delay-Locked Loop | 151 |
| 6.2.1. Statistics of the DLL in Rayleigh Fading Channel | 153 |

| | |
|---|------------|
| 6.2.2. Time Tracking Loop Operation | 161 |
| 6.3. Summary | 164 |
| 7. Conclusions and Future Work | 165 |
| 7.1. Conclusions..... | 165 |
| 7.2. Future Work | 170 |
| Appendix I: Moments of Random Variables | 172 |
| Appendix II: Derivation of equations for P_d and P_{fa} | 174 |
| Appendix III: Derivation of equation (6.41) | 175 |
| Publications | 178 |
| References..... | 187 |

LIST OF FIGURES

| | |
|--|----|
| Figure 1.1. Evolution of mobile communication systems | 3 |
| Figure 2.1. Time/frequency occupancy of FH-SS system | 15 |
| Figure 2.2. Time/frequency occupancy of TH-SS system | 17 |
| Figure 2.3. Time/frequency occupancy of DS-SS system | 18 |
| Figure 2.4. Basic baseband DS-SS operation: transmitter structure | 19 |
| Figure 2.5. Power spectrum of data and PN signal | 20 |
| Figure 2.6. Basic baseband DS-SS operation: receiver structure..... | 21 |
| Figure 2.7. An m stage Galois feedback LFSR generator..... | 28 |
| Figure 2.8. Discrete autocorrelation function of PN sequence | 30 |
| Figure 2.9. Generation of Gold sequence using two preferred m -sequences..... | 32 |
| Figure 3.1. Filtering effect of the mobile channel..... | 37 |
| Figure 3.2. A three-path mobile channel..... | 38 |
| Figure 3.3. Sketch of a typical exponential MIP..... | 45 |
| Figure 3.4. Sketch of the Doppler power spectrum | 46 |
| Figure 3.5. Plot of the normalised psd, $S_y(f)$ | 49 |
| Figure 3.6. Rayleigh fading simulator using the Gaussian filtering method | 50 |
| Figure 3.7. Jakes model of a Rayleigh fading simulator..... | 52 |
| Figure 3.8. Pdf of Rayleigh fading channel using the Jakes method | 53 |
| Figure 3.9. TDL model for frequency selective Rayleigh fading channel..... | 54 |
| Figure 3.10. (a) broadband jammer (b) partial-band jammer..... | 61 |
| Figure 4.1. Block diagram of the synchronisation process | 64 |
| Figure 4.2. Basic components of the PN code acquisition circuit | 67 |
| Figure 4.3. Two-dimensional serial search strategy of the PN code uncertainty region | 69 |

| | | |
|--------------|---|-----|
| Figure 4.4. | A serial realisation of the maximum-likelihood search strategy | 71 |
| Figure 4.5. | Block diagram of the serial search strategy | 72 |
| Figure 4.6. | A coherent detector implementation..... | 74 |
| Figure 4.7. | Non-coherent detector implementation | 75 |
| Figure 4.8. | Active correlator structure | 76 |
| Figure 4.9. | Baseband, digital MF correlator structure | 78 |
| Figure 4.10. | Block diagram of a non-coherent D -dwell PN code acquisition circuit.... | 79 |
| Figure 5.1. | The proposed double dwell acquisition circuit..... | 85 |
| Figure 5.2. | The CA-CFAR Processor | 87 |
| Figure 5.3. | Flow graph of the proposed double dwell acquisition circuit..... | 88 |
| Figure 5.4. | Reduced flow-graph of the state transition diagram..... | 111 |
| Figure 5.5. | The expanded H_1 region for the double dwell acquisition system | 112 |
| Figure 5.6. | An expanded $H_0(z)$ for the i th cell in the H_0 region..... | 114 |
| Figure 5.7. | Choosing a P_{fa} (Ricean factor, $k_R = 0$ dB)..... | 118 |
| Figure 5.8. | Plot showing the effect of SNR on P_{fa} (Ricean factor, $k_R = 0$ dB)..... | 119 |
| Figure 5.9. | Plot showing the effect of k_R on P_d | 120 |
| Figure 5.10. | Plot showing the effect of k_R on $E\{T_{acq}\}$ | 121 |
| Figure 5.11. | Performance comparison of the proposed and the MF-LL methods | 122 |
| Figure 5.12. | Comparison of the proposed and the MF-LL methods in AWGN and Rayleigh fading channel..... | 123 |
| Figure 5.13. | Effect of N on P_d ($f_D T_c = 10^{-4}$) | 125 |
| Figure 5.14. | Effect of Doppler shift on P_d ($N = 64$)..... | 126 |
| Figure 5.15. | Effect of Doppler shift on G / N | 127 |
| Figure 5.16. | Plot of normalised $E\{T_{acq}\}$ for different values of N | 128 |

| | |
|--|-----|
| Figure 5.17. Plot of normalised $E\{T_{acq}\}$ for different length of PDI | 129 |
| Figure 5.18. Theoretical and simulation results of the proposed circuit in terms of P_{fa} | 130 |
| Figure 5.19. Theoretical and simulation results of the proposed circuit in terms of P_d | 130 |
| Figure 5.20. Theoretical and simulation results of the proposed circuit in terms of $E\{T_{acq}\}$ | 131 |
| Figure 5.21. Comparison of the normalized $E\{T_{acq}\}$ of the adaptive and non-adaptive methods | 132 |
| Figure 5.22. The expanded H_1 region for the frequency selective fading channel | 134 |
| Figure 5.23. Plot of $E\{T_{acq}\}$ for a frequency selective Rayleigh fading channel using an exponential MIP with $\eta = 0.6$ | 136 |
| Figure 5.24. Plot of $E\{T_{acq}\}$ for frequency selective Rayleigh fading channel using a uniform MIP | 137 |
| Figure 5.25. Plot showing the effect of MAI ($P_{fa} = 10^{-5}$ and $E_c / N_0 = -5$ dB are parameters)..... | 138 |
| Figure 5.26. Normalised $E\{T_{acq}\}$ versus K showing the effect of t' ($k_R = 0$ dB) | 139 |
| Figure 5.27. Plot showing the effect of CW jammer on $E\{T_{acq}\}$ ($P_{fa} = 10^{-5}$ and $E_c / N_0 = -5$ dB) | 141 |
| Figure 5.28. Plot of $E\{T_{acq}\}$ vs. P_{fa} and P_d (J / S varying from 0 – 50 dB and $E_c / N_0 = -5$ dB) | 142 |
| Figure 5.29. Mitigating the effect of a CW jammer by increasing N ($E_c / N_0 = -5$ dB and no frequency offset) | 143 |
| Figure 5.30. Degradation in SNR due to Δf for different values of N | 144 |
| Figure 5.31. Effect of Δf on normalized $E\{T_{acq}\}$ | 145 |
| Figure 6.1. The autocorrelation function of a rectangular pulse | 149 |
| Figure 6.2. A Non-coherent DLL tracking circuit | 152 |
| Figure 6.3. Tracking error function for different values of T_d / T_c | 163 |

LIST OF TABLES

| | |
|---|----|
| Table 2.1. Application of spread spectrum communication | 13 |
| Table 2.2. Cross-correlation properties of m-sequences and Gold sequences | 31 |
| Table 2.3. Walsh and PN sequences applications in CDMA systems | 33 |

CHAPTER 1

General Overview

1.1. Introduction

Simply put, communications involves the transmission of information from one point to another. The wide variety of information sources result in either analogue or digital messages that have to be conveyed from one end (usually the transmitter) to the receiving end (the receiver). A message is transmitted through a channel. This could be a fixed wire between the transmitter and the receiver, as is usually the case in the Public Switched Telephone Networks (PSTN) landline system and this is called a *wireline* channel. On the other hand, the channel could be the atmosphere between the transmitter and receiver, as usually the case in mobile telephone systems and this is called a *wireless* channel. Since the transmitters are not hard-wired to the receivers, such systems are known as wireless communications systems. Wireless communications has been one of the fastest growing fields in the engineering sector in the past decade. The rapid growth in wireless communications is both technologically and user driven [1]. Technologically, the past decade has experienced significant advancements in the areas of Digital Signal Processing (DSP), digital Radio Frequency (RF) circuit fabrication, new large-scale circuit integration, and other miniaturization technologies, which make portable radio equipment smaller, cheaper, and more reliable.

The 'anywhere-anytime' communication has led to the rapid growth in the number of subscribers both in the developed world and in the developing world where the landline phone system is still developing. One of the challenges facing the industry is how to cope with the increasing number of subscribers together with their respective service demand. While the most important service being demanded by the increasing number of subscribers is still voice, there is now the growing need for mobile systems to cope with multimedia services. These additional services were taken into consideration when the International Telecommunications Union (ITU) laid out the framework for the standardisation of the third generation of mobile systems commonly known as 3G under the umbrella of International Mobile Telecommunications 2000 (IMT-2000) [2, 3].

The first generation (1G) of wireless systems was first deployed in the late 1970's [1]. These were analogue systems. Second and third generations (2G and 3G) of mobile systems are all digital systems. Figure 1.1 shows the block diagram of the evolution of mobile systems from 1G to 3G. Full details of the evolution of mobile communications systems can be found in [1]. It is seen from the diagram that the evolution can be described by the increasing bit rates the system is expected to support. However, the spectrum to support these services is scarce. This therefore calls for efficient utilisation of available spectrum. The way the spectrum is shared amongst the users is determined by the multiple access technique employed. 1G system is based on Frequency Division Multiple Access (FDMA). FDMA is a multiple access technique whereby the available frequency spectrum is divided in a disjoint manner among the users. This has placed a limit on the number of subscribers that can use the spectrum at any given time. Advanced Mobile Phone Systems (AMPS) in North America and Total Access

Communications Systems (TACS) in Europe are based on FDMA. With the advancement in digital communications, capacity improvement was achieved in the form of Time Division Multiple Access (TDMA). In TDMA, each user is allocated a time slot for transmission. This means that each FDMA channel can be further subdivided in time among users, thereby increasing the capacity. Global System for Mobile communication (GSM) is a typical example of a system that is based on TDMA. Since the spectrum is divided in time, there is still a limit on capacity.

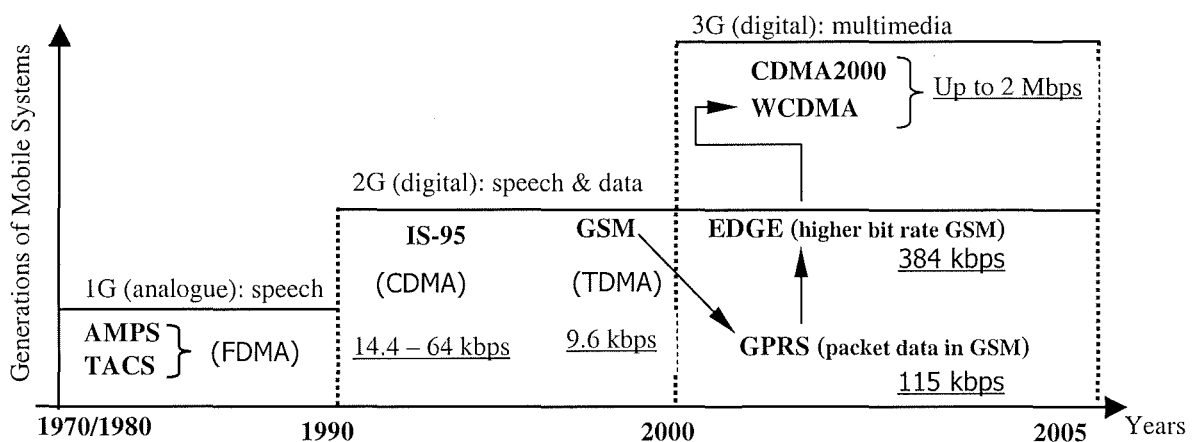


Figure 1.1. Evolution of mobile communications systems

In view of this, a new technique for multiple access was commercialised by Qualcomm® in 1993 and it is known as Code Division Multiple Access (CDMA) [4]. In CDMA, instead of dividing up the spectrum among users, all users are allowed into the same spectrum but are distinguished by their own unique PN code. This means that each user now constitutes source of interference in the system. Thus the capacity limit is determined by the amount of interference the system can tolerate. This means that the capacity of a CDMA system is interference limited [5]. It was shown in [6] that CDMA can provide much more capacity than FDMA and TDMA systems. Apart from its

capacity advantage, CDMA also has other advantages inherent in it as a result of the use of the PN code for its implementation. These advantages include voice privacy, low probability of intercept, anti-jamming capability and protection against multipath. These advantages will be explained in Chapter 2. The first CDMA system to be deployed was IS-95 (also called CDMA0ne). Its technological and commercial successes led the IMT-2000 group to accept CDMA as the air interface standard for 3G. Two major 3G standards are CDMA2000 in North America and Wideband CDMA (WCDMA) in Europe [2, 3]. From Figure 1.1, it is seen that existing GSM systems are migrating towards WCDMA through General Packet Radio Switching service (GPRS) and Enhanced Data rate for GSM Evolution (EDGE).

The technology that made CDMA possible is known as spread spectrum communication [7–10]. This is a transmission technique that uses PN code to spread the information-bearing signal to a bandwidth in excess of the minimum bandwidth required to transmit that signal. Though CDMA can provide improved capacity when compared to the other systems, its implementation is quite challenging. Two important implementation areas in SS communication systems, especially in CDMA, are *power control* and *PN code synchronisation* [7–11]. For efficient operation of CDMA systems, these two areas have to be properly implemented. The latter is being addressed in this thesis.

1.2. Synchronisation in Digital Communications Systems

Digital communications is the transmission of information in digital form. In most cases, the information source is analogue in form and has to be converted to digital form

using DSP. At the receiver, depending on the intended use, the received signal can be used in the digital form, or reconverted to an analogue form. In comparison to analogue communications systems, the implementation of digital communications systems is more complex. In digital communications systems, *synchronisation*^{1.1} is an important implementation area. This is a means of estimating some parameters in the received signal so that it is properly aligned with its locally generated version. Some important parameters that are estimated include: carrier frequency; carrier phase; bit time; symbol time; frame time and so on [12]. These types of synchronisations are necessary in digital communications systems, as the output of the demodulator must be sampled periodically in order to recover the transmitted information. For example, if each bit of transmitted digital signal is to be recovered correctly, the demodulator must be sampled at a time that takes into consideration the delay in the received signal. Since this delay cannot be known with certainty, it means that there should be a technique to estimate the delay so that the demodulator can be sampled at the right sampling instant. This therefore calls for a synchronisation circuit. For coherent communication, all the above types of synchronisation are necessary, particularly for the carrier frequency and phase synchronisation. For non-coherent communication systems, the carrier phase synchronisation is not necessary.

For CDMA systems, because of the use of PN codes for spreading the signal at the transmitter and the subsequent use of the same PN code for despreading the signal at the receiver, there is an additional type of synchronisation known as PN code synchronisation. Two major ways to achieve synchronisation are by the use of the

^{1.1}Carrier synchronisation is also important in coherent analogue communication.

hardwire synchroniser and the *recovery synchroniser* techniques. In the *hardwire synchroniser*, a separate channel is used to transmit the reference information that is necessary for the efficient demodulation of the received signal. For example, in CDMA systems, the information signal is spread with the PN code and transmitted in one channel. The same PN code without the message is transmitted in another channel, and therefore the two received signals will experience the same propagation delay. This will be expensive to implement and it will also negate the security and secrecy that the system was designed to achieve in the first place [10]. For the case of the *recovery synchroniser*, the synchronisation information is recovered from the received input signal without any other knowledge of the transmitter information. Though this will also involve an additional cost in implementing a synchroniser in the receiver; but for CDMA systems, the major advantages are still intact. To simplify the implementation of synchronisers in CDMA receivers, an unmodulated PN signal is initially transmitted using a pilot channel. The receiver now synchronises to this PN signal by using the synchronisation circuit to extract the necessary synchronisation parameters. Using these estimated parameters; the same PN code is now locally generated at the receiver. Once this is done, the transmitter can start spreading the message with the PN code and subsequently transmit it. Then by despreading the received signal with the locally generated PN signal, the original message can be efficiently recovered.

1.3. Motivation for this Thesis

There are a lot of publications on the acquisition of PN codes in SS systems as will be seen cited in appropriate sections of this thesis. Some of the published results are circuits that are based on serial, parallel or hybrid (serial-parallel) search schemes. For

low complexity circuit that will be suitable for portable users' equipment, the *serial search* is preferred [10, 11]. In [13], the performance analysis of an acquisition method known as *multiple dwell* serial search; was carried out. In this method, multiple tests of the phase of the received signal are performed before the final declaration of acquisition. It was shown that by using this method, the performance of the circuit, in terms of speed of acquisition, could be improved. However, as the number of dwells increases, so does the complexity. In terms of trade-off between complexity and speed of acquisition, a double dwell was shown to be a good compromise [13]. In the course of the review of literature on PN code acquisition circuits; this research was started with an intensive study of two acquisition circuits from which a new circuit was designed. An adaptive circuit using CA-CFAR processor was proposed in [14]. The use of CA-CFAR technique is very popular in the field of radar analysis [15]. It is used to adaptively set up a threshold based on the noise variation in the mobile environment. The work presented in [14] was a double dwell acquisition circuit where the second dwell was implemented with another MF of length longer than that used in the first dwell. It was a non-coherent detector and the analysis was carried out in an Additive White Gaussian Noise (AWGN) channel only. The circuit was implemented with the assumption that there was no frequency offset. Frequency offset causes degradation of the signal-to-noise ratio (SNR) and this degradation increases as the correlation length increases, resulting in performance degradation in non-coherent detectors [9–11]. Frequency offset cannot be avoided due to imperfections in large-scale manufactured oscillators used in the down-conversion section of these detectors as oscillators are always specified with a frequency tolerance level of parts per millions (ppm). There is also the problem of Doppler shift that causes variation of the received carrier frequency.

Thus, in order to use the non-coherent detector, the effect of frequency offset has to be considered. In [9], a method to mitigate the effect of frequency offset was proposed. In this method, a small correlation length that will not be severely affected by the expected frequency offset was used. However, since the correlation length is directly related to the circuit output SNR, the SNR at the output of the circuit will be small as well. In order to improve the SNR, the output of the correlator is accumulated over a number of intervals, in what is called *post detection integration* (PDI) [9]. If the number of intervals is L , it means that PDI is of length L . However, the analysis in [9] was done for a non-adaptive acquisition circuit. Also, the possible use of PDI to implement multiple dwell PN code acquisition system was stated in [9] but numerical results were not given to illustrate the effectiveness of this technique. A thorough study of [9] and [14] now motivated this research. This led to the design of a new adaptive detector for the acquisition of PN code sequence. The motivation was to utilise the best features of [9] and [14] in the design of a new circuit. This was achieved as follows. The adaptive nature of the proposed circuit is based on the CA-CFAR technique as implemented in [14] but the implementation of the second dwell is by PDI as suggested in [9]. The proposed circuit was designed and analysed taking into consideration the effect of fading, jamming, multiple access interference (MAI) and frequency offset. Some of these conditions were not considered in [9] and [14]. With stated trade-offs in terms of complexity and speed of acquisition between the proposed circuit and the circuits from which it was derived, the overall results obtained showed that the proposed method could improve the acquisition time performance of the code acquisition process.

1.4. Contributions of this Thesis

In order to study the performance of the proposed circuit, the theory behind the proposed circuit was studied and mathematically modelled. New sets of equations for the proposed circuit in terms of P_d , P_{fa} and $E\{T_{acq}\}$ were derived. In the first instance, the performance of the circuit was considered in a Ricean fading channel. This type of channel is characterised by the presence of a non-faded specular component and diffuse multipath fading components. This is the scenario of mobile systems operating in rural areas [16]. The second set of equations relating the circuit were derived for a frequency selective and frequency non-selective Rayleigh fading channel. This typically captures the operation of mobile systems operating in sub-urban and urban areas where the received signal is made up of multipath fading components with no specular component [16]. Numerical results were used to show the performance of the proposed circuit. Also, where appropriate, simulation results were used for independent validation of the theoretical results. The contribution of these results from the industrial point of view is that it provides the opportunity for possible physical realisation of the circuit since it brings about improved acquisition time performance of the code acquisition process. The strong agreement between the theoretical and simulation results validates this claim. From an academic point of view, this will present the reader with an understanding of how to carry out the mathematical analysis of a circuit taking into consideration the time varying nature of the environment it is expected to operate in.

It is also intended that the material presented in this thesis should be educative enough by ensuring that all aspect of synchronisation (acquisition and tracking) of SS signals are adequately covered. Therefore, a study of code tracking was done. A mathematical

analysis of a non-coherent DLL tracking circuit was carried out. This will present the reader with an understanding of how the tracking circuit works in conjunction with the acquisition circuit.

Overall, it is intended that this thesis will serve as a motivation and reference for future work and research in the field of synchronisation in particular and SS communications in general.

1.5. Layout of the Thesis

In Chapter 2, SS communications is briefly studied. Specifically, its application in CDMA systems is explained. The importance of PN codes in the implementation of SS systems is also discussed in this chapter. In Chapter 3, a mobile channel is studied, as the proposed acquisition circuit will be operating in a mobile channel that will be characterised by fading and interference. In Chapter 4, a literature review of PN code synchronisation is done with emphasis on acquisition. This will lay the foundation for the analysis of the proposed circuit to be carried out in Chapter 5. In Chapter 5, the proposed PN code acquisition circuit is presented and its performance analysed. In Chapter 6, a brief study of a PN code tracking is done with particular emphasis on non-coherent delay-locked loop. Conclusions and future work are presented in Chapter 7.

CHAPTER 2

Spread Spectrum and CDMA

2.1. Introduction

Spread Spectrum (SS) communications is a transmission technique in which the information-bearing signal is transmitted in a bandwidth that is much larger than the minimum required transmission bandwidth in order to gain one or more operational advantages. Such operational advantages include multiple access, voice privacy, low probability of intercept, protection against multipath, anti-jamming and so on. This wide bandwidth is achieved with the aid of PN codes. In [17, pp.1], a complete definition of SS is given as follows:

“SS is a means of transmission in which the signal occupies a bandwidth in excess of the minimum necessary to send the information; the band spread is accomplished by means of a code which is independent of the data, and a synchronised reception with the code at the receiver is used for despreading and subsequent data recovery.”

In the above definition, it is important to note the importance of synchronisation. This means that without synchronisation, no effective communication can take place in systems using SS modulation. This technique was initially used in the military and was patented by Hedy Lamarr and George Anthiel in 1941 [7]. The intention was to cause radio guided missiles to be disguised in such a way that they would be difficult to intercept. This technique, known as Frequency Hopping Spread Spectrum (FH-SS) is

achieved by transmitting signals using randomly selected carrier frequencies. Such random frequencies were obtained with the aid of a PN code. The signal can only be intercepted if the interceptor knows the PN code that was used to generate these random frequencies. This is the advantage of low probability of interception or detection. Another advantage of SS communication is that it can be used for multiple access. Since each user has its own unique PN code that is uncorrelated with that of the other users (in practice the codes of the users are not completely uncorrelated), then they can transmit their signals in the same spectrum. At the receiver, the intended user's code is correlated with all the received codes but only the signal of the desired user is recovered. The use of SS for multipath protection can be explained as follows. The duration of each PN chip (*chip* is used to distinguish each of the PN code sequence from *bit* used to represent each of message data sequence) is known as chip time, given as T_c . A receiver normally receives signal from multiple paths, some adding constructively while others destructively. This results in a dispersed signal in the time domain. However, in the SS receiver, any received signal that is not within T_c is rejected. This therefore offers protection against the destructive effect of multipath signals. Similar to the low probability of detection is the advantage of privacy. In mobile communications, it will be difficult for an eavesdropper to listen to a message meant for another user as each user has its own unique secret PN code. Table 2.1 summarises the advantages and applications of SS communications [8–10].

Table 2.1. Applications of spread spectrum communication [8]

| Purposes | Military | Commercial |
|---------------------------|----------|------------|
| Antijamming | ✓ | ✓ |
| Multiple access | ✓ | ✓ |
| Low detectability | ✓ | |
| Message privacy | ✓ | ✓ |
| Selective calling | ✓ | ✓ |
| Identification | ✓ | ✓ |
| Navigation | ✓ | ✓ |
| Multipath protection | ✓ | ✓ |
| Low radiated flux density | ✓ | ✓ |

A conventional digital modulation technique will exchange power increase for improved system performance. However, SS modulation technique exchanges bandwidth increase for improved system performance. It can be deduced that these system performance improvement methods are possible as far as Shannon capacity equation [1] is satisfied. The Shannon capacity equation is given by:

$$C = B_s \log_2(1 + S/N) \quad \text{bits/sec} \quad (2.1)$$

where C is the maximum number of bits that can be transmitted per second with a probability of error close to zero, B_s is the channel bandwidth in Hertz and S/N is the system SNR.

A conventional communication system will use a bandwidth, B_s Hz and a high SNR satisfying (2.1). But for a SS system, the bandwidth will be W_s Hz ($W_s \gg B_s$). However, since C has to be constant for error-free communication, then the SNR for the

SS system has to be reduced accordingly. This means that a low SNR (such as a signal power below noise power level) can be used to transmit information as far as (2.1) is satisfied. At the transmitter of a SS system, before transmission, the desired message signal is modulated by a PN code that causes the signal bandwidth to be expanded from B_s Hz to W Hz with a corresponding decrease in SNR. This operation at the transmitter is known as *spreading*. At the receiver, the received wideband signal is demodulated by the same PN code resulting in the restoration of the signal to its original bandwidth and SNR. This operation at the receiver is known as *despreading*. If the received signal is corrupted by an interfering signal like a jammer, the jammer is spread, as it is only processed once (that is, demodulation operation at the receiver) by the PN code. On the other hand, the desired signal is despread, as it is processed twice (that is, modulation at the transmitter and demodulation at the receiver) by the same PN code. Thus, spreading a signal reduces its power (usually below noise power level) and despreading restores the signal power to its original value. The result of the spreading operation on the jammer is to reduce its power level at the receiver. This means that, at the receiver, the desired signal has a SNR advantage over the jammer. The SNR advantage resulting from the spreading and despreading operations is known as the processing gain (P_G) and it is given as the ratio of the transmission bandwidth, W_s to the original bandwidth of the unmodulated data signal, B_s as:

$$P_G = W_s / B_s \quad (2.2)$$

The implication of (2.2) is that the higher the value of P_G , the better the anti-jamming performance of the SS system. In short, the randomness of the PN code and the P_G are the main reasons for the advantages of SS systems as depicted in Table 2.1.

There are three main types of SS systems. These are FH-SS, Direct Sequence SS (DS-SS) and Time Hopping SS (TH-SS). There are also a hybrid schemes, which tends to combine any two of the three main types of SS systems and they have their relative merits [10].

2.1.1. FH-SS

In FH-SS, the narrowband signal is hopped from one frequency to another in a random manner with the aid of the PN code. The block diagram is shown in Figure 2.1. The complex baseband signal $c(t)$ at the output of the frequency hopping signal generator has the form given as [10]:

$$c(t) = \sum_i \exp(j(2\pi f_i t + \phi_i)) p_{T_h}(t - iT_h) \quad (2.3)$$

where $p_{T_h}(t)$ is a basic pulse shape of duration, T_h known as the hopping time and f_i is a pseudo-randomly generated sequence of i frequency shifts with random phases of ϕ_i uniformly distributed over $[0, 2\pi]$. This f_i is used to drive a frequency synthesiser to produce real-valued RF carrier-modulated version of $c(t)$.

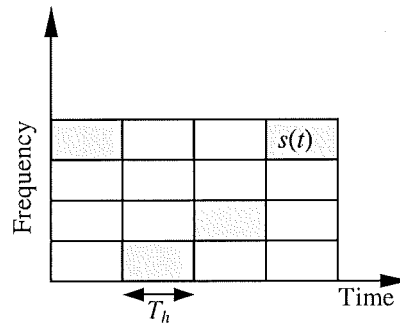


Figure 2.1. Time/frequency occupancy of FH-SS system

By using the scheme of multiplicative modulation [10], the data signal $d(t)$ can be combined with the SS signal $c(t)$ to give the transmitted signal $s(t)$ for a FH-SS system as:

$$s(t) = \text{Re}\{d(t)c(t)e^{j(2\pi f_c t + \theta_T)}\} \quad (2.4)$$

where f_c is the carrier frequency, θ_T is the phase of the signal uniformly distributed over $[0, 2\pi]$. $\text{Re}\{x\}$ denotes the real part of x .

The major advantage of FH-SS system [18] is that when used for multiple access, its near-far performance is better than DS-SS system and synchronisation is much easier. Another advantage is that a greater P_G can be achieved using this method when compared to the DS-SS system. The major disadvantage is that a highly sophisticated frequency synthesiser is necessary and coherent demodulation is difficult because of the problem in maintaining phase relationships during hopping.

2.1.2. TH-SS

In TH-SS, the signal is hopped pseudo-randomly from one location to another within a time interval, as shown in Figure 2.2. The output of a TH-SS signal generator is given as [10]:

$$c(t) = \sum_i p(t - (i + a_i / M_T)T_s) \quad (2.5)$$

where the pulse waveform $p(t)$ has duration of, at most, T_s / M_T . Time, instead of the frequency is segmented into intervals, T_s , with each interval containing a single pulse pseudo-randomly located at one of the M_T locations within the interval. The transmitted signal $s(t)$ is as given by (2.4) with $c(t)$ given by (2.5).

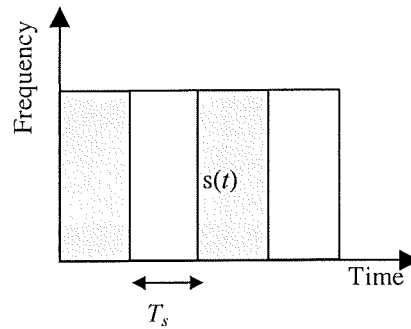


Figure 2.2. Time/frequency occupancy of TH-SS system

The near-far performance of a TH-SS system is similar to that of FH-SS system. They are both *avoidance* SS systems [18]. The random hopping of the signal makes the possibility of it being at the fixed frequency of the jammer to be quite remote. That is, the probability of it being jammed is quite low; and, if jammed, only a portion of the signal is actually jammed. So hopping the signal can be viewed as a means of avoiding the jammer. The major disadvantage of TH-SS system is that code synchronisation takes a long time and it also involves the use of a frequency synthesiser, which is an additional complexity [18].

2.1.3. DS-SS

In DS-SS, the signal is directly multiplied by the PN code sequence in such a way that the power spectral density of the signal is collapsed below the noise level. In this type of SS system, the signal is spread to a wide bandwidth before transmission as shown in Figure 2.3.

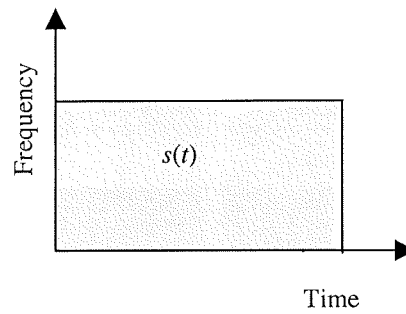


Figure 2.3. Time/frequency occupancy of DS-SS system

The waveform at the output of a DS-SS signal generator is given as:

$$c(t) = \sum_i c_i p_{T_c}(t - iT_c) \quad (2.6)$$

The output sequence $|c_i| = 1$ is linearly modulated onto a sequence of pulses, $p_{T_c}(t)$ of duration T_c , called the chip time or duration. The transmitted signal is given by (2.4) with $c(t)$ given by (2.6).

The major advantage of DS-SS system is that its implementation, in terms of the spreading and despreading of the data signal, is quite easy. It is just a simple direct multiplication. It does not involve the use of a frequency synthesiser, as in the other types of SS systems. Coherent demodulation of the signal is possible and no synchronisation among users is necessary when used for multiple access. DS-SS system is also described as an *averaging* SS system [18]. In contrast to avoidance SS system, averaging SS systems transmit in the same bandwidth as the interfering signal all the time. However, at the receiver, the P_G is used to spread the interfering signal to a wide bandwidth. By using appropriate narrow band filter, the effect of the interfering signal on the desired signal is considerably reduced as most of the interferences are filtered

out. The major disadvantage is that synchronisation is more difficult in this system as synchronisation has to be done to a fraction of T_c . The near-far effect is more prevalent in this system, necessitating the need for a complex power control algorithm [18].

2.2. Implementation of DS-SS System

As already stated, DS-SS modulation is simply the direct multiplication of the data signal with the PN code before transmission. At the receiver, the received signal is multiplied again with the same PN code that was used at the transmitter, thus recovering the data signal. Figure 2.4 shows the baseband representation of the transmitter of DS-SS modulation technique.

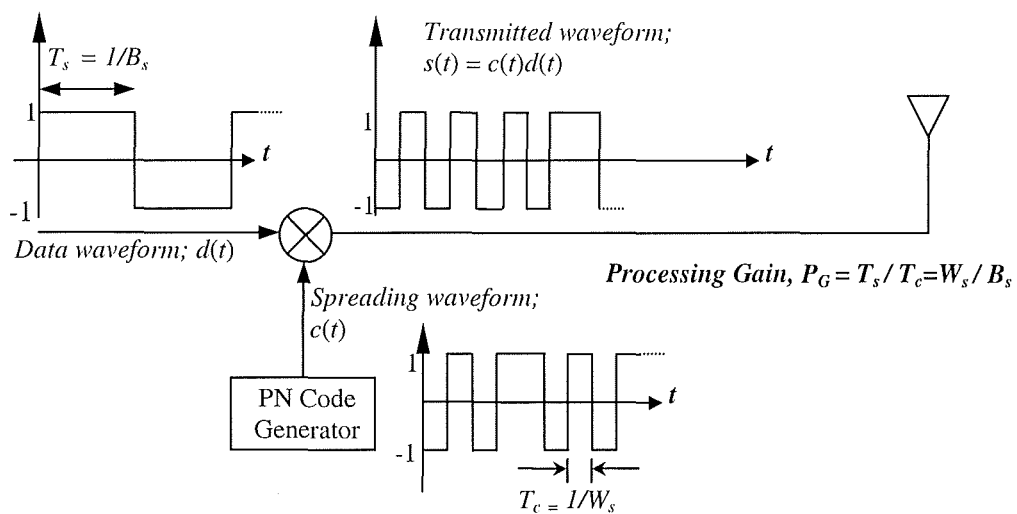


Figure 2.4. Basic baseband DS-SS operation: transmitter structure

The power spectral density (psd) of the data signal, $d(t)$ with rate of $1 / T_s$ bits/sec is given by [17]:

$$S_d(f) = T_s \sin^2(fT_s) \quad (2.7)$$

The psd of the PN signal, $c(t)$ [and also that of $s(t) = c(t)d(t)$] is given by [17]:

$$S_c(f) = T_c \sin^2(fT_c) \quad (2.8)$$

The power spectra of (2.7) and (2.8) are sketched in Figure 2.5.

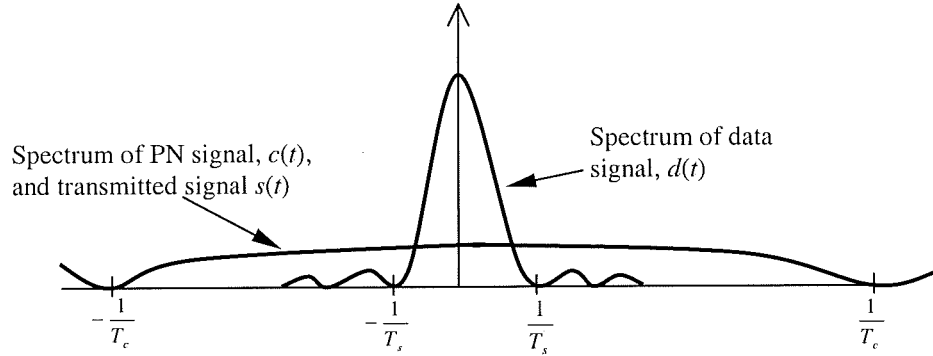


Figure 2.5. Power spectra of data and PN signal

From Figure 2.5, it is seen that the spectrum of the data signal is collapsed to a small value over a wide bandwidth as a result of the spreading operation. The transmitted signal is basically given as:

$$s(t) = c(t)d(t) \quad (2.9)$$

The power spectrum of the transmitted data, $s(t)$ will be the same as that of $c(t)$ since $W_s \gg B_s$.

The data signal $d(t)$ is recovered at the receiver using the basic demodulator shown in Figure 2.6. The received signal is assumed to be corrupted by AWGN, $n(t)$ and other interferences, $I(t)$. Thus the received signal, $r(t)$ is given as:

$$r(t) = c(t)d(t) + I(t) + n(t) \quad (2.10)$$

To recover the signal $d(t)$, $r(t)$ is multiplied by $c_r(t)$, locally generated at the receiver.

This will give a value $y(t)$ as:

$$y(t) = r(t)c_r(t)$$

$$= c_r(t)c(t)d(t) + c_r(t)I(t) + c_r(t)n(t)$$

$$= \underbrace{d(t)}_{c_r(t)=c(t)} + c_r(t)I(t) + c_r(t)n(t) \quad (2.11)$$

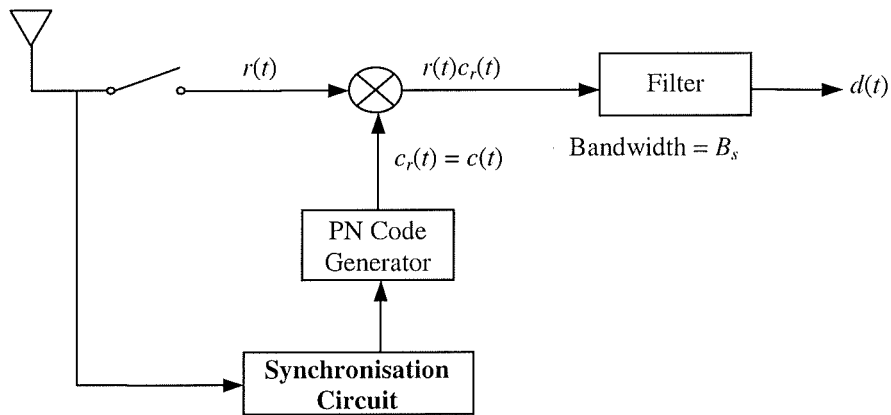


Figure 2.6. Basic baseband DS-SS operation: receiver structure

The first part of (2.11) was obtained by using property (iii) of PN codes to be discussed in Section 2.4. By using this property, $c^2(t) = 1$. Multiplication of $I(t)$ by $c_r(t)$ will spread it to a wide bandwidth, W_s . However, the bandwidth of $d(t)$ is B_s ($B_s \ll W_s$). By filtering $y(t)$ with a lowpass filter of bandwidth B_s , $d(t)$ is recovered while a very large portion of the interfering signal and noise will be filtered out.

2.3. Code Division Multiple Access

Code Division Multiple Access (CDMA) uses SS modulation for multiple access whereby users are identified by their own unique PN code and they occupy the same spectrum. Since CDMA is based on SS modulation, it therefore has all the advantages of SS communication. The three main types of CDMA systems are FH-CDMA, TH-CDMA and DS-CDMA. It is the DS-CDMA that is used in commercial mobile

communications [3, 4]. The reason being the ease of implementation as outlined in the advantages of DS-SS systems. The capacity, K (number of users) in a CDMA system (assuming the receiver is a single-user detector) is given from [9] as:

$$K \approx \frac{4P_G}{E_b / I_0} \quad (2.12)$$

where E_b / I_0 is the bit-energy-to-noise-density^{2.1}.

From (2.12), as the number of users increases for a fixed P_G , it means decrease in E_b / I_0 (note that the users constitute the bulk of the interference, I_0), leading to degradation in the system quality. The reverse is the case if the interference is reduced. Thus, it is seen that the capacity of CDMA systems is interference limited. As the users increase, the performance of the system degrades gradually in what is called graceful degradation, which shows the soft capacity of a CDMA system [5].

The transmitter and receiver structures for DS-CDMA system with K asynchronous users is just the elaboration of Figures 2.4 and 2.6 respectively. Therefore, the transmitted baseband signal for the k th user is given from (2.9) as:

$$s(t) = \sum_{k=1}^K c_k(t)d_k(t) \quad (2.13)$$

The received signal is given by:

$$r(t) = \sum_{k=1}^K c_k(t)d_k(t) + n(t) \quad (2.14)$$

To recover the message signal, $d_1(t)$ of user 1, $r(t)$ is multiplied with the local PN signal for user 1, $c_{r,1}(t)$ to obtain:

^{2.1} The conventional notation for Gaussian noise density is N_0 (W/Hz), but since the density will be dominated by interference from other users (all the users are in the same spectrum), the notation I_0 is employed to indicate the inclusion of this additional interference.

$$\begin{aligned}
\tilde{d}_1(t) &= \sum_{k=1}^K c_{r,1}(t)c_k(t)d_k(t) + c_{r,1}(t)n(t) \\
&= c_{r,1}(t)c_1(t)d_1(t) + \sum_{k=2}^K c_{r,1}(t)c_k(t)d_k(t) + c_{r,1}(t)n(t) \\
&= d_1(t) + I_0(t)
\end{aligned} \tag{2.15}$$

where the first term in (2.15) is the desired message signal for user 1. The second term is the interference given by:

$$I_0(t) = \sum_{k=2}^K c_{r,1}(t)c_k(t)d_k(t) + c_{r,1}(t)n(t) \tag{2.16}$$

From (2.15), the received message $\tilde{d}_1(t) \approx d_1(t)$ due to the presence of the other users' interference, $I_0(t)$. It is seen that as the number of users increases, $I_0(t)$ will increase and this will lead to degradation in the quality of $\tilde{d}_1(t)$. The amount of degradation the system can tolerate now determines the capacity of the system.

Another important area worth mentioning in DS-CDMA systems is the *near-far effect*. This is a result of mobile stations (MS) near to the base station (BS) and thus received with higher signal power cause interference to MS farther from the BS that are received with a lower signal power. This can be controlled by using power control algorithms [7–9]. There are two main types of power control algorithms, such as *open-loop* and *closed-loop* power control. The MS uses the open-loop power control algorithm to adjust its transmitted power based on the power it receives from the forward link. If the received forward link power is very high, the MS will reduce its power, and vice versa. However, as both the forward and reverse links are separated in frequency, this power control algorithm is not effective as it only provides a rough estimate of the average power of all the users in the system. The implication of this is that the MS might set its

power too high, or too low. This is why an additional power control algorithm known as closed-loop power control is required. The closed-loop power control is administered by the BS. If the BS determines that the power of an MS is too high or too low, it sends a command to that MS to lower or raise its power. Since all MSs communicate with a BS, it means they are all properly controlled to the same power. However, it is clear that only MSs that are already synchronised and engaged in data transmission could take advantage of this closed-loop power control algorithm. If an MS is yet to be synchronised, it can only rely on open-loop power control. The issue of open-loop power control will be revisited in Chapter 5 when the effect of MAI on the performance of the proposed circuit is being considered.

2.3.1. Call Processing in DS-CDMA Systems

Call processing has to do with the exchange of messages between the mobile phone or MS and its server BS in order to negotiate the origination and termination of calls. Call processing procedures are similar for CDMA IS-95 and CDMA2000 [19, 20]. To use an MS, it has to be powered on and when the user sees the logo of the service provider, calls can be made and received. If this is not possible, the user assumes there is no service available, or reception is poor, and may have to wait or move to another area for better reception. One of the steps in call processing is called the *initialisation process*. It is the step that the MS has to follow or execute in order to recognise, access and set up configuration parameters. The initialisation process includes the acquisition and synchronisation to the pilot channel. Briefly, the following are the call processing states in the order they occur when an MS switched on [19]:

- MS Initialisation State: the MS performs system acquisition and synchronisation.
- MS Idle State: in this state, the MS monitors messages transmitted through signalling and control channels, such as Forward Paging Channels (FPChs), Quick Paging Channels (QPChs), and so on.
- System Access State: here, the MS attempts to access the system by sending messages or responding to orders from the server BS. Such orders include directing the MS to use a traffic channel.
- MS control on the Traffic Channel State: communication is established between an MS and a BS during a call with the aid of Fundamental Channels (FChs) and Dedicated Control Channels (DCChs) to send and receive data messages and speech.

Only the MS initialisation state is further explained here, as it has to do with the synchronisation of the PN signal. Details of call processing could be found in [19].

2.3.1.1. MS Initialisation State

On power up, the MS selects the system to be used. The system to use here is CDMA. The band of frequency is also selected (800 MHz for IS-95 and 1900 MHz for CDMA2000). The next step is the *synchronisation* stage. The MS acquires and synchronises itself to a BS. This is done with the aid of a pilot PN code transmitted by the BS using the Forward Pilot Channel (FpiCh). Finally, the MS gathers more information about the CDMA network timing and configuration parameter.

The synchronisation process is basically as follows. The FpICH is specifically meant for the transmission of a synchronisation signal – which is basically the PN signal without data – to MS. The CDMA BS must always transmit this signal. The pilot channels transmit the first row of the Walsh Hadamard matrix, which is an all 0's code of length 64 (see Section 2.4.1). These Walsh codes are I/Q (quadrature) modulated by I - and Q short PN sequences of length 32,767 chips. The MS tries to synchronise to this PN signal with the aid of the synchronisation circuit in two stages. The first stage is the coarse synchronisation, where the MS roughly synchronises the phase of its locally generated PN code to the received PN code, with the aid of the acquisition circuit. The second stage is called the fine synchronisation stage and this involves the use of the tracking circuit to fine-tune this roughly-acquired phase, and to keep track of it through the duration of the communication. It is seen that, without synchronisation, the call processing cannot be completed in CDMA systems. Therefore, the need for PN code synchronisation cannot be overemphasised. The synchronisation process for WCDMA is quite different and mention will be made of it in Chapter 7.

2.4. Generation of PN Codes

From the definition of SS, it was stated that the wide bandwidth is achieved with the aid of PN codes (also known as spreading codes). A PN code is a long string of ones (+1) and zeros (-1) that have properties of random noise. They are usually generated using well-configured Linear Feedback Shift Registers (LFSR). Unlike random noise, PN codes are generated from deterministic sources. The reason being that if it is completely random, then it will not be possible to regenerate the same codes at the receiver in order to despread the signal. Alternatively, it is possible to send the spreading codes as a

reference signal that can now be used to despread the signal. The obvious drawback of such tactics, as pointed out in [10], is that the message can easily be deciphered by any receiver (intended or not) that has access to both transmitted signals. Also, there is a relatively poor performance at low SNR. Thus, for effective operation, the codes have to be stored in, or regenerated by, the intended receiver that knows the algorithm of the code sequence generator that was used to generate the spreading code at the transmitter. In this case, the unintended receiver does not know the algorithm that was used to generate the code, and so the code appears random, hence the term *pseudo-random* code. In a nutshell, the PN code should have properties resembling that of random noise, but it should be easily generated from a deterministic source. There are several types of PN code generators discussed in virtually all the literature on SS communications [10]. The most commonly used code generator is the LFSR. Different configurations of LFSR result in the following types of PN sequences:

- i. Maximal length sequence.
- ii. Gold sequence.
- iii. Kasanmi sequence.

Figure 2.7 shows the basic component of an m stage LFSR generator for generating maximal length sequence, or m -sequence. This type of LFSR is known as the *Galois feedback generator* [10, 21]. It is made up of m delay elements and the output, ζ_0 is fed back into the registers through the connecting taps, φ_m and mod-2 adders. The tap weights, φ_m ($m = 1, 2, \dots$) are elements of the binary Galois field, $GF(2)$. Using D as the delay operator, the elements stored in the registers of m delay elements are given by the symbols of the field elements over $GF(2^m)$ in polynomial form as:

$$\beta(D) = \beta_0 + \beta_1 D + \dots + \beta_{m-1} D^{m-1} \quad (2.17)$$

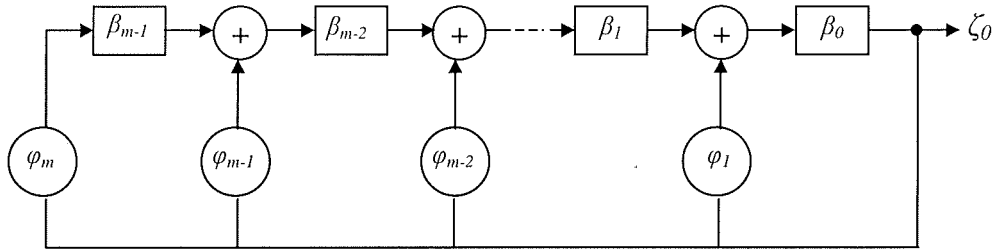


Figure 2.7. An m -stage Galois feedback LFSR generator

At a clock pulse, the output ζ_0 is recorded and the contents of the delay elements are shifted one place to the right. At the same time, ζ_0 is also sent back to the delay elements in the shift registers through the connecting taps φ_m ($m = 1, 2, \dots$) after the mod-2 addition is done. At every clock pulse, the output is taken out, and at the same time, fed back into the shift register. Not all the taps are connected and so the tap connection is given by the polynomial [21]:

$$\varphi(D) = 1 + \sum_{i=1}^m \varphi_i D^i \quad (2.18)$$

where $\varphi(D)$ is a special class of irreducible polynomial known as *primitive* polynomial [21]. A polynomial $\varphi(D)$ of degree m is a primitive polynomial, if the smallest integer M for which $\varphi(D)$ divides $D^M + 1$ is $M = 2^m - 1$. For example, a 4 stage LFSR with $\varphi(D) = 1 + D + D^4$ means that the feedback connections are in taps φ_1 and φ_4 . The output sequence of the shift register is given by [21]:

$$\zeta(D) = \frac{\beta^{(0)}(D)}{\varphi(D)} \quad (2.19)$$

where $\beta^{(0)}(D)$ is the polynomial used to indicate the initial condition of the shift register content.

Normally, the period of the output cycles from the LFSR generator should be 2^m . However, if all the delay elements are filled with 0, then the output will always be 0 as there will be no transition or change in the output at every clock pulse. To avoid this situation, the all-zero state is excluded and the period is now given as $2^m - 1$. Thus the largest code that can be generated by a shift register of m delay elements is $2^m - 1$ and this is known as maximal-length sequence, or m -sequence, for short. Thus the period of an m -sequence is given as $M = 2^m - 1$.

Consider the following example for clarification:

Let the initial condition of a 3 stage LFSR contents in Figure 2.7 be given as [1 0 1].

This means that $\beta^{(0)}(D) = 1 + D^2$. Thus the period is $M = 2^3 - 1 = 7$. Let the characteristic polynomial of the shift register be given by $\phi(D) = 1 + D + D^3$. Then by using (2.19), the sequence produced is given as:

$$\zeta(D) = \frac{1 + D^2}{1 + D + D^3} = 1 + D + D^3 + D^6 \dots \quad (2.20)$$

Thus $\zeta(D) = [1 \ 1 \ 0 \ 1 \ 0 \ 0 \ 1]$. The dotted line in (2.20) is used to indicate that the sequence repeats after the last output for the period, which is D^6 .

The following are some of the properties of m -sequence:

- i. There is an approximate balance of zeros and ones (2^{m-1} ones and $2^{m-1} - 1$ zeros). This is also commonly known as the balance property.
- ii. In any period, half of the runs of consecutive zeros or ones are of length one, one-fourth are of length two, one-eighth are of length three, and so on. This is commonly known as the run-length property.

- iii. The normalised autocorrelation of the m -sequence is equal to 1, at zero phase shift, and $-1/M$ (normally approximated to 0 for $M \gg 1$) at any other shifts.

This is known as the autocorrelation property.

Given an m -sequence c_i for $i = 1, 2, \dots$; and a shifted version of it c_{i+k} , the discrete autocorrelation function is given as:

$$R_c(k) = \sum_{i=1}^M c_i c_{i+k} = \begin{cases} 1 & k = 0, \pm L, \pm 2L, \dots \\ -1/M & \text{otherwise} \end{cases} \quad (2.21)$$

The plot of the discrete autocorrelation function is shown in Figure 2.8.

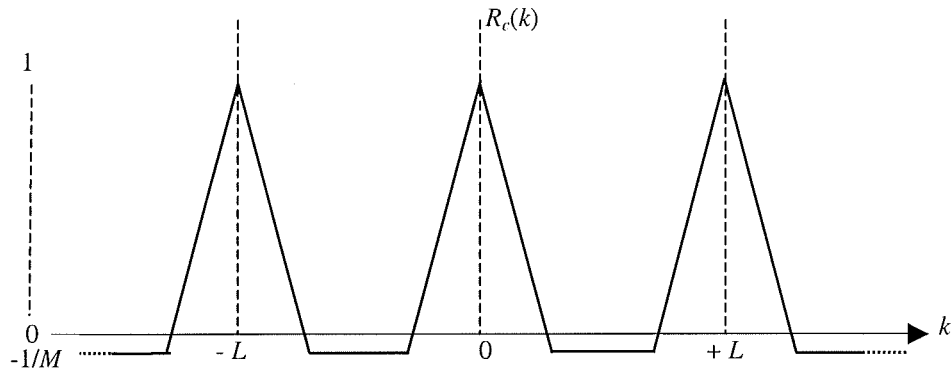


Figure 2.8. Discrete autocorrelation function of PN sequence

2.4.1. PN Codes in CDMA Systems

m -sequences have good autocorrelation properties, but their cross-correlation properties are poor. For this reason their use in certain applications is restricted. In CDMA systems, it is desired that the cross-correlation between users be as small as possible to limit the interference experienced in the system. m -sequences have cross-correlation values that are many valued. The maximum cross-correlation value, denoted as R_{\max} , increases as the length M of the sequence as shown in Table 2.2. Though there are some m -sequences that have small cross-correlation values, these m -sequences are few [22]

and thus there is a limitation of the use of m -sequence in CDMA systems. However, since the correlation among different shifts of the same m -sequence is almost zero, they are used for BS identification. In a synchronous transmission in CDMA systems, as in the forward link of IS-95 CDMA and CDMA2000, all base stations are time-synchronised by GPS. Hence, each base station is identified by a unique offset of the same m -sequence [19 – 23].

Table 2.2. Cross-correlation properties of m -sequences and Gold sequences from [22]

| m | $M = 2^m - 1$ | m -sequences | | | Gold sequences | |
|-----|---------------|----------------|------------|-----------------|----------------|-----------------|
| | | Number | R_{\max} | $R_{\max}/R(0)$ | R_{\max} | $R_{\max}/R(0)$ |
| 3 | 7 | 2 | 5 | 0.71 | 5 | 0.71 |
| 4 | 15 | 2 | 9 | 0.60 | 9 | 0.60 |
| 5 | 31 | 6 | 11 | 0.35 | 9 | 0.29 |
| 6 | 63 | 6 | 23 | 0.36 | 17 | 0.27 |
| 7 | 127 | 18 | 41 | 0.32 | 17 | 0.13 |
| 8 | 255 | 16 | 95 | 0.37 | 33 | 0.13 |
| 9 | 511 | 48 | 113 | 0.22 | 33 | 0.06 |
| 10 | 1023 | 60 | 383 | 0.37 | 65 | 0.06 |
| 11 | 2047 | 176 | 287 | 0.14 | 65 | 0.03 |
| 12 | 4095 | 144 | 1407 | 0.34 | 129 | 0.03 |

In order to improve on the cross-correlation properties of m -sequence, method of generating codes with good cross-correlation properties were developed by Gold [24, 25] and Kasami [26]. Gold sequences are constructed by taking a pair of specially selected m -sequences, called *preferred m -sequences*, and then a mod-2 sum of these two sequences are formed for each of M cyclically shifted versions of one sequence relative to the other sequence. The Gold sequence generated is of length M . This is shown in Figure 2.9. Comparing m -sequence and Gold sequence performance as shown in Table

2.2, it is seen that significant improvement in the cross-correlation property of PN sequence is achieved by using Gold sequence.

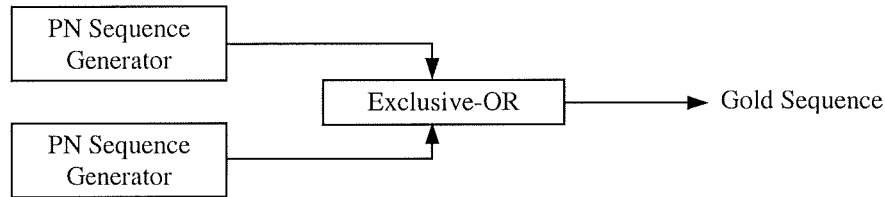


Figure 2.9. Generation of Gold sequence using two preferred m -sequences

There is also another important code used in CDMA systems, known as *Walsh* code. In CDMA, Walsh codes are used for channelisation, that is, separating individual users in the forward link. In the reverse link, they are used for orthogonal modulation. They are generated by code-word rows of special square matrices known as Hadamard matrices [23]. These matrices contain one row of all zeros with the remaining rows each having an equal number of 1's and 0's. The Hadamard matrix is given by:

$$H_{2N} = \begin{bmatrix} H_N & H_N \\ H_N & \overline{H_N} \end{bmatrix} \quad (2.22)$$

In (2.22) $\overline{H_N}$ are the same but inverted elements of H_N .

The seed matrix is given as:

$$H_2 = \begin{bmatrix} 0 & 0 \\ 0 & 1 \end{bmatrix} \quad (2.23)$$

Higher order matrices are generated by recursion using the seed matrix. The Walsh codes are then selected from the rows of the matrix. In CDMA systems, each Walsh code is selected from rows of Hadamard matrix of order 64. Walsh codes are orthogonal to each other and thus they are defined by the equation:

$$\sum_{i=0}^{M-1} w_x(i\tau)w_y(i\tau) = 0, \quad x \neq y \quad (2.24)$$

where $w_x(i\tau)$ and $w_y(i\tau)$ are the x th and y th members of an orthogonal set, M is the length of the set, and τ is the symbol duration.

Another type of code that is used in WCDMA is the *variable-length orthogonal codes* [23]. They are also constructed from modified Hadamard matrices. These codes are needed in order to support multimedia services in 3G CDMA systems. Different bit rates are assigned different spreading code according to a tree-based code assignment structure. Further details of the different codes used in CDMA systems are found in the references cited in this section. Table 2.3 gives a brief detail of the applications of the codes discussed so far in CDMA systems.

Table 2.3. Walsh and PN sequences applications in CDMA systems

| | CDMA (IS-95)/CDMA2000* | | WCDMA | |
|---------------------|---|--|--|---|
| | Forward link | Reverse link | Forward link | Reverse link |
| Channelisation code | Walsh orthogonal sequence of length 64 | Long PN code of length $2^{42}-1$ chips. | Variable-length orthogonal sequences | Variable-length orthogonal sequences |
| Scrambling code | Different offset of an m -sequence with a period of 32,767 ($2^{15}-1$) chips (a common PN for all users of a cell) | Different offset of an m -sequence with a period of 32,767 ($2^{15}-1$) chips (a distinct offset for each users) | 10 ms of a $2^{18}-1$ chip Gold sequence (a common PN for all users of a cell) | Very large set of Kasami sequences. Optional: 10 ms of a $2^{41}-1$ chip Gold sequence. |

*CDMA2000 uses variable-length orthogonal sequences for channelisation in both forward and reverse link.

2.6. Summary

The purpose of this chapter was to introduce the theory behind SS communications and CDMA. A definition of SS was stated and the main types of SS systems available were briefly explained. The importance of PN code sequences in SS communications was stated. The application of SS in commercial mobile communications in the form generally known as CDMA was briefly discussed. Two important implementation areas in CDMA systems were mentioned. These are power control and PN code synchronisation. This thesis is concentrated on the latter. A brief explanation of the major steps in call processing in CDMA system was given. From this study, it was clear that the first step in call processing is the MS initialisation state. This mainly involves PN code synchronisation. Further study of PN code acquisition will be done in Chapter 4.

CHAPTER 3

Mobile Radio Channel and Interferences

3.1. Introduction

One of the driving forces for the large market growth in mobile communication systems is as a result of the possibility of 'anywhere-anytime' communication. This is achieved as the receiver is not tied to a wired circuit like the traditional landline (fixed) telephone system. However, unlike the landline system, the radio channel imposes fundamental limits on the range, data rate and quality of wireless communication. The most important factors that influence the performance limits of mobile systems are the propagation environment and user mobility pattern. A radio wave is an electromagnetic wave propagating from the transmitter antenna through the atmosphere to the receiver antenna. The dielectric of free space, ϵ_r , is unity. However, in the wireless channel, due to the presence of gases and water vapour, ϵ_r is no longer unity, and decreases with height, and so does the refractive index, $\sqrt{\epsilon_r}$ [8]. Thus, the propagating wave will undergo reflection, absorption, refraction, diffraction and scattering depending on the type of objects they come in contact with. Such objects include buildings, bridges, hills, trees and so on. The presence of these objects might also block the direct path, also known as the line-of-sight (LOS) path between the transmitter and receiver, a phenomenon known as shadowing. The shadowing effect is expected to be more

prevalent in the urban environment. This results in signal reception to be mainly by non-line-of-sight (NLOS). In the rural area, it will be mainly by LOS [16]. Also, as the distance between the BS and the MS increases, the signal strength is attenuated according to the inverse square law of electromagnetic propagation in free space. Since the MS is moving, the speed at which it moves also affects the quality of the received signal. The net effect of these factors is that the MS will receive multiple components of the transmitted signal, some adding constructively while others destructively, a phenomenon termed fading.

Thus, for effective deployment of cellular system, a thorough study of the factors in the wireless link that limit the performance of the system has to be carried out. This means specifying models to capture different environmental conditions in the areas where the cellular system is to be deployed. For example, the propagation model used in specifying microwave link transmission from one tower to another tower will be different from that used in a BS to a MS. The same is true for the models used in a rural area to those used in a sub-urban or urban area. Apart from fading, wireless systems also suffer from other form of interference including jamming, multiple access interference (MAI), inter- and intra-cell interference, and so on. Fading results from fluctuations in the amplitude and phase of the transmitted signal, leading to the attenuation of the average power of the received signal. Interference, on the other hand, directly results in the reduction of the available SNR. This research focuses on signal transmission and reception in a cellular system, where the emphasis is on the mobile-to-base station and vice-versa. It is therefore the aim of this chapter to study the characteristics of the mobile channel.

3.2. Characterisation of a Wireless Channel

As already stated, the transmitted signal undergoes a variety of effects as it propagates through the atmosphere, and this mostly results in fading. From [27], a filter can be defined as a system or network that selectively changes the wave shape, amplitude-frequency and/or phase-frequency characteristics of a signal that is passed through it. Therefore, the wireless channel can be represented by a filter as shown in Figure 3.1 with impulse response $\tilde{h}(\tau)$ or frequency response $H(f)$ (where \leftrightarrow is used to denote a Fourier transform pair).

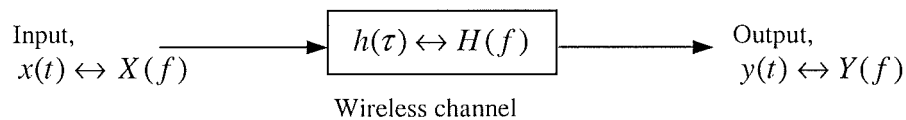


Figure 3.1. Filtering effect of the mobile channel

In Figure 3.1, the input signal into the wireless channel (that is, the signal from transmitter) is $x(t)$ and $y(t)$ is the output signal from the wireless channel (that is the input signal into the receiver). In system design, mathematical models are used to represent these effects. In short, due to the random nature of the channel, the mathematical models mainly describe the statistical distribution of the channel in terms of its probability density function (pdf). The choice of model used depends on factors including the type of environment (that is whether rural or urban area), propagation type, (that is whether microwave tower-to-tower link or BS to MS) and so on. Figure 3.2 depicts a typical propagation environment for a cellular system.

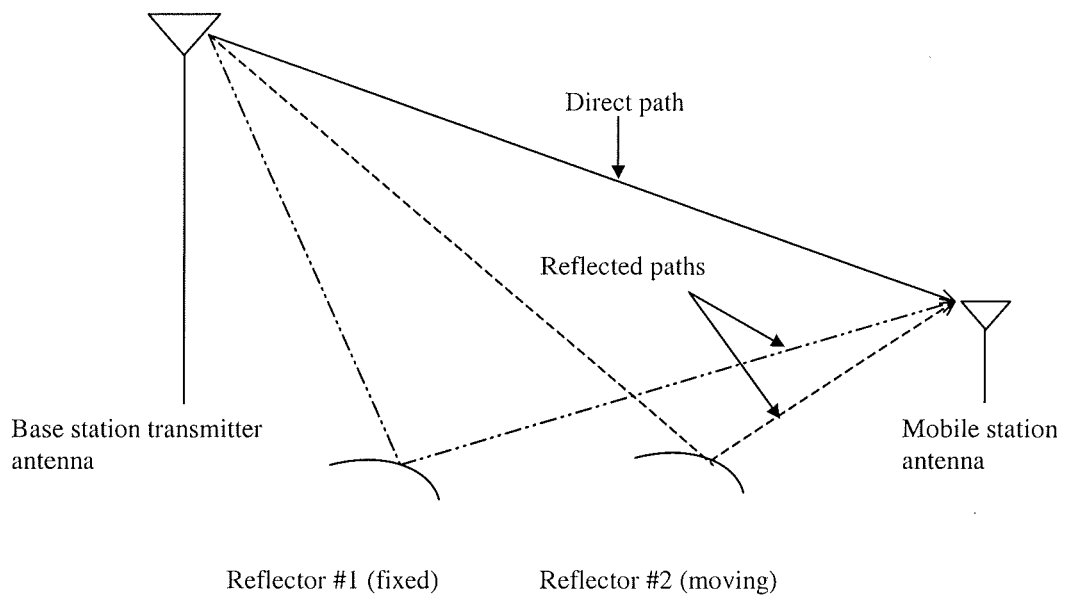


Figure 3.2. A three-path mobile channel

From Figure 3.2, it is seen that the signal is made up of a LOS path, and two NLOS paths. These multipath signals will arrive at different times as a result of the difference in distance travelled. The BS antenna height is usually between 30-91 m and the MS antenna height varies in the range of 1-3 m [28]. Normally, the MS is embedded in the surroundings. Figure 3.2 typically represents the propagation model that is usually common in a rural environment, as there is the high likelihood of a LOS path.

3.3. Classification of Fading

There are two basic terms used to describe fading in wireless systems. These are *large-scale* and *small-scale fading*. By noting the filtering effect of a wireless channel, the lowpass equivalent response of a mobile channel can be modelled by a complex impulse response given by:

$$\tilde{h}(\tau, t) = \tilde{h}_l(d, p(t))\tilde{h}_s(\tau, p(t)) \quad (3.1)$$

where $\tilde{h}_l(d, p(t))$ models the effect of large-scale fading as a function of position, $p(t)$ at distance d . $\tilde{h}_s(\tau, p(t))$ accounts for the small-scale fading effect at position $p(t)$ at time τ .

3.3.1. Large-Scale Fading

The large-scale fading, $\tilde{h}_l(d)$ [short for $\tilde{h}_l(d, p(t))$] describes the attenuation in signal strength, or power, as the distance, d between the mobile and the BS increases. This attenuation is known as the path loss [16, 28-32]. It also takes into consideration terrain features between the mobile and the base station. Here it is assumed that the base station is always fixed^{3.1}. Thus if d is the distance between the base and mobile station, then the large-scale fading, in dB, can be given as [30]:

$$\tilde{h}_l(d) = L(d_0) + 10n \log_{10}(d/d_0) + X_\sigma \quad (3.2)$$

where $L(d_0)$ is the path loss in free-space given by $(4\pi d_0 f_c / \nu)^2$ with d_0 a reference distance usually chosen to be less than or equal to 1 km. f_c is the carrier frequency in Hz, ν is the speed of signal propagation in free space in m/s. n , the path loss index, depends on the frequency, antenna heights and propagation environment. From measurements, it is approximately 2.2 on the average [31]. X_σ is a zero mean Gaussian variable with standard deviation ranging from 6-10 dB, and is site-distant dependent [30].

It is seen that large-scale fading as given by (3.2) is mainly distance dependent. Therefore, the distance, d , between the base and mobile station is an important

^{3.1} In military communications, BS is not always fixed

parameter when evaluating large-scale fading. It can be concluded that large-scale fading varies very little with change in time. This means that by properly noting the coverage area when deploying base stations; and based on gathered information about terrain features in the mobile environment, it is possible to have some measure of control over the large-scale fading effect. For the case of small-scale fading; as will be shown later, a small change in time can lead to large change in the received signal envelope, and this poses a major problem in the analysis and design of communication systems.

3.3.2. Small-Scale Fading

Small-scale fading, $\tilde{h}_s(\tau, p(t))$ is the fluctuation in signal envelope due to multipath and the speed at which the mobile is moving. From Figure 3.2, the received signal is made up of three parts, but, in most cases, the number of paths is usually many and can be generalised into L_p paths. These L_p paths can be grouped into *discrete* and *diffuse* multipath channel [31]. The received signal in a discrete multipath channel is a made up of discrete component paths. A diffuse multipath channel is a channel with each path being a continuum of many component paths.

Assume that the output of the wireless channel is given as:

$$y(t) = \sum_{l=1}^{L_p} \alpha_l(t)x(t - \tau_l(t)) \quad (3.3)$$

where $x(t)$ is the transmitted signal, $\alpha_l(t)$ and $\tau_l(t)$ are respectively the attenuation and propagation delay associated with the l th multipath component. It is seen from (3.3) that both the attenuation and the delay are a function of time and consequently whenever there is a relative movement between the transmitter and receiver, these factors will

change accordingly. Assuming that the input signal into the wireless channel in Figure 3.1 is a modulated signal given by:

$$x(t) = A(t) \cos(2\pi f_c t + \phi(t)) \quad (3.4)$$

where $A(t)$ is the amplitude of the signal and f_c is the carrier frequency with phase, $\phi(t)$ uniformly distributed in $[0, 2\pi]$. The complex envelope of the signal is given as:

$$\tilde{x}(t) = A(t)e^{j\phi(t)} \quad (3.5)$$

Substituting (3.4) into (3.3) gives:

$$\begin{aligned} y(t) &= \sum_{l=1}^{L_p} \alpha_l(t) A(t - \tau_l(t)) \cos[2\pi f_c (t - \tau_l(t)) + \phi(t - \tau_l(t))] \\ &= \sum_{l=1}^{L_p} \alpha_l(t) A(t - \tau_l(t)) \operatorname{Re} \left\{ e^{[j\phi(t - \tau_l(t))]} e^{[-j2\pi f_c \tau_l(t)]} e^{(j2\pi f_c t)} \right\} \end{aligned} \quad (3.6)$$

$\operatorname{Re}\{x\}$ denotes the real path of x . Therefore, since $\alpha_l(t)$ and $A(t)$ are both real, (3.6) can be written as:

$$y(t) = \operatorname{Re} \left\{ \sum_{l=1}^{L_p} \alpha_l(t) A(t - \tau_l(t)) e^{[j\phi(t - \tau_l(t))]} e^{[-j2\pi f_c \tau_l(t)]} e^{(j2\pi f_c t)} \right\} \quad (3.7)$$

By using (3.5), it is seen that:

$$A(t - \tau_l(t)) e^{[j\phi(t - \tau_l(t))]} = \tilde{x}(t - \tau_l(t)) \quad (3.8)$$

Thus,

$$y(t) = \operatorname{Re} \left\{ \sum_{l=1}^{L_p} \alpha_l(t) \tilde{x}(t - \tau_l(t)) e^{[-j2\pi f_c \tau_l(t)]} e^{(j2\pi f_c t)} \right\} \quad (3.9)$$

The complex attenuation can be defined as:

$$\tilde{\alpha}_l(t) = \alpha_l(t) e^{[-j2\pi f_c \tau_l(t)]} = \alpha_l(t) e^{-j\theta_l(t)} \quad (3.10)$$

Thus,

$$y(t) = \text{Re} \left\{ \sum_{l=1}^{L_p} \tilde{\alpha}_l(t) \tilde{x}(t - \tau_l(t)) e^{(j2\pi f_c t)} \right\} \quad (3.11)$$

It is apparent from (3.11) that the envelope of the lowpass received signal is:

$$\tilde{y}(t) = \sum_{l=1}^{L_p} \tilde{\alpha}_l(t) \tilde{x}(t - \tau_l(t)) \quad (3.12)$$

Equation (3.12) describes the channel input-output relationship and this corresponds to a linear time-varying (LTV) system with impulse response given as:

$$\tilde{h}_s(\tau, t) = \sum_{l=1}^{L_p} \tilde{\alpha}_l(t) \delta(t - \tau_l(t)) \quad (3.13)$$

where $\delta(\cdot)$ is the Dirac delta function.

In equation (3.13) τ is the elapsed time and thus $\tilde{h}_s(\tau, t)$ is the impulse response of the channel at time t assuming that the impulse is applied at time $t - \tau$. This is the channel impulse response for a discrete multipath channel. For a diffuse multipath channel, ($L_p \rightarrow \infty$) and the channel impulse response is given as [32]:

$$\tilde{h}_s(\tau, t) = \alpha(\tau, t) e^{-j2\pi f_c \tau} \quad (3.14)$$

where $\alpha(\tau, t)$ denotes the attenuation of the received signal component at delay τ , and at time instant t . Equations (3.13) and (3.14) show that, for small scale fading, the wireless channel can be represented mathematically by a filter with impulse response $\tilde{h}_s(\tau, t)$.

From (3.10), if τ_l changes by $1/f_c$ (which is a very small value) then $\theta_l(t)$ will change by 2π (a large value) and therefore a large change in $\tilde{\alpha}_l(t)$. Assume that a mobile system is operating at $f_c = 900$ MHz, then $1/f_c = 1.1 \times 10^{-9}$ sec, which is a very small

value. This small change in τ can lead to large change in the received signal envelope. For large number of paths, this results in a larger number of random changes in $\tilde{\alpha}_i(t)$ and the central limit theorem [32] can be used to model $\tilde{h}_s(\tau, t)$ as a complex Gaussian process in t .

3.3.2.1. Pdf of Ricean and Rayleigh Fading Channel

If the mean of $\tilde{h}_s(\tau, t)$ is zero, but with variance σ^2 (indicating the presence of only NLOS signals), the pdf of the channel envelope $R=|\tilde{h}_s(\tau, t)|$ is Rayleigh distributed and it is given by [32]:

$$f_R(r) = \frac{r}{\sigma^2} e^{-r^2/2\sigma^2}, \quad r \geq 0 \quad (3.15)$$

However, if $\tilde{h}_s(\tau, t)$ has a non-zero mean (indicating the presence of a LOS and other NLOS signals), the envelope, R has a Ricean pdf given by [32]:

$$f_R(r) = \frac{r}{\sigma^2} e^{-(r^2+A^2)/2\sigma^2} I_0\left(\frac{rA}{\sigma^2}\right), \quad r \geq 0 \quad (3.16)$$

The parameter A^2 represents the power of the LOS signal and $I_0(x)$ is the zero order modified Bessel function of the first kind. The Ricean pdf is usually described by a factor known as the Ricean fading factor, k_R (dB) [30], where k_R is the ratio of the power of the LOS path to the NLOS paths, given by:

$$k_R = 10 \log_{10}\left(\frac{A^2}{2\sigma^2}\right) \quad (\text{dB}) \quad (3.17)$$

If $k_R = -\infty$, then there is no LOS path and (3.16) reduces to (3.15). If $k_R = \infty$, then propagation is mainly by LOS and the channel is purely an AWGN channel.

Apart from the Ricean and Rayleigh statistical channel models, there are other channel models in the literature, but these two models have been shown to be quite adequate for most analysis [16, 30- 32]. Typical statistical models include the Suzuki distribution, the Nakagami- m distribution and Weibull distribution [16, 32].

3.3.2.2. Important Parameters

To mathematically model the time-varying nature of the channel, $\tilde{h}_s(\tau, t)$ is treated as a *wide sense stationary* (WSS) random process in t with an autocorrelation function given as [45]:

$$R_{\tilde{h}_s, \tilde{h}_s}(\tau_1, \tau_2, \Delta t) = E\left\{\tilde{h}_s^*(\tau_1, t)\tilde{h}_s(\tau_2, t + \Delta t)\right\} \quad (3.18)$$

where $E\{x\}$ denotes the expectation of x , and $*$ is used to indicate a complex conjugation. In most multipath channels, the attenuations and phase shift associated with the various scattered paths are uncorrelated. This is known as *uncorrelated scattering* (US) [31] and, when it is combined with the WSS, it leads to the WSSUS assumption. Using this WSSUS assumption:

$$R_{\tilde{h}_s, \tilde{h}_s}(\tau_1, \tau_2, \Delta t) = R_{\tilde{h}_s, \tilde{h}_s}(\tau_1, \Delta t)\delta(\tau_1 - \tau_2) \quad (3.19)$$

where $\delta(\cdot)$ is the Dirac delta function.

Therefore the autocorrelation function can be written as:

$$R_{\tilde{h}_s, \tilde{h}_s}(\tau, \Delta t) = E\left\{\tilde{h}_s^*(\tau, t)\tilde{h}_s(\tau, t + \Delta t)\right\} \quad (3.20)$$

If $\Delta t = 0$, the resulting autocorrelation function $R_{\tilde{h}_s, \tilde{h}_s}(\tau, 0) \equiv R_{\tilde{h}_s, \tilde{h}_s}(\tau)$ is the average power output of the channel as a function of the time delay τ , and this is called the *multipath intensity profile* (MIP). The range of value of τ over which $R_{\tilde{h}_s, \tilde{h}_s}(\tau)$ is greater than zero is called the *multipath spread* of the channel denoted as T_m . The maximum value of T_m

is given as T_{max} and it is the delay τ for which $R_{\bar{h}_s, \bar{h}_s}(\tau)$ is very small. Two types of MIP are the *exponential* and *constant* MIP [33]. Figure 3.3 is a plot of a typical exponential MIP.

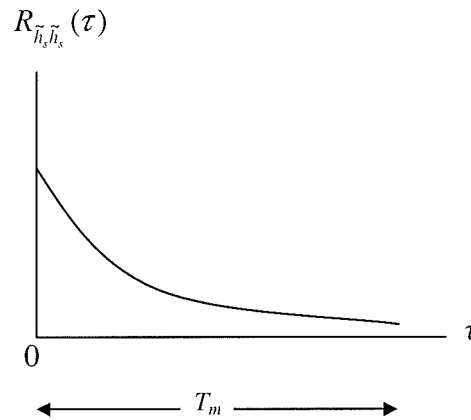


Figure 3.3. Sketch of a typical exponential MIP

Assume that the symbol duration of a data signal is given by T_s . The channel is said to be *frequency selective* if $T_{max} \gg T_s$. This is equivalent to the situation whereby the channel bandwidth is much less than the signal bandwidth. In this case, the channel filters out, or separates the received signal. This will cause intersymbol interference, affecting the performance of the system. However, if $T_{max} \ll T_s$, the channel is not frequency selective and so it is called a *frequency non-selective* fading channel. This is equivalent to the case whereby the channel bandwidth is larger than the signal bandwidth. In this case all the multipath components of the signal arrive within a short fraction of a symbol time. Therefore a single ray can be used to represent a frequency non-selective Rayleigh fading channel; where the single ray represents the multiplicative effects of all the multipath components within the channel bandwidth [31].

Taking the Fourier transform of (3.20), the *scattering function* [33] of the channel is obtained and given as:

$$S(\tau, \lambda) = F\{R_{\tilde{h}_r, \tilde{h}_s}(\tau, \Delta t)\} = \int_{-\infty}^{\infty} R_{\tilde{h}_r, \tilde{h}_s}(\tau, \Delta t) e^{j2\pi\lambda\Delta t} d\Delta t \quad (3.21)$$

For a given τ , $S(\tau, \lambda)$ describes the psd in the frequency variable λ , the *Doppler frequency variable*. The *Doppler power spectrum*, $S(\lambda)$ is obtained by setting $\tau = 0$ in (3.21). This is given as:

$$S(\lambda) = \int_{-\infty}^{\infty} R_{\tilde{h}_r, \tilde{h}_s}(0, \Delta t) e^{j2\pi\lambda\Delta t} d\Delta t \quad (3.22)$$

$S(\lambda)$ is a power spectrum that gives the signal intensity as a function of the Doppler frequency variable λ . This is shown in Figure 3.4.

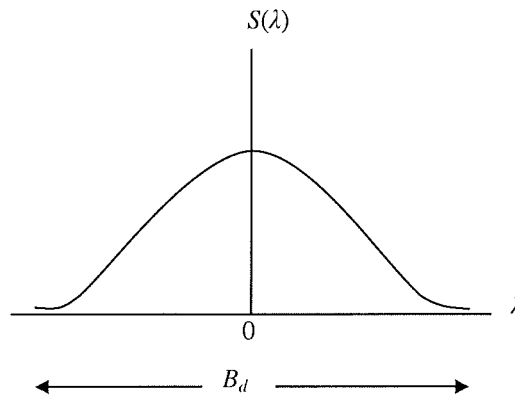


Figure 3.4. Sketch of the Doppler power spectrum

From Figure 3.4, the Doppler spread, B_d is the bandwidth of the Doppler power spectrum and it indicates how fast the channel is fading. Since the symbol duration is T_s , the signal bandwidth, B_s is approximately the inverse of the symbol duration, i.e. $B_s \approx 1/T_s$. If $B_d \gg B_s$, the channel is said to be *fast fading* and if $B_d \ll B_s$, the channel is said to be *slow fading*.

3.3.3. Computer Simulation of Rayleigh Fading Channel

The purpose of the study of mathematical models of fading channel is to use such models in system design and analysis. As is always the case, when there is no closed form solution to a particular problem in the design of a circuit, computer simulation is another way to analyse such a circuit. However, in situations where there is a closed form solution to the proposed circuit, the use of computer simulation is therefore a means of verifying the theoretical result. However, in simulation, field measurement of the mobile environment is rarely used. This will be time consuming and often inconclusive, due to the variation of signal in different environments. The general method is to use the computer to design a fading simulator [34] that will mimic the mobile environment. However, a good fading simulator should be able to approximately duplicate the assumed statistical properties of the fading channel. The property studied here is the channel pdf as given by (3.15).

To verify these theoretical results obtained in Chapter 5, Monte Carlo simulation was used. In the simulation, the signal was transmitted through a frequency non-selective Rayleigh fading channel simulator. The accuracy of the results will mostly depend on how the fading channel simulator pdf approximates the theoretical pdf. Therefore, it is important that a study of the different methods of generating a fading channel with the aid of computer be studied. There are two methods of building a fading simulator [1, 34]. One is by the *Gaussian noise filtering* method and the other by the method of *summation of sinusoids*. A brief description of these two methods will be shown and the simulation result using the summation of sinusoids will be given.

3.3.3.1. Gaussian Noise Filtering Method

The starting point for the design of a fading simulator is to transmit an unmodulated carrier. The received bandpass signal $y(t)$ in a frequency non-selective Rayleigh fading channel can be given as [29]:

$$y(t) = \alpha_I(t) \cos 2\pi f_c t - \alpha_Q(t) \sin 2\pi f_c t \quad (3.23)$$

where,

$$\alpha_I(t) = \sum_{l=1}^{L_p} \alpha_l \cos \phi_l(t) \quad (3.24a)$$

$$\alpha_Q(t) = \sum_{l=1}^{L_p} \alpha_l \sin \phi_l(t) \quad (3.24b)$$

$\alpha_I(t)$ and $\alpha_Q(t)$ are the inphase and quadrature components of the bandpass signal and are independent zero mean Gaussian processes with same variance.

A simple way to build a Rayleigh fading simulator is to implement (3.23). This involves passing two i.i.d. Gaussian processes of zero mean and same variance through a channel (filter). If a white noise is passed through a filter, the spectrum is affected, but the pdf still remains the same [29]. In order to use this method, it is necessary to design a filter that can preserve the spectrum of white noise after filtering. It is quite challenging to design this kind of filter. The psd of $y(t)$, is given as [29]:

$$S_y(f) = \begin{cases} \frac{\Omega}{2\pi f_D} \frac{1}{\sqrt{1-(f/f_D)^2}}, & f \in [-f_D, f_D] \\ 0 & \text{otherwise} \end{cases} \quad (3.25)$$

where $\Omega = E[\alpha_I^2(t)] + E[\alpha_Q^2(t)]$ and $f_D = v/\lambda$ is the maximum Doppler shift in Hz, with v given as the mobile speed (in m/s) and λ is the wavelength (in m).

If (3.25) is normalised by $\pi f_D / 2$, then

$$S_y(f) = \frac{\Omega}{\sqrt{1 - (f/f_D)^2}}, \quad f \in [-f_D, f_D] \quad (3.26)$$

This is shown in Figure 3.5 for $f_D = 100$ Hz.

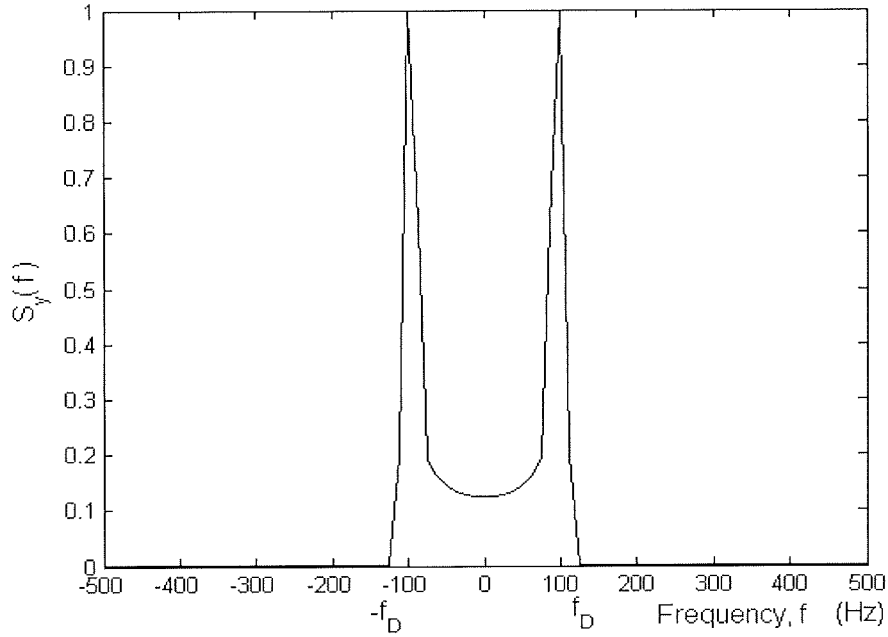


Figure 3.5. Plot of the normalised psd, $S_y(f)$

From [33], the output psd of a channel is given as:

$$S_y(f) = |H(f)|^2 S_x(f) \quad (3.27)$$

where $S_x(f) = \Omega$ Watts/Hz, is the psd of the input white Gaussian noise.

The transfer function of the channel is thus given as:

$$\begin{aligned} H(f) &= \sqrt{S(f)/\Omega} \\ &= \left(1 - (f/f_D)^2\right)^{-1/4} \quad f \in [-f_D, f_D] \end{aligned} \quad (3.28)$$

Equation (3.27) means that if a white Gaussian noise of psd $S_x(f) = \Omega$ Watts/Hz is filtered by a filter of transfer function given by (3.28), the output psd is the squared amplitude response of the in-phase and quadrature filters as shown in Figure 3.6. The output envelope is a Rayleigh fading envelope as long as the two different noise sources are independent Gaussian random processes.

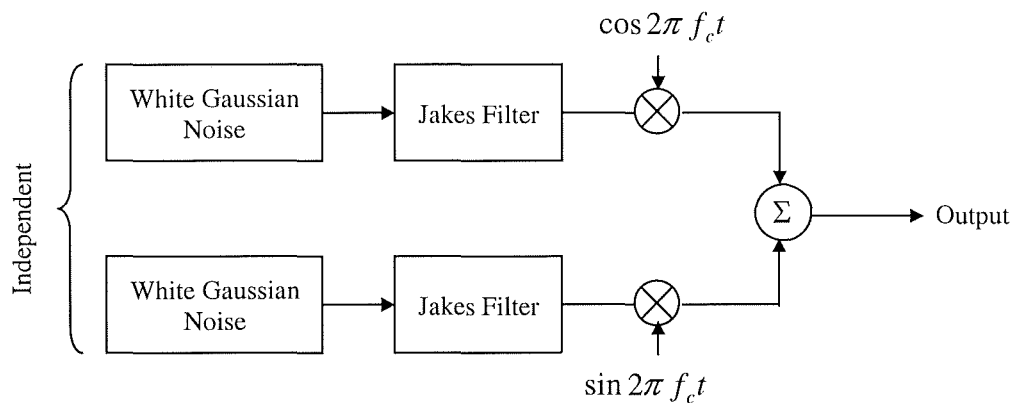


Figure 3.6. Rayleigh fading simulator using the Gaussian filtering method [1]

The challenge is to build a filter that can approximate the spectrum, $S_y(f)$ as shown in Figure 3.5. One technique is to use a finite impulse response (FIR) filter [29, 33] by windowing to approximate the spectrum. The major disadvantage is that a filter of very long length is required in order to approximate this spectrum. The major advantage of this method is the ease by which uncorrelated noise can be generated, and thus multiple uncorrelated fading waveforms can be generated.

3.3.3.2. Summation of Sinusoids Method

Jakes [34] proposed an alternative method of implementing a Rayleigh fading simulator known as summation of sinusoids. Jakes showed that the summation of a large number L of sinusoids, each of different frequencies is a close approximation of Gaussian

process. The basic idea is to generate two quadrature signals as in (3.23) (assuming equal strength multipath components, that is, $\alpha_l = 1$) and when they are added together, the envelope of the signal is Rayleigh distributed with uniform phase. Writing (3.23) as

$$Y(t) = Y_I(t) + jY_Q(t) \quad (3.29)$$

From [46], $Y_I(t)$ and $Y_Q(t)$ can be given as:

$$Y_I(t) = 2 \sum_{l=1}^L \cos \beta_l \cos w_l t + \sqrt{2} \cos \Phi \cos w_m t \quad (3.30a)$$

$$Y_Q(t) = 2 \sum_{l=1}^L \sin \beta_l \cos w_l t + \sqrt{2} \sin \Phi \cos w_m t \quad (3.30b)$$

where $w_m = 2\pi v / \lambda$ represents the maximum Doppler frequency in radians/sec, v as the mobile speed in m/sec, and λ is the wavelength of the transmitted signal. $w_l = w_m \cos(2\pi l / La)$ with $La = 4L + 2$. It must be noted that the phase of the output signal $Y(t)$ should be random and uniformly distributed in $[0, 2\pi]$ in order to generate the Gaussian process. The conditions for this are [29, 34]:

$$E[Y_I^2(t)] = E[Y_Q^2(t)] \text{ and } E[Y_I(t)Y_Q(t)] \approx 0 \text{ for values of } \Phi = \pi/4 \text{ and } \beta_l = \pi l / L; \text{ or}$$

$$E[Y_I^2(t)] \approx E[Y_Q^2(t)] \text{ and } E[Y_I(t)Y_Q(t)] = 0 \text{ for values of } \Phi = 0 \text{ and } \beta_l = \pi l / (L + 1).$$

From the above conditions, it is seen that the effect of the choice of Φ and β_l on the distribution of $Y(t)$ is negligible. The case where $\Phi = 0$ is used in this research as it makes the implementation of the simulation easier. Figure 3.7 is the diagram for this method, which again as the Gaussian filtering method is the implementation of (3.29). Comparing Figure 3.6 with Figure 3.7, it is seen that the initial implementation of the Jakes method in the physical form could be cumbersome as it involves a large number of oscillators and associated components. However, its software implementation is quite

easy when compared to the Gaussian method as it does not involve the design of filters but just the generation of sinusoids, which are already available as built-in functions in most software simulation tools like Matlab®.

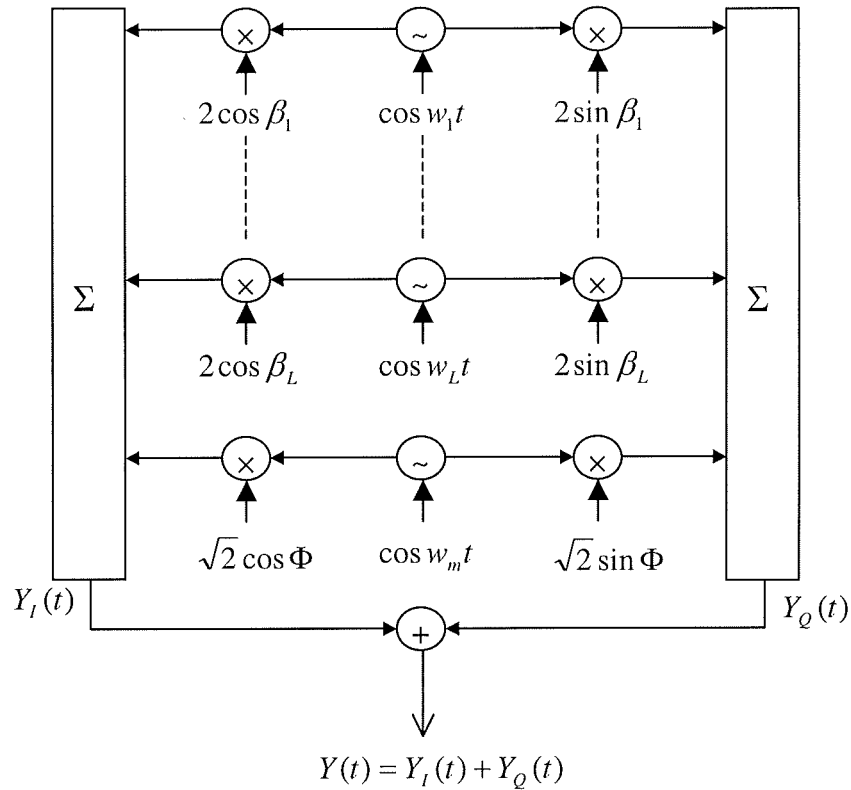


Figure 3.7. Jakes model of a Rayleigh fading simulator

Figure 3.8 compares the Rayleigh pdf of the theoretical and simulation results. The close agreement between theory and simulation shows the accuracy of this method.

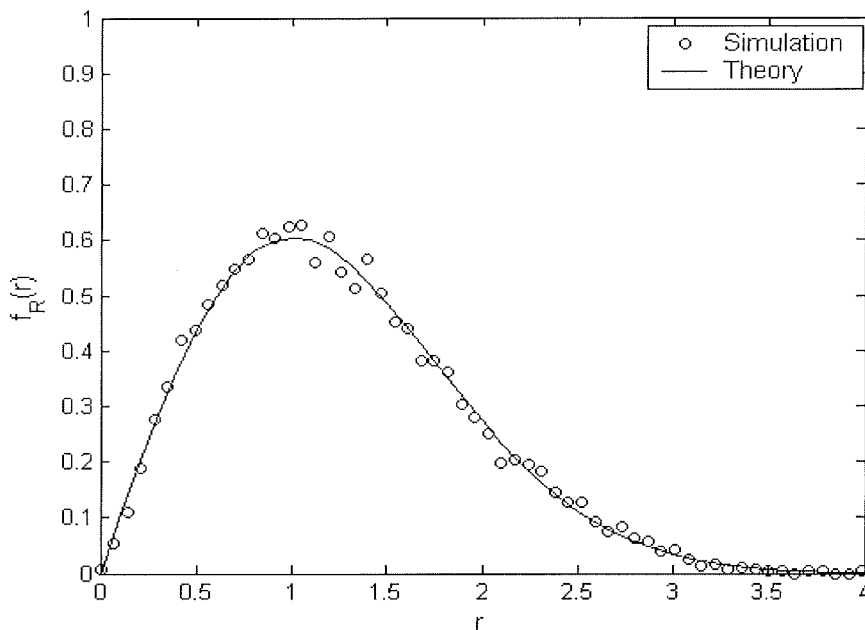


Figure 3.8. Pdf of Rayleigh fading channel using Jakes method

3.3.4. TDL Model of Frequency Selective Rayleigh Fading Channel

As discussed in the previous sections, in a mobile environment, due to the omni-directional antenna and NLOS propagation, the received signal is a continuum of multiple signals of varying amplitudes and phases, and thus a variation in received signal level. If these multiple signals can be separated into distinct parts, then the channel is frequency selective fading, otherwise it is frequency non-selective fading. A commonly used model for frequency selective fading channel is the tapped delay line (TDL) model [32] as shown in Figure 3.9. In this figure, a tap of spacing equal to the symbol duration represents each multipath signal. For a DS-SS system, the spacing between taps is the chip duration, T_c of the spread spectrum signal.

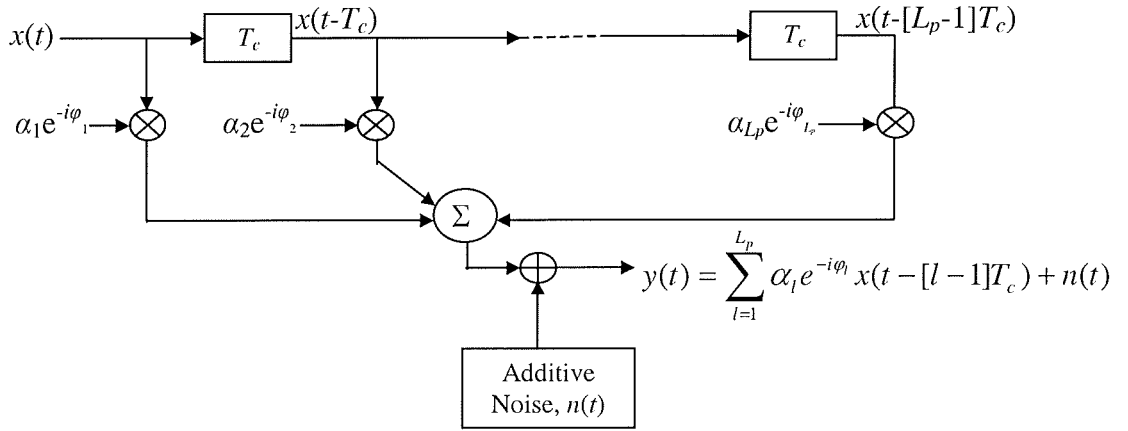


Figure 3.9. TDL model for frequency selective Rayleigh fading channel

It is assumed that each tap is multiplied by a complex Gaussian random process of envelope, $\tilde{\alpha}_l(t) = \alpha_l(t)e^{-j2\varphi_l(t)}$ with amplitudes $\alpha_l(t)$ and phases $\varphi_l(t)$ assumed to be i.i.d. random variables uniformly distributed in $[0, 2\pi]$. The magnitude of each tap weight $R = |\alpha_l(t)|$ is assumed to be an i.i.d. Rayleigh random variables of zero-mean and variance $E\{\alpha_l^2\} = \sigma_l^2$. With this assumption, the pdf of the l th resolvable path is Rayleigh distributed. Since $\{\alpha_l(t)\}$ represents the tap weights corresponding to L_p different delays, $\tau = lT_c$, $l = 1, 2, \dots, L_p$, the uncorrelated scattering assumption stated in Section 3.3.2.2 implies that each of the taps are uncorrelated, and they are also statistically independent due to the i.i.d. assumption. With these assumptions, it is shown in [32] that the number of resolvable paths is a function of the multipath spread, T_m and it is given as:

$$L_p = \lfloor T_m / T_c \rfloor + 1 \quad (3.31)$$

where $\lfloor x \rfloor$ is the integer $\geq x$.

It can be deduced from Figure 3.3 and (3.31) that as T_m increases, the number of paths increases, but the power associated with each path decreases accordingly. The received signal in a frequency selective Rayleigh fading channel is given from Figure 3.9 as:

$$y(t) = \sum_{l=1}^{L_p} \alpha_l e^{-i\phi_l} x(t - [l-1]T_c) + n(t) \quad (3.32)$$

It is seen that the case where $T_m = 0$ represents the frequency non-selective Rayleigh fading channel.

Two types of MIP considered in this research are the exponential and uniform MIP. Using an exponential MIP with a decaying rate specified by η , the average power in each resolvable path is given as [35]:

$$E[\alpha_l^2] = \sigma_l^2 = C e^{-(l-1)\eta} \quad (3.33)$$

C is a normalisation factor used to normalise the fading power to unity and so the solution to (3.33) using equation for geometric series from [36] gives C as:

$$C = \frac{1 - e^{-\eta}}{1 - e^{-\eta L_p}} \quad (3.34)$$

Then substituting (3.34) into (3.33), the average power in each resolvable path is given as:

$$\sigma_l^2 = \frac{1 - e^{-\eta}}{1 - e^{-\eta L_p}} e^{-(l-1)\eta} \quad (3.35)$$

For a uniform MIP ($\eta = 0$), using l'Hôpital's rule [36], the limit of (3.34) as η goes to zero is:

$$\lim_{\eta \rightarrow 0} C = \frac{1}{L_p} \quad (3.36)$$

By substituting (3.36) into (3.33), the average power in each resolvable path for the case of uniform MIP is given as:

$$\sigma_i^2 = \frac{1}{L_p} \quad (3.37)$$

This tap delay line multipath model together with derived equations for the exponential and constant MIP will be used in the analysis of the proposed circuit later in Chapter 5 when the performance analysis of the proposed circuit is considered in frequency selective fading channel.

3.4. Interference in Mobile Networks

Problems such as dropped calls, noisy channels, poor voice quality, lost connections, and so on are common in all wireless services, especially mobile telephony. The quality of service (QoS) of the network is determined by the mobile user sensitivity to the frequency of occurrence of these problems. For a good QoS, it is expected that the mobile network should be able to address these problems especially in the presence of the mobility of the user [37]. These problems are often a result of fading and interference [38]. However, it should be noted that SS systems provide a good measure of immunity to interference by utilising its P_G . However, prior to synchronisation, the system cannot take advantage of this processing gain. It is the aim of this section to define interference and study some of its sources.

3.4.1. Definition of Interference

Interference^{3,2} or jamming can be defined as the disturbance or interruption to a radio

^{3,2} Interference and jamming are used interchangeably here, but jamming is used in military communications to indicate intentional interference.

signal due mainly to the presence of the interrupting signal in the same spectrum (on-frequency jamming) with the desired signal. However, disruption to reliable communication can also occur even if the interfering signal is not in the same spectrum (off-frequency jamming) with the desired signal, a typical example is the jamming resulting from the process of inter-modulation. The direct effect of interference in a network is to reduce the available SNR at the receiver, not the transmitter, and if not properly mitigated, will lead to a poor QoS. At the front end of every receiver is the presence of AWGN, which has a psd N_0 (Watts/Hz) that is flat in all frequencies. However, the receiver usually filters out most of this noise power. As far as the energy per bit, E_b (Watts-Sec) of the transmitted signal is high, there is always enough SNR available for demodulation. The SNR with no interference can be given as:

$$SNR = \frac{E_b}{N_0} \quad (\text{dB}) \quad (3.38)$$

Now, considering the situation where a jamming psd N_J (Watts/Hz) is present at the receiver, then the available Signal-to-Interference-Noise Ratio (SINR) is given by:

$$SINR = \frac{E_b}{N_0 + N_J} \quad (\text{dB}) \quad (3.39)$$

From (3.39), it is seen that if N_J increases, the SINR will decrease accordingly. Let the jammer power, J be given by:

$$J = W_J N_J \quad (3.40)$$

where W_J is effective bandwidth of the jamming signal.

If the jammer has a high power that is limited to a fixed value, J at a bandwidth $W_J < W_s$ (where W_s is the bandwidth of the SS signal), then for the jammer to jam a SS signal of wide bandwidth W_s , the jammer has to reduce N_J in order to make $W_J = W_s$. If

N_j is reduced, it can be seen from (3.39) that the SINR will be increased. This is one of the methods that a SS system achieves its anti-jamming capability [39]. The larger the bandwidth, W_s of the SS signal, the more advantage is taken of the processing gain to mitigate the effect of the jammer.

The anti-jamming capability of SS systems is based on the assumption that the received PN signal is already synchronised with the locally generated at the receiver. Without synchronisation, the system cannot take advantage of the P_G . This research focuses on the synchronisation of spread spectrum signals and thus the processing gain cannot be used in improving the performance of the acquisition circuit rather the circuit is expected to perform satisfactorily in the presence of these interferences. Possible solutions on how to mitigate the effect of the interference will be discussed in Chapter 5.

3.4.2. Sources of Interference

Interferences can be either intentional or unintentional. Unintentional interference is usually the by-product of another legitimate communication activity and could be on- or off-frequency sources. On the other hand, intentional interferences are on-frequency sources of malicious signals transmitted with the sole purpose of disrupting reliable communication. In military warfare, intentional interferences are a common place.

3.4.2.1. Unintentional Interferences

The success of 2G has resulted in the rolling out of 3G and now the emphasis is on 4G. The spectrum available for commercial and private wireless services is scarce and

service providers are faced with the problem of trying to provide good QoS using this scarce resource. This means there must be co-existence between existing systems and new systems. A particular example is the co-existence of the analogue standard AMPS and CDMA systems in North America [19]. Also, cell towers are tightly packed with antennae from different mobile service providers. Within the VHF and UHF spectrum are other communication service providers like commercial radio broadcasters, navigation and satellite systems and so on. Thus the communication sky is crowded with signals from different sources and so there is a high likelihood of unintentional interference. Some examples of unintentional interferences are [38]:

- I.** Improperly Configured Transmitter: This is usually the case where a mobile operator is transmitting at the frequency of another service provider as a result of a fault or incorrect setting at the offending transmitter. Once this is identified, the operator is usually willing to reconfigure the transmitter.
- II.** Cell Overlap: BSs or cell sites are usually configured to operate within a coverage area. Sometimes incorrect antenna tilt, excess transmitter power, or a change in the environment can cause a particular BS to exceed its specified coverage for a particular channel. For example, if the forest of trees blocking a particular BS is cut down, then the coverage limit could be exceeded.
- III.** Inter-modulation Products: Interferences resulting from inter-modulation products can disrupt reliable communication. When one or more external signals enter the non-linear final amplifier stage of a transmitter (the interfering transmitter), they mix with the signal of the interfering transmitter, creating a new signal that appears as a new frequency

component in the communication band. The power associated with these new products could be high enough to disrupt reliable communication. It is possible that the interfering transmitter is in a different frequency band from the mobile network, but the new frequency component could be high enough to now occupy the band of the mobile systems. This is an example of an off-frequency interference source. Details of intermodulation can be further studied in [28, 38].

- IV. Harmonics from Broadcast Transmitters: Commercial radio and TV stations can produce substantial energy in harmonics of their signals and this can also disrupt reliable communication. For example, a 5 Megawatt TV transmission can produce a harmonic signal of about 5 watts [38] which can interfere with nearby mobile communications.

3.4.2.2. Intentional Interferences

In military communications, jamming or intentional interference is a common place. SS is a technology that is useful in battling the jammer. There are different types of jammer and some of them are discussed below.

- I. Broadband and Partial-band Jammer: A broadband jammer spreads Gaussian noise of total power J over the bandwidth of the SS system, W_s . The jammer noise density, N_J is J/W_s (Watts/Hz). If the jammer decides to concentrate its energy over a portion of the spectrum, then a partial-band jammer results. In that case, the jammer has traded bandwidth occupancy for greater power spectral density. These types of jammer are shown in Figure 3.10.

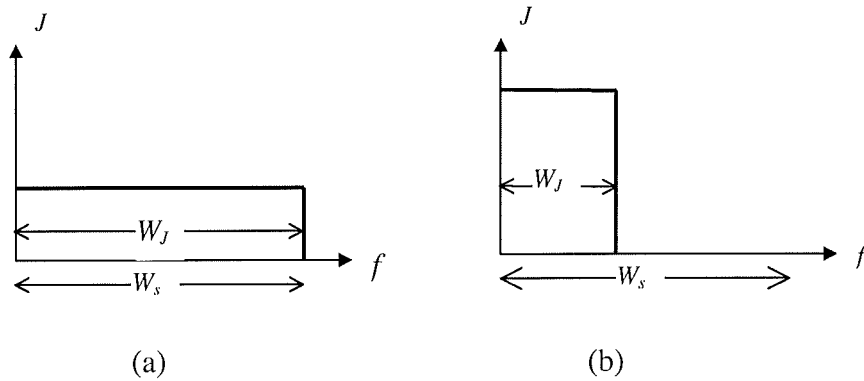


Figure 3.10. (a) broadband jammer (b) partial-band jammer

- II.** Pulse Jammer: This is very common in tactical military communications. In this case, it is assumed that the jammer can trade duty cycle for increase jammer power. This is similar to the partial-band jammer, except that the jammer is only present a fraction, ρ of time (where $0 < \rho < 1$). During this time, the jammer psd is increased to a level N_J / ρ . Thus the lower the value of ρ , the higher the jammer psd and the shorter the time the signal is present, but with serious degradation in circuit performance. Details of these and other types of jammer are studied in [10].

3.4.2.3. Multiple Access Interference

When spread spectrum is used for commercial mobile communication, a technology known as CDMA, as explained in Chapter 2, all the users occupy the same spectrum but are distinguished by their own unique PN code. The signal of the desired user can be extracted in the presence of the other users by cross-correlating the desired user code with that of the other users since their respective PN codes are uncorrelated. However, the noise power content resulting from the cross-correlation operation is not exactly

zero and this leads to increased noise power as the number of users increases. This type of interference is known as *multiple access interference* (MAI). The effect of MAI on the acquisition circuit performance will also be studied in Chapter 5.

3.5. Summary

In this chapter, a study of the channel models specified for wireless channels in rural and urban areas as well as interferences in mobile networks has been carried out. This will make it easier to understand the performance analysis of the proposed PN code acquisition circuit to be presented in Chapter 5. Sources of performance degradation in mobile systems include fading, intentional/unintentional interference and MAI. For the case of fading, the large-scale fading is mainly characterised as path loss and it increases as the distance between the MS and the BS increases. Therefore, when a cellular system is deployed, the effect of large-scale fading can be considered constant as the MS is always assumed to be within its coverage area. However, small-scale fading results from the fact that the mobile receives multiple signals that undergo rapid fluctuations in amplitude and phase for a relatively small movement in the position of the mobile, which is a major problem in mobile systems. The statistical characterisation of the distribution of the channel using the Rayleigh and Ricean model was specified. This chapter concluded with a study of interference in mobile networks and how it can affect the performance of mobile systems.

CHAPTER 4

Introduction to PN Code Acquisition

4.1. Introduction

As already stated, synchronisation is carried out in two steps: *coarse synchronisation* or *acquisition* and *fine synchronisation* or *tracking*. Acquisition involves obtaining a coarse estimate of the phase shift between the transmitted PN code and that at the receiver so that the received PN code will be aligned or synchronised with the locally generated PN code. After acquisition, tracking follows. Figure 4.1 is a block diagram representation of the basic components of the synchronisation process in SS systems. The *correlator* block compares the received PN signal with a locally generated signal, and, if the two signals are properly aligned, with the aid of the *acquisition decision* block, a decision is made to this effect and the *tracking circuit* enabled by toggling the switch S_1 from position 1 to position 2. If the tracking operation is successful, then synchronisation is declared. Once synchronisation is achieved, S_2 is closed and the PN signal from the *local PN code generator* is used to despread the received signal. Thereafter, data demodulation as in conventional communication systems follows.

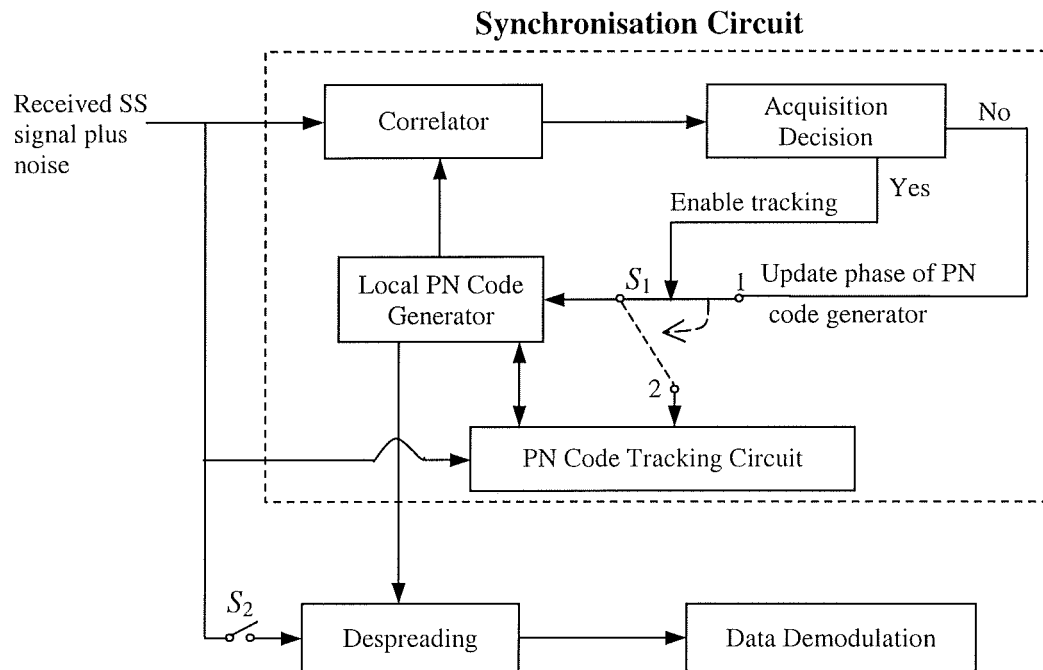


Figure 4.1. Block diagram of the synchronisation process

This research mainly focuses on the acquisition aspect of synchronisation. Therefore, the rest of the chapter will be dedicated to the study of PN code acquisition. Before the end of this chapter, the following questions will be answered. How is the delay in the received signal looked for? This depends on the *search strategies*. What type of devices to be used in doing this search? This involves the use of *correlators*. Once a particular search strategy and a correlator have been chosen, then how long will it take to search a cell? This is known as the *dwell time*? What are the *threshold* setting techniques that are used in acquisition decision? Finally the tools for *performance measures* will also be studied.

4.2. PN Code Acquisition Problem Definition

The acquisition problem normally involves estimating the delay, τ between the received PN code and the locally generated PN code, to within the chip duration, T_c . That is $\tau \leq T_c$, and this is within the tracking range of the PN code tracking circuit. Therefore, if $\tau > T_c$, the received and locally generated PN codes are out-of-phase and no effective despreading can take place at the receiver. When the two codes are not synchronised, the received signal still remains spread and the SNR will always be low, as the circuit cannot take advantage of the P_G at this time. This means that the code synchronisation is usually done at low SNR. Also taking into consideration the deteriorating effect of mobile environment, such as fading and jamming, not to mention that for good quality of service, this synchronisation process has to be done as fast as possible; the code synchronisation process is quite challenging.

The acquisition process mainly involves the correlation of the received signal with a locally generated signal and looking for the point of maximum autocorrelation. The delay estimate, $\hat{\tau}$ which gives the maximum autocorrelation value, is taken as the delay in the transmitted signal. Assume that the transmitted signal in a DS-CDMA system with K asynchronous users is given by:

$$s(t) = \sum_{k=1}^K \sqrt{2S_k} d_k(t) c_k(t) \cos(\omega t + \theta_k) \quad (4.1)$$

where S_k is the k th user average power, $d_k(t)$ is data signal of the k th user, ω is the carrier frequency in radians/sec,

spreading PN signal given as $c(t) = \sum_{i=-\infty}^{\infty} c_i p_{T_c}(t - iT_c)$; where $|c_i| = 1$ is the i th chip of the PN code sequence of length W and $p_{T_c}(t)$ is the unit rectangular pulse^{4.1} of duration T_c . In most SS systems, especially CDMA systems, the code synchronization process is usually completed before data is sent [19]. Then, the received signal in an AWGN channel is given by:

$$r(t) = \sum_{k=1}^K \sqrt{2S_k} c_k(t + \tau_k T_c) \cos(\omega t + \omega_D + \theta_k) + n(t) \quad (4.2)$$

where τ_k is the delay in the received PN signal of the k th user normalised to the chip duration T_c , ω_D is the Doppler shift in radians/sec and $n(t)$ is the AWGN with a one-sided power spectral density (PSD) given as N_0 Watts/Hz.

Assume that the transmitted signal is meant for User 1 and defining the locally generated PN signal as $c_1(t + \hat{\tau}_1 T_c)$, it is seen that the received signal, $r(t)$ will overlap with the locally generated signal if $\hat{\tau}_1 = \tau_1$. That is, if $c_1(t + \hat{\tau}_1 T_c) = c_1(t + \tau_1 T_c)$, then $c_1(t + \hat{\tau}_1 T_c)c_1(t + \tau_1 T_c) = 1$ from property (iii) of m -sequence (Section 2.4), and the data signal can be despread successfully. Determining this position of the delay in the received signal is the code acquisition problem. Figure 4.2 shows the block diagram of a PN code acquisition circuit. In the figure, the received signal, $r(t)$ is correlated with the locally generated PN signal, $c_1(t + \hat{\tau}_1 T_c)$ in the *correlator*. This correlation is done for a specified time interval, known as the *dwell time*, t_d . The output y is compared with a threshold, T_h that was set up by a *threshold setting device*. If $y \geq T_h$, it means that the

^{4.1} For ease of analysis, it is assumed that the received pulse is a rectangular pulse. But in practice, a Nyquist filter is used for pulse shaping and thus the shape will be determined by the value of the roll-off factor.

received signal is in phase with the locally generated signal, and thus tracking is enabled. However, the circuit can falsely indicate that $y \geq T_h$, this will still cause the

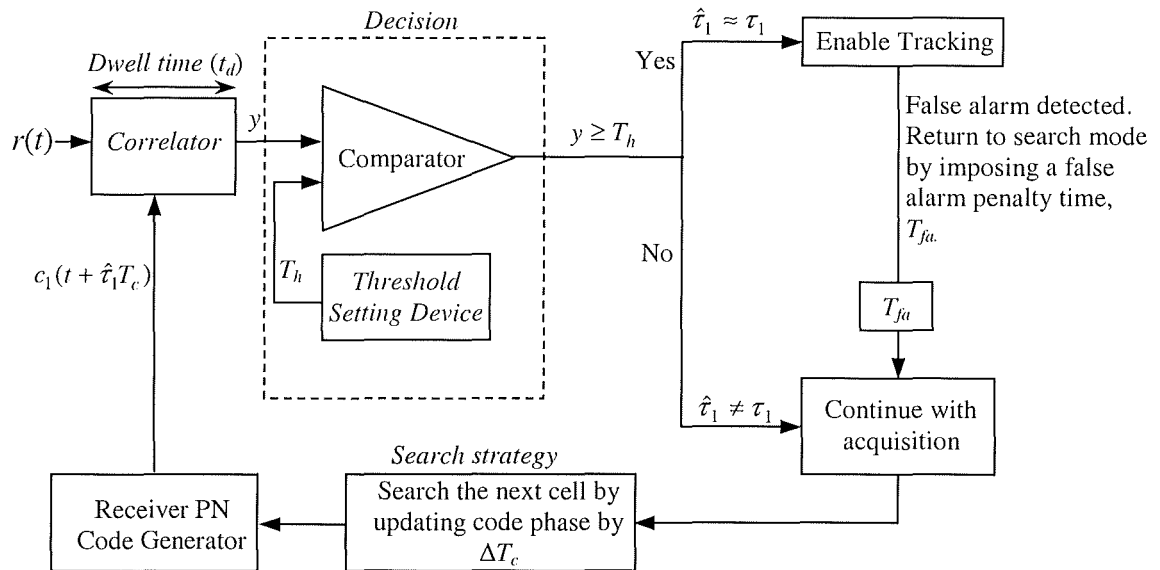


Figure 4.2. Basic components of the PN code acquisition circuit

tracking circuit to be enabled, and once this false acquisition is detected, the circuit returns to the search mode with a penalty time known as false alarm penalty time, T_{fa} . This false acquisition can be identified in two major ways. In the first instance, the tracking loop may not lock, indicating that the acquired phase is not within the tracking range of the tracking circuit (a condition for the tracking circuit to lock). However, in the second instance, if the tracking circuit happens to lock with this false phase, it is certain that data demodulation will not be effective (no recognisable information will be available to the user of interest if data demodulation is attempted with this false phase). Therefore, the circuit will return to the search mode once this is observed, incurring T_{fa} . If $y < T_h$, it means the received signal is out-of-phase with the locally generated PN

signal. Therefore, the acquisition process is continued by updating the code phase of the local PN code generator determined by the type of *search strategy* used, and the process repeats. However, it is also possible that $y < T_h$ when the correct phase is received, in this case the circuit will miss the correct code phase and the search process will continue.

4.2.1. Search Strategies

In signal transmission and reception, due to the uncertainty of range between transmitter and receiver, the relative dynamic movement (velocity) of the receiver with respect to the transmitter and oscillator instability, the signal is normally received with some delay in time and offset in frequency. This delay in time and offset in frequency, normally called *time* and *frequency uncertainties*, which are denoted here as T_u and F_u respectively must be estimated if the despreading of the signal is to be achieved. The art of estimating these uncertainties in the received PN signal in order to bring it into a coarse alignment with the locally generated PN signal is known as code acquisition [40]. The uncertainties in time and frequency are usually bounded into a specified interval or region. This is the *uncertainty region*. Thus the uncertainty region is a two dimensional region in time and frequency domain as shown in Figure 4.3. In the figure, the uncertainty region is divided up (quantised) into sub-regions δt and δf . These smaller uncertainty regions are referred to as *cells*. For now, it is assumed that only one cell is the correct estimate of the position of the delay in the incoming PN signal. This correct cell can be called the *synchro cell*. This is usually the intersection between the time and frequency uncertainty regions as shown in the shaded area of the figure. At this synchro cell position, the received signal is in phase with the locally generated signal.

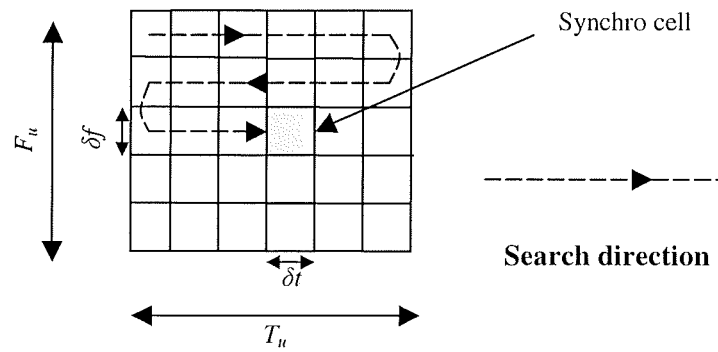


Figure 4.3. Two-dimensional serial search strategy of the PN code uncertainty region

The remaining out-of-phase cells are therefore known as *non-synchro cells*. However, depending on how the uncertainty region is searched and the effect of multipath channels, the number of synchro cells could be more than one. This will be made clearer in Chapter 5. The procedure used in searching through the uncertainty region for the synchro cell is known as the search strategy.

In using Figure 4.3, it is assumed that there is no prior information about the position of the synchro cell and thus the search can start anywhere. If there is a prior information, a different search strategy could be used [10, 11]. From the figure, it is seen that the synchro cell could still be determined by doing the search using only the time uncertainty region and neglecting the frequency uncertainty region. This means that a one-dimensional search in the time uncertainty region can be carried out and the frequency uncertainty neglected. This is the technique used by some authors [7 – 11], and is used in this thesis. It is clear that, by neglecting the frequency uncertainty, the performance of the circuit will be affected. Its manifestation is in loss in the available SNR as the frequency uncertainty increases [9, 11]. This may not cause any severe

degradation in circuit performance for small frequency uncertainty, but for large frequency uncertainty, the performance of the circuit is heavily degraded. By using the dimensions in the figure, the total number of cells in code chips in the uncertainty region is given as:

$$W = \frac{T_u \times F_u}{\delta t \times \delta f} \quad (4.3)$$

In this thesis, the number of cells in the uncertainty region is given as:

$$W = T_u / \delta t \quad (4.4)$$

where the frequency uncertainty is neglected, that is $F_u / \delta f = 1$. Normally, δt is of the order of a fraction of the chip duration T_c . If Δ indicates the incremental order in which the code is searched, then:

$$W = T_u / \Delta T_c \quad (4.5)$$

If $T_u = MT_c$, where M is the PN code length, then $W = M / \Delta$.

The search step-size, Δ is usually taken as 1, $\frac{1}{2}$, $\frac{1}{4}$. . . , depending on the pull-in range of the code-tracking circuit [10]. From (4.5), the smaller the value of Δ , the more the number of cells and consequently the more the number of possible synchro cells.

4.2.1.1. Maximum-likelihood Search Strategy

This search method requires parallel correlation of all the possible cells in the uncertainty region with the received signal and choosing the cell with the largest correlation value as the synchro cell. If there are W cells in the uncertainty region, the number of such detectors will be equal to W , as well [7, 10]. Alternatively, a serial realisation of the maximum-likelihood technique is obtained by using just one circuit whereby all W cells are correlated serially and the correlated values stored [10]. The cell that gives the maximum correlation value is chosen as the synchro cell. A serial

realisation of this strategy is shown in Figure 4.4. The advantage of using this search strategy is that a definite decision on acquisition is made with just only one search of the uncertainty region. For SS systems with long PN codes, as may be needed in situations of large processing gain, the complexity of the parallel implementation, or the long time needed to do the serial implementation of this strategy is often prohibitive. Therefore, a different search strategy is worth considering.

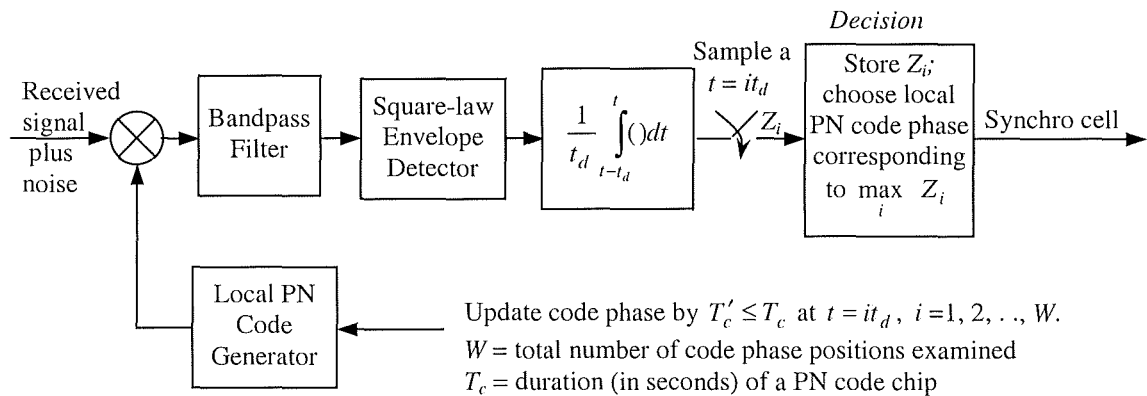


Figure 4.4. A serial realisation of the maximum-likelihood search strategy from [10]

4.2.1.2. Serial Search Strategy

The serial search is the search strategy generally employed in code acquisition process [10, 11]. This involves searching the code uncertainty region cell-by-cell until the synchro cell is determined. This is similar to the implementation in Figure 4.4 except that the decision device is not based on selecting the largest. Rather it based on comparing each correlation output with a predetermined threshold. This is shown in Figure 4.5. At each sampling instant, the output after a dwell time t_d is compared with a threshold. If this value is greater than the threshold, acquisition is declared. Thus there is no need to search all the cells before a decision is made as with the maximum-likelihood strategy. A noticeable advantage is when acquisition is achieved

the first time sampling is done. The disadvantage is that the circuit might falsely declare acquisition, or might miss the synchro cell. This might lead to multiple searches of the whole uncertainty region, before the declaration of acquisition, thereby increasing the acquisition time. However, this technique is simple and easy to implement and generally used in most acquisition circuits.

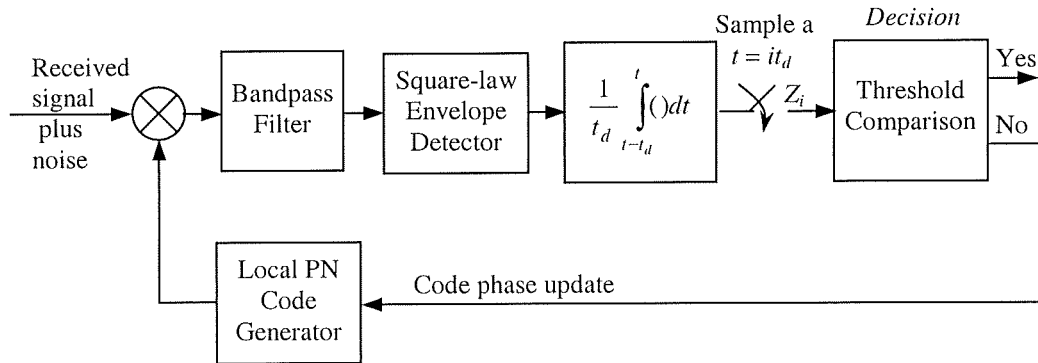


Figure 4.5. Block diagram of the serial search strategy from [10]

4.2.1.3. Parallel Search Strategy

Parallel search technique involves searching different phases of the received signal simultaneously by using q correlators in parallel. The outputs from the correlators are stored and the largest value is compared to a threshold. If this value is greater than the threshold, then acquisition is declared. Otherwise the search is continued by testing a new set of q phases. Since not all the phases are tested simultaneously, a false acquisition is also possible. Thus it is different from the maximum-likelihood technique in this regard. If the number of cells to be searched is W , the time taken to search the uncertainty region is less than the serial search by a factor of W / q . As the number of the detectors q is increased, the time taken to search the cells reduces, but the complexity increases accordingly. If $q = W$, this is similar to the parallel implementation

of the maximum-likelihood technique already discussed. Parallel search has been investigated in [35, 41, 42] and the results presented in these publications confirmed the advantages of this strategy.

4.2.1.4. Hybrid Search Strategy

This is normally a combination of the parallel search and serial search strategies by choosing a compromise in terms of trade-off between speed of acquisition and complexity. A thorough analysis of the hybrid scheme has been carried out in [43] and it was shown that, by proper implementation, performance close to the parallel search strategy could be obtained.

4.2.1.5. Sequential Estimation Strategy

In this method, initially proposed by Ward [44], the receiver to be synchronised demodulates the incoming PN signal (in exactly the same way that a PSK signal will be demodulated in conventional digital system). The demodulated PN sequences are loaded into the local PN sequence generator and a trial check for synchronisation is made. An improved method for this technique is studied in [45]. This method has been shown to give fast synchronisation at high SNR when considered in AWGN channel. Its performance is heavily degraded by noise and thus not generally used in most SS applications [10].

4.2.2. Detector Structure

Having studied the search strategy segment from Figure 4.2, in this section, the *detector* segment is studied. The detector is used for correlating the received signal with the

locally generated signal. It should be noted that the received signal, $r(t)$ in (4.2) is carrier modulated and, therefore, if accurate estimate of the carrier frequency and phase is available at the receiver, the detector will perform *coherent correlation* of the received signal with the locally generated signal. However, since SNR is low as a result of spreading, accurate estimate of the carrier phase cannot be guaranteed and therefore the correlation is performed neglecting the carrier phase. This is known as *non-coherent correlation*. The correlation is done over a finite time, known as the dwell time, t_d . The output of the detector for the coherent case is given by:

$$y(\varepsilon) = \int_0^{t_d} r(t)c_1(t + \hat{\tau}_1 T_c) \cos(\omega t + \omega_d t + \theta_1) dt \quad (4.6)$$

This is shown in Figure 4.6.

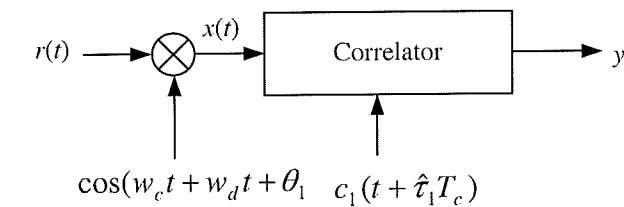


Figure 4.6. A coherent detector implementation

If the maximum-likelihood technique is used, the estimate of the delay of the received signal is the value of ε maximising (4.6).

For the non-coherent case, the carrier phase is ignored and the envelope of the detector output is used in the decision process. The detector structure is shown in Figure 4.7. It is made up of in-phase (I) and quadrature (Q) branches. This will enable the effect of the

carrier phase to be ignored since the non-coherent combining after squaring will eliminate the phase error.

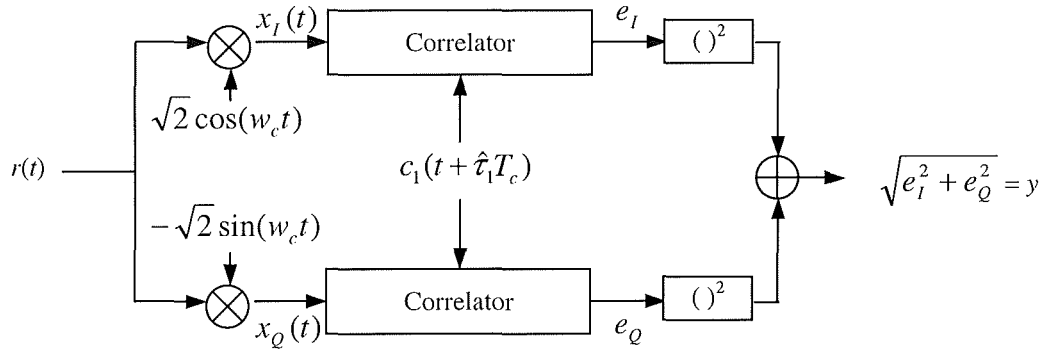


Figure 4.7. A non-coherent detector implementation

The outputs of the correlators for the I and Q branches [neglecting double frequency terms and $n(t)$] are given as $e_I = y_I(\varepsilon)\cos\theta_1$ and $e_Q = y_Q(\varepsilon)\sin\theta_1$. Where $y_I(\varepsilon)$ and $y_Q(\varepsilon)$ are given as:

$$y_I(\varepsilon) = y_Q(\varepsilon) = \int_0^{t_d} r(t)c_1(t + \hat{\tau}_1 T_c) dt \quad (4.7)$$

It is seen from Figure 4.7 that the carrier phase, θ_1 is eliminated after squaring and summing. Again, if the maximum-likelihood technique is used, the estimate of the delay of the received signal is the value of ε maximising (4.7). However, the performance of non-coherent detector is degraded by frequency error.

The correlators in Figures 4.6 and 4.7 could be active or passive devices. This means that the correlation of the locally generated signal with the received signal can be performed by using either active integration or passive integration.

4.2.2.1. Active Correlator

The active correlation [10, 40] involves actively generating the local PN signal and multiplying it chip-by-chip with the received signal and summing the output at the end of the dwell time, t_d . Therefore the time to do the correlation is dependent on the number of received code chips correlated. If a code length of M chips of the received signal are correlated, then the dwell time is given as $t_d = MT_c$, where T_c is the chip duration. Consequently, for long code length, the correlation time will be too long since each correlation interval involves the active generation of a new set of PN codes from the generator. This limits the search speed. The active correlator is shown in Figure 4.8. Major advantages of the active correlator are that it consumes less power when implemented, and it is not restricted to a specified code length, as the case for MF.

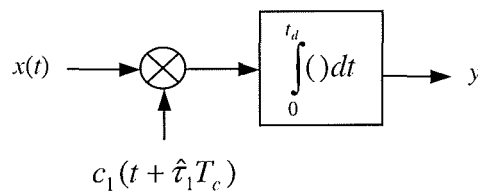


Figure 4.8. Active correlator structure

4.2.2.2. Passive Correlator

The passive correlator [40] is based on the well-known principle of MF [46]. A MF is the linear filter that maximises the SNR at its output and has an impulse response that is a time-reverse and delayed version of the waveform of the received signal. In order to maximise the SNR, the impulse response of the filter must be “matched” to that of the input signal. Given a transmitted signal $x(t)$ of duration T , the impulse response of the MF is given as:

$$h(t) = \begin{cases} x(T-t); & 0 \leq t \leq T \\ 0; & \text{otherwise} \end{cases} \quad (4.8)$$

The output of the MF is given by:

$$\begin{aligned} y(t) &= \int_{\tau=0}^T x(t-\tau)h(\tau)d\tau \\ &= \int_{\tau=0}^T x(t-\tau)x(T-\tau)d\tau \end{aligned} \quad (4.9)$$

For the impulse response of the MF to be “matched” to that of the input signal, its output must be sampled at $t = T$. It is seen from (4.9) that $y(t)$ will be maximum at this sampling time. Instead of correlating the received sequence chip-by-chip with the local sequence, a given length, N of the PN sequence is stored in the MF. This means that the filter is matched to an N -chip segment of the possible M -chip transmitted waveform with $N < M$. If T_c is the chip duration, then $T = NT_c$ and therefore $x(t)$ is given by:

$$x(t) = \sum_{i=0}^{N-1} c_i p_c(t - iT_c) \quad (4.10)$$

where $|c_i| = 1$ is the i th chip of the PN sequence and $p_c(t)$ is the pulse shape of the chips.

Equation (4.10) is implemented by using an N/Δ of shift register [10, 11, 47] as shown in Figure 4.9. The signal, $x(t)$ is made to slide through it and the output is taken at each sampling instant of the MF, which is the chip duration T_c . Thus the passive method using the MF is much faster than the active correlator method by order of $1/M$. However, there is the problem that successive outputs of the MF will be highly correlated. But it has been shown [11] that for $N \gg 1$, successive correlation intervals are statistically independent.

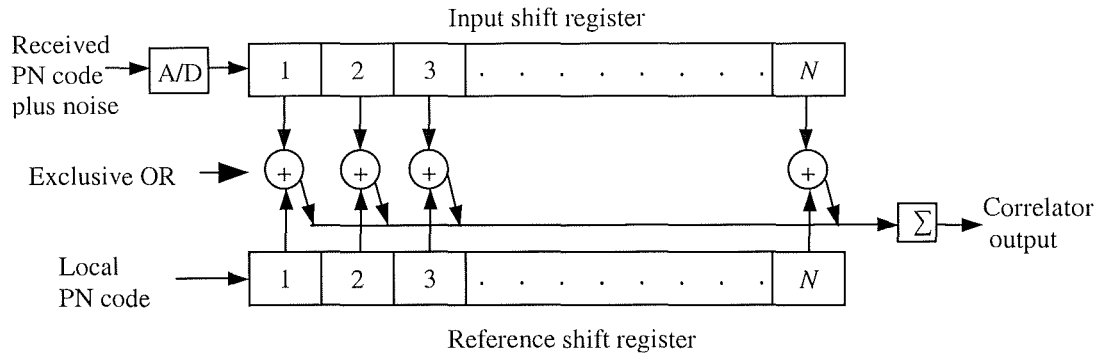


Figure 4.9. Baseband, digital MF correlator structure from [47]

It is also important to note that a MF is more complex to design and consumes more power than the serial correlator [40]. This device can be implemented using charged coupled devices (CCD) [40, 48], surface acoustic wave (SAW) convolvers [49], or the use of discrete time correlators, [40, 47].

4.2.3. Dwell Time

So far it has been assumed that the received signal is correlated with the locally generated PN signal for duration of t_d sec and the output compared to a threshold. If the output is above the threshold, then, acquisition is declared (in the absence of false alarm) and the tracking mode enabled. This is known as single dwell acquisition system. Such schemes are useful in the ML search strategy. For other search strategies (e.g. the serial search) where false alarm is a major problem, it is necessary to confirm that the selected phase is the correct estimate of the delay in the received signal before enabling the tracking circuit. This is achieved by employing a multiple dwell system [13]. This is where multiple tests of the same phase of the received signal are carried out before the final declaration of acquisition. The dwell times are given as $t_{d1}, t_{d2}, \dots, t_{dD}$ as shown in

Figure 4.10. Consider the basic operation of a double dwell system as an example. If in the first dwell, t_{d1} the output of the correlator is found to be above a threshold, T_{h1} , another correlation is done for another dwell time, say t_{d2} , (usually $t_{d2} > t_{d1}$). If after t_{d2} , the correlator output is found to be above another threshold T_{h2} (where $T_{h2} > T_{h1}$), then acquisition is finally declared and the tracking circuit enabled. One reason for using a multiple dwell is to avoid as much as possible the undesired effect of false alarm.

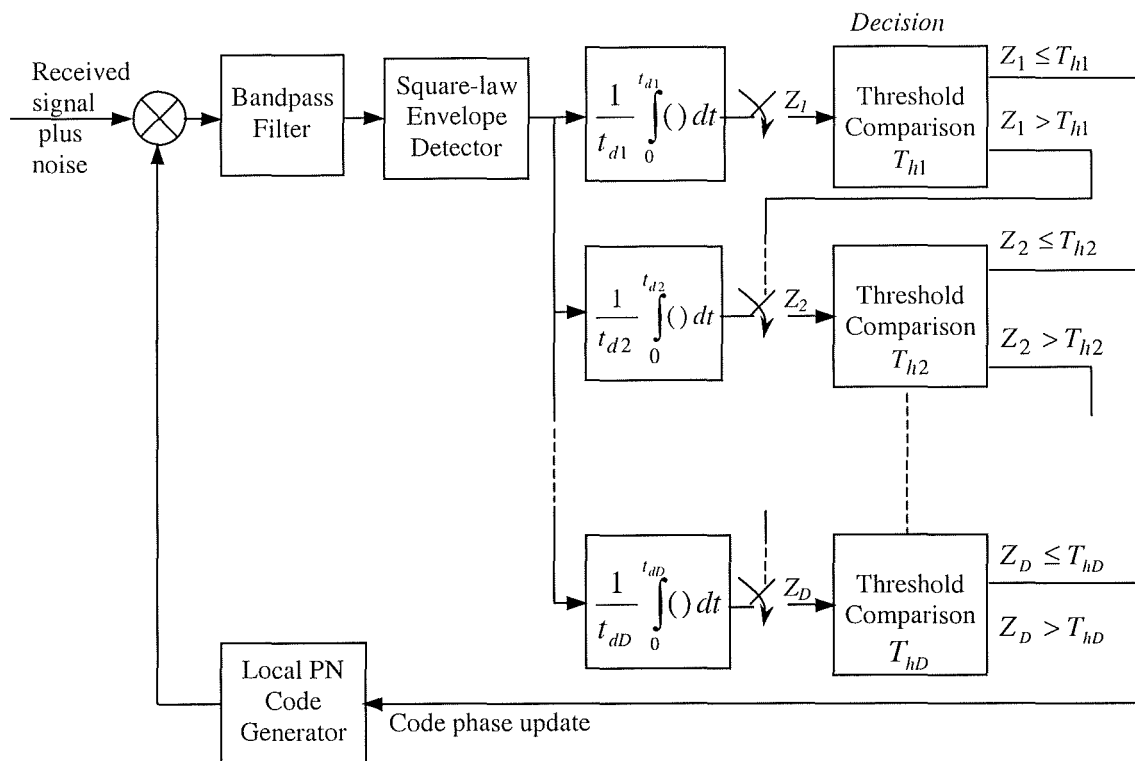


Figure 4.10. Block diagram of a non-coherent D -dwell PN code acquisition circuit [10]

Another reason for using a multiple dwell system is that, by proper implementation, the time to declare acquisition can be significantly reduced when compared to the single dwell [13]. In short, unless a single dwell system declares acquisition at the first decision instant (which is rare); a multiple dwell performs better than a single dwell.

This is easily understood by noting that for a multiple dwell system, the dwell time in the first dwell is made very short and so it takes a short time to identify a synchro cell and activate the second dwell. The dwell time of the second dwell is made longer than that in the first dwell and so on. Thus, the reliability of the detection circuit is improved. The same time is also used in the first dwell to identify a non-synchro cell before searching the next cell. However, for a single dwell, in order to ensure a reliable detection, a dwell time that is much longer than that used in the first dwell of a multiple dwell system must be used. However, since it is assumed that there is only one synchro cell and a larger number of non-synchro cells, the time spent in searching these non-synchro cells is longer for a single dwell than for a multiple dwell as the time for the first dwell of a multiple dwell is shorter.

4.2.4. Threshold Setting

An important unit in the code acquisition circuit is the *decision* device. This is where the threshold is set and a decision made whether acquisition is achieved, or not. A thorough analysis of the different types of threshold setting rules used in the decision unit of the acquisition circuit was carried out in [50]. The threshold setting rules include the maximum selection, fixed threshold and adaptive threshold. The maximum selection method involves selecting the maximum value from a set of correlation results. The fixed threshold method involves comparing the value at the output of the correlator to a predetermined fixed threshold value. The adaptive method involves using an adaptive technique to adaptively select the threshold based on the noise variation in the environment in which the circuit is deployed. The maximum selection method is usually associated with the ML search strategy. For parallel acquisition circuits, the

maximum selection is usually used in conjunction with the fixed threshold or adaptive threshold. For the serial search, it could be either fixed threshold or adaptive threshold. The importance of threshold setting cannot be over-emphasised, as too high a threshold will reduce the probability of detecting the synchro cell even though it will reduce the probability of false alarm. This means a high likelihood of missing the synchro cell. However, too low a threshold will lead to a high detection probability and the same time a high false alarm in the circuit. It is therefore clear that if the threshold is not properly chosen, the time to achieve synchronisation may be too long.

4.2.5. Performance Measures

PN code acquisition has to be done in an environment that is characterised by AWGN, fading, jamming and so on. Also, in most acquisition systems, there is no prior information about the position of the delay in the received signal. It is seen that the above factors therefore make the acquisition process a random process due to their random nature. Therefore the code acquisition process has to be modelled probabilistically. The main performance measure parameters are: the probability of detection, P_d ; the probability of miss detection, P_m ; and the probability of false alarm, P_{fa} . Taking into consideration all these probabilities, it is now left to determine the average time it takes the circuit to declare acquisition. This is known as the mean acquisition time, $E\{T_{acq}\}$ and is one of the most important circuit performance measures [10, 11]. In short most of the references cited in this thesis on code acquisition use $E\{T_{acq}\}$ as the main parameter measure.

In code acquisition circuit analysis, as in conventional signal detection, there are two hypotheses, H_1 and H_0 [10]. H_1 is the hypothesis that the received signal is in-phase with the locally generated PN signal and H_0 is used when they are out-of-phase. If the output of the correlator is y , and the threshold as T_h , then under H_1 :

$$P_d = Pr(y \geq T_h) \quad (4.11)$$

$$P_m = Pr(y < T_h) \quad (4.12)$$

Under H_0 :

$$P_{fa} = Pr(y \geq T_h) \quad (4.13)$$

Once this false alarm is detected, the acquisition circuit returns to the search mode with a false alarm penalty time, T_{fa} .

$E\{T_{acq}\}$ is therefore a function of P_d , P_m , P_{fa} and T_{fa} :

$$E\{T_{acq}\} = f(P_d, P_m, P_{fa}, T_{fa}) \quad (4.14)$$

4.3. Summary

The purpose of this chapter was to carry out a literature review on PN code acquisition techniques. This will make for easy understanding of the analysis of the proposed circuit, which is presented in Chapter 5. A glaring fact from the reviewed literature showed that the acquisition process mainly entails correlating the received PN signal with a locally generated PN signal. The phase of the received signal that gives the maximum autocorrelation value is taken as the synchro cell. The correlation can be performed using active or passive correlator. Faster acquisition can be achieved using the passive correlator. However it is more complex than the active correlator. It was also stated that the serial search is the preferred search strategy as it is less complex than the

other search strategies. The importance of threshold setting in serial search was stressed. Finally, the parameters for performance measures were stated and it was emphasised that the mean acquisition time is an importance parameter measure.

CHAPTER 5

Adaptive PN Code Acquisition

5.1. Introduction

In this chapter, the proposed PN code acquisition circuit is presented and its performance is analysed in a mobile environment. In the first instance, the different segments that make up the circuit are described. This will make for a better understanding of how the circuit works as a single unit. Thereafter, mathematical equations relating the performance of the circuit in a mobile environment are derived. Specifically, the equations relating the P_d , P_{fa} and $E\{T_{acq}\}$ are derived and the effect of the varying mobile environment on these parameters are theoretically studied. Some of the numerical results from the theoretical analysis are validated by Monte Carlo simulation.

5.2. The Proposed Circuit

The proposed circuit is a double dwell adaptive acquisition circuit shown in Figure 5.1. A MF is used for the correlation operation. Since the uncertainty region, W in chips is large, and by recalling from Figure 4.3 that only one cell is the synchro cell, it means that there are many non-synchro cells. For better performance, it is necessary for the circuit to detect and reject these non-synchro cells as fast as possible. This can be

achieved by using a multiple dwell acquisition system as discussed in Section 4.2.3. An MF of a short length is used in the first dwell of the proposed circuit. The shorter the length of the MF, the less time spent in the first dwell and therefore more non-synchro cells can be quickly discarded. However, it will be made clearer in due course that the probability of detection, P_d is directly related to the length of the MF. Therefore, to improve the detection performance of the circuit, a longer dwell time is used in the second dwell. This is achieved by the use of post detection integration (PDI) [9]. The PDI is implemented by summing L successive outputs of the MF and making a decision thereafter.

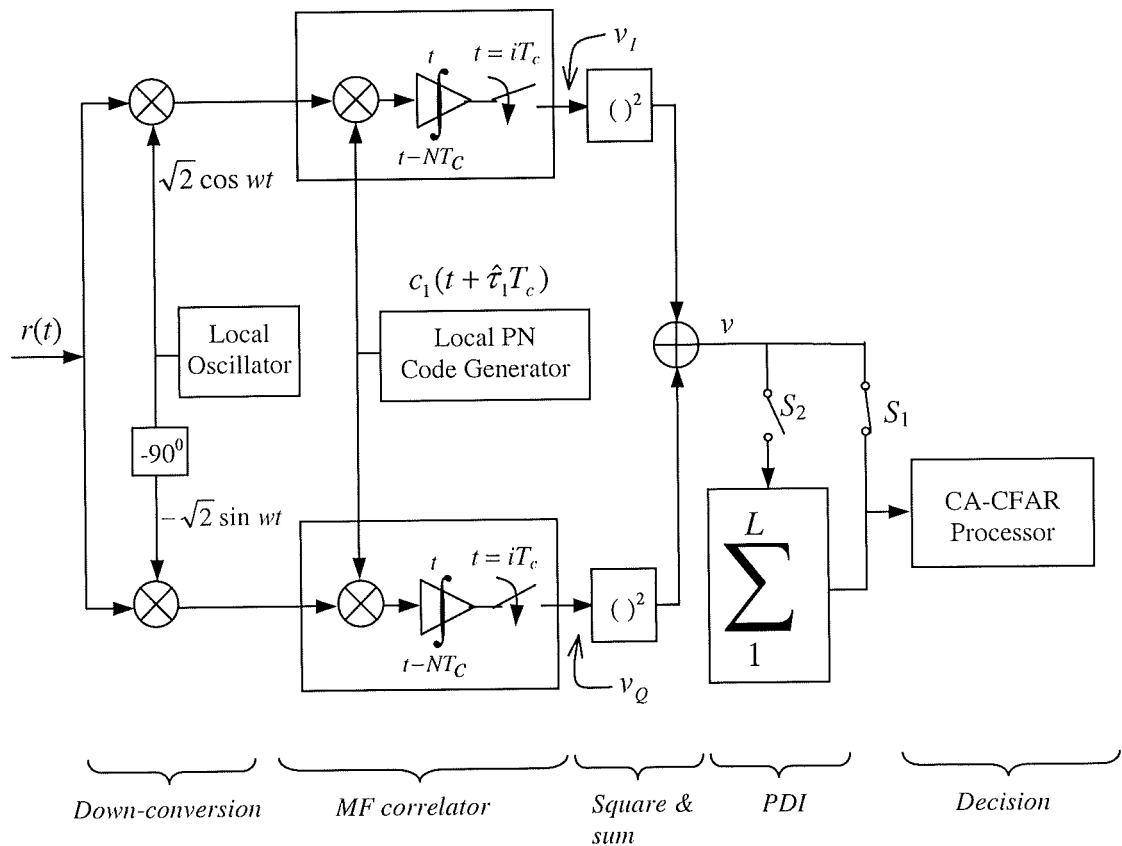


Figure 5.1. The proposed double dwell acquisition circuit

At the front end of the acquisition circuit is the *down-conversion* segment. This approximately converts the carrier modulated PN signal to baseband by eliminating the carrier frequency. This is as a result of the non-coherent nature of the circuit as the SNR is too low to do carrier phase acquisition prior to PN acquisition. In the down-conversion process, there is usually error in frequency known as frequency offset [9 – 11]. This affects the performance of the circuit and it will be shown later in this chapter that by using a shorter length MF in the implementation of the circuit, this effect of frequency offset can be mitigated. For now it can be stated that the purpose of using a shorter length MF in a multiple dwell acquisition system is to improve cell search performance of the acquisition circuit in terms of speed of acquisition. After the down-conversion, the next segment of the circuit is the *MF correlator* that does baseband matched filtering of the received signal. The received PN signal is correlated with its replica, which is locally generated at the receiver. Normally, the maximum autocorrelation value corresponds to the situation where the two PN codes are properly aligned. This might not be the case all the time, leading to false alarm. The next segment of the circuit is the *square and sum*. This is necessary to eliminate the carrier phase error by combining the signals from the *I* and *Q* arms of the detector. The output of the detector is taken to the decision segment where a decision is made (that is, whether acquisition is completed, or not). The *PDI* segment is used to implement the second dwell. This is achieved by combining *L* successive outputs of the MF in order to improve the SNR and making a decision, thereafter.

The *decision* segment is an adaptive circuit based on the cell averaging constant false alarm rate (CA-CFAR) technique [14, 15]. This is shown in Figure 5.2. The CA-CFAR

processor is made up of $n + 1$ windows. Prior to acquisition decision, out-of-phase correlation samples from the MF, which are basically noise power samples from the mobile environment, are stored in the n windows. This ensures that only noise samples are in the windows. The summed output of the n windows, u is scaled by a fixed factor T_r ($r = 1, 2$ for first and second dwell respectively) resulting in the threshold, $T_h = T_r u$. The value from the MF for the cell under test is then stored in the window v . In using the CA-CFAR technique, it is assumed that the noise samples in the n windows are of equal power. If this is not the case, other techniques, such as Smaller Of all CFAR (SO-CFAR) and Greater Of all CFAR (GO-CFAR), could be used [51].

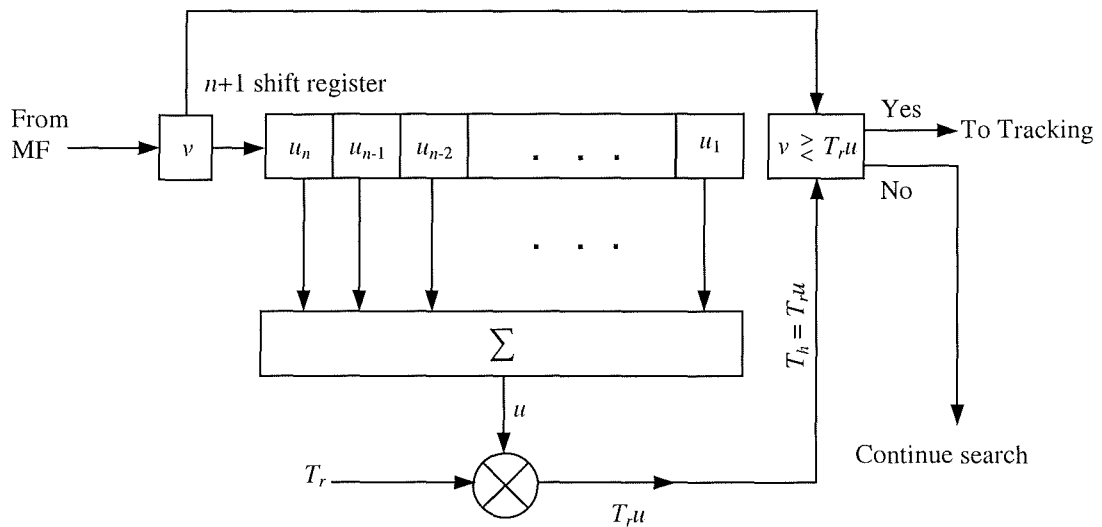


Figure 5.2. The CA-CFAR processor

If in the first dwell, $v \geq T_1 u$, it is assumed that the received signal is aligned with the local signal, and the second dwell is enabled by closing S_2 and opening S_1 in Figure 5.1. Finally, if after L PDI, $v \geq T_2 u$, then acquisition is declared and tracking enabled. If the foregoing conditions do not hold for any of the dwells, that cell is rejected

immediately and the next cell is searched. It is seen from Figure 5.2 that, as the noise power in the mobile environment varies, u and therefore the threshold, $T_r u$ will vary accordingly. Thus the circuit can adapt to changing noise power. Unlike a non-adaptive circuit that uses fixed threshold value, the threshold value is not fixed but made to vary by the scaling factor, T_r , that fixes the false alarm rate of the system. Figure 5.3 is a flow graph of the search process in the double dwell acquisition circuit.

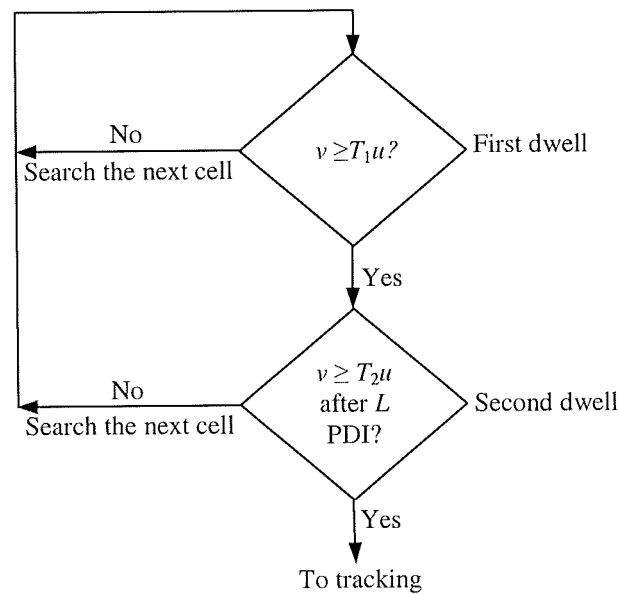


Figure 5.3. Flow graph of the proposed double dwell acquisition circuit

5.3. Performance Analysis

5.3.1. The Channel Model

In wireless communication systems, the most challenging aspect of the channel is the Rayleigh fading multipath channel [32, 52]. In most cases, especially in sub-urban and urban areas, signal propagation is mainly by NLOS. The channel can be frequency selective or frequency non-selective. In order to provide a base line for performance analysis and comparison, the performance of the circuit is first studied in a Ricean

fading channel. Secondly, its performance is analysed in a frequency non-selective Rayleigh fading channel and finally a frequency selective Rayleigh fading channel. In the following analysis, it is assumed that the Rayleigh fading is slow enough that the amplitude and phase remain constant during each correlation interval, but fast enough that successive correlation intervals are independent [9]. It is also assumed that the channel is wide sense stationary [32].

5.3.1.1. Ricean Fading Channel

In CDMA systems, data transmission is only done after successful PN code acquisition [19], and thus the effect of data on the acquisition process is not considered here. Let the transmitted signal, $s(t)$ be given as:

$$s(t) = \sqrt{2S}c(t)\cos(\omega t + \theta) \quad (5.1)$$

where S is the signal power in Watts, $c(t) = \sum_{i=-\infty}^{\infty} c_i p_{T_c}(t - iT_c)$ is the PN code waveform. $|c_i| = 1$ is the i th chip of the PN code sequence and $p_{T_c}(t)$ is the rectangular waveform with duration equal to the chip duration, T_c . ω is the carrier frequency in radians/seconds and θ is the phase of the carrier.

In the study of the mobile fading channel in Chapter 3, it was shown that small-scale fading channel introduces time-variant amplitude fluctuation, carrier phase jitter and propagation delay to the real signal transmitted through it. Thus the impulse response of a Ricean fading channel can be given as:

$$\tilde{h}(t) = \{A e^{j\phi} + \alpha(t)e^{-j\phi(t)}\}\delta(t - \tau) \quad (5.2)$$

where the first term in (5.2) represents the deterministic component due to LOS signal. The second term represents the diffused components of the Rayleigh faded signal. $\delta(\cdot)$ is the Dirac delta function. $\alpha(t)$ and $\varphi(t)$ are respectively the overall gain and phase shift resulting from the superposition of the multipath components. The phases $\varphi(t)$ of the diffuse components are uniformly distributed over $[0, 2\pi]$. The component due to Rayleigh fading in (5.2) can also be expressed in terms of its in-phase and quadrature components, $x(t)$ and $y(t)$ as:

$$\alpha(t)e^{-j\varphi(t)} = x(t) + jy(t) \quad (5.3)$$

where $x(t)$ and $y(t)$ are zero-mean i.i.d. Gaussian random process with same variance given as $E[\alpha^2(t)] = \sigma^2$. The ratio of the power of the LOS signal, to the NLOS signal, is usually given by the Ricean factor, $k_R = 10\log_{10}(A^2/2\sigma^2)$ dB (Section 3.3.2.1).

Using (5.1) and (5.2), the received signal can be given as:

$$r(t) = \tilde{h}(t)s(t) + n(t) \quad (5.4)$$

Assuming a DS-CDMA system with K asynchronous users^{5.1}, the received signal can be expressed as:

$$\begin{aligned} r(t) = & \sqrt{2S} \sum_{k=1}^K A_k c_k(t + \tau_k T_c) \cos(\omega t + \psi_k) + \sqrt{2S} \sum_{k=1}^K x_k(t) c_k(t + \tau_k T_c) \cos(\omega t + \theta_k) \\ & + \sqrt{2S} \sum_{k=1}^K y_k(t) c_k(t + \tau_k T_c) \sin(\omega t + \theta_k) + n(t) \end{aligned} \quad (5.5)$$

where τ_k is the delay in the receive PN signal of the k th user normalised to the chip duration, T_c . θ_k represents the carrier phases of the users' received signal uniformly

^{5.1} $k = 1$ represents the signal of the desired user that is being acquired.

distributed over $[0, 2\pi]$. $\psi_k = \phi_k + \theta_k$ and are also uniformly distributed over $[0, 2\pi]$.

$n(t)$ takes the effect of AWGN into consideration and it is given from [8] as:

$$n(t) = \sqrt{2} [n_I(t) \cos wt - n_Q(t) \sin wt] \quad (5.6)$$

where $n_I(t) = n_Q(t)$ is the double-side psd given as $N_0 / 2$ Watts/Hz.

The I - Q MF performs non-coherent correlation of the received signal with a locally generated PN signal as shown in Figure 5.1. The I and Q components of the locally generated PN signal is given as:

$$I(t) = \sqrt{2} c_1(t + \hat{\tau}_1 T_c) \cos wt \quad (5.7a)$$

$$Q(t) = -\sqrt{2} c_1(t + \hat{\tau}_1 T_c) \sin wt \quad (5.7b)$$

where $\hat{\tau}_1$ is an estimate of τ_k .

Thus the output of the MF is given as:

$$v_I = \int_0^{NT_c} r(t) I(t) dt \quad (5.8a)$$

$$v_Q = \int_0^{NT_c} r(t) Q(t) dt \quad (5.8b)$$

The code acquisition process is to make $c_1(t + \hat{\tau}_1 T_c) \approx c_1(t + \tau_1 T_c)$, i.e. $\hat{\tau}_1 \approx \tau_1$.

Let $\hat{\tau}_1 - \tau_k = pT_c + \zeta_k$; where $p = \left\lfloor \frac{|\hat{\tau}_1 - \tau_k|}{T_c} \right\rfloor$ is an integer number of code chips, and ζ_k

is the residual code offset uniformly distributed in $0 < \zeta_k \leq T_c$. This is a generalisation for $k = 1, 2, 3, \dots, K$ users. For the desired user, the situation where $p = 0$ represents the case $c_1(t + \hat{\tau}_1 T_c) \approx c_1(t + \tau_1 T_c)$. This is known as the acquisition state and denoted as the H_1 state. Also under the H_1 state, $c_1(t + \hat{\tau}_1 T_c) \neq c_k(t + \tau_k T_c)$ for $k = 2, 3, 4, \dots, K$. When

$p > 0$, then $c_1(t + \hat{\tau}_1 T_c) \neq c_k(t + \tau_k T_c)$ for $k = 1, 2, 3, \dots, K$, and this is indicated by the state where acquisition cannot occur and is known as the H_0 state.

From [53], the cross-correlation of $c_1(t + \hat{\tau}_1 T_c)$ with $c_k(t + \tau_k T_c)$ is given as:

$$\begin{aligned} R_{c_1 c_k}(p, \zeta_k) &= \frac{1}{NT_c} \int_0^{NT_c} c_1(t + \hat{\tau}_1 T_c) c_k(t + \tau_k T_c) dt \\ &= \frac{1}{N} \sum_{i=0}^{N-1} c_{1,i} c_{k,i+p} \left(1 - \frac{\zeta_k}{T_c}\right) + \frac{1}{N} \sum_{i=0}^{N-1} c_{1,i} c_{k,i+p+1} \frac{\zeta_k}{T_c} \end{aligned} \quad (5.9)$$

Let $\delta_k = \frac{\zeta_k}{T_c}$ (thus $0 < \delta_k < 1$), thus (5.9) can be expressed as:

$$R_{c_1 c_k}(p, \delta_k) = \frac{1}{N} \sum_{i=0}^{N-1} c_{1,i} c_{k,i+p} (1 - \delta_k) + \frac{1}{N} \sum_{i=0}^{N-1} c_{1,i} c_{k,i+p+1} \delta_k \quad (5.10)$$

It should be noted that the two terms in (5.10) are uncorrelated. Using results from appendix I, the variance of $R_{c_1 c_k}(p, \delta_k)$ is the sum of the variances of the individual terms. This property is assumed in all analysis involving $R_{c_1 c_k}(p, \delta_k)$. Without losing the generality, it is assumed that the carrier phase, θ_1 of the desired user is zero and taken as the reference. The I and Q components at the output of the MF are given as:

$$v_I = v_{ls} + v_{ls-mai} + v_{nl} + v_{nl-mai} + N_{AW} \quad (5.11a)$$

$$v_Q = v_{ls} + v_{ls-mai} + v_{nl} + v_{nl-mai} + N_{AW} \quad (5.11b)$$

where v_{ls} represents the output of the MF due to the LOS component from the desired user, v_{ls-mai} represents the output of the MF due to the LOS component from the other users (which is the MAI term), v_{nl} represents the output of the MF for the desired user due to the NLOS Rayleigh faded signal, v_{nl-mai} represents the output of the MF due to

the NLOS Rayleigh faded signal of the other users. N_{AW} represents the effect of AWGN. It is assumed that the I and Q components are i.i.d. and have the same means and variances; so it is sufficient to do the analysis for one the components (the I component).

From (5.11a), neglecting double frequency terms:

$$v_{ls} = v_l \cos \phi_1 \quad (5.12)$$

and therefore,

$$v_l = \int_0^{NT_c} \sqrt{S} A_1 c_1(t + \hat{\tau}_1 T_c) c_1(t + \tau_1 T_c) dt \quad (5.13)$$

Writing (5.13) as:

$$v_l = \sqrt{S} A_1 N T_c X \quad (5.14)$$

where the autocorrelation function, X is given as:

$$X = \frac{1}{N T_c} \int_0^{N T_c} c_1(t + \hat{\tau}_1 T_c) c_1(t + \tau_1 T_c) dt \quad (5.15)$$

Then by using (5.10), X can be expressed as:

$$X = \frac{1}{N} \sum_{i=0}^{N-1} c_{1,i} c_{1,i+p} (1 - \delta_1) + \frac{1}{N} \sum_{i=0}^{N-1} c_{1,i} c_{1,i+p+1} \delta_1 \quad (5.16)$$

Under H_1 hypothesis, $p = 0$, then:

$$X = \frac{1}{N} \sum_{i=0}^{N-1} c_{1,i} c_{1,i} (1 - \delta_1) + \frac{1}{N} \sum_{i=0}^{N-1} c_{1,i} c_{1,i+1} \delta_1 \quad (5.17a)$$

$$X = \frac{1}{N} \sum_{i=0}^{N-1} c_{1,i}^2 (1 - \delta_1) + \frac{1}{N} \sum_{i=0}^{N-1} c_{1,i} c_{1,i+1} \delta_1 \quad (5.17b)$$

$$X = (1 - \delta_1) \quad (5.17c)$$

Note that by using property (iii) of PN code, the second term in (5.17b) is approximated to 0 (actually it is $-\delta_1/N$).

Using (5.17c), the mean of the v_l is given as:

$$\begin{aligned} E[v_l] &= \sqrt{S} A_1 T_c N (E[X]) \\ &= \sqrt{S} A_1 T_c N (1 - \delta_1) \end{aligned} \quad (5.18)$$

Using (5.12) and (5.17) the mean of v_{ls} is given as:

$$\begin{aligned} \mu_{ls, H_1} &= E[v_{ls}] = E[v_l] \cos \phi_1 \\ &= \sqrt{S} A_1 T_c N (1 - \delta_1) \cos \phi_1 \end{aligned} \quad (5.19)$$

The variance (var for short) of v_{ls} is given as:

$$\sigma_{ls, H_1}^2 = \text{var}[v_{ls}] = \text{var}[v_l] \cos^2 \phi_1 \quad (5.20)$$

The variance of v_l in (5.20) is given as:

$$\begin{aligned} \text{var}[v_l] &= E[v_l^2] - (E[v_l])^2 \\ &= S A_1^2 N^2 T_c^2 (1 - \delta_1)^2 - [\sqrt{S} A_1 N T_c (1 - \delta_1)]^2 = 0 \end{aligned} \quad (5.21)$$

By using (5.20) and (5.21), the variance of v_{ls} is 0.

From (5.11a),

$$v_{ls-mai} = \left[\sum_{k=2}^K \int_0^{NT_c} \sqrt{2S} A_k c_1(t + \hat{\tau}_1 T_c) c_k(t + \tau_k T_c) \cos(wt + \psi_k) \right] \sqrt{2} \cos wt dt \quad (5.22)$$

Neglecting double frequency terms,

$$v_{ls-mai} = \sum_{k=2}^K \int_0^{NT_c} \sqrt{S} A_k c_1(t + \hat{\tau}_1 T_c) c_k(t + \tau_k T_c) \cos \psi_k dt \quad (5.23)$$

The mean of (5.23) is zero since the other users PN signals are uncorrelated with that of the desired user. The variance, however, is given as:

$$\begin{aligned}
\sigma_{ls-mai, H_1}^2 &= \text{var}[v_{ls-mai}] = E[v_{ls-mai}^2] \\
&= E\left\{\left(\sum_{k=2}^K \int_0^{NT_c} \sqrt{S} A_k c_1(t + \hat{\tau}_1 T_c) c_k(t + \tau_k T_c) \cos \psi_k dt\right)^2\right\} \\
&= SN^2 T_c^2 \sum_{k=2}^K A_k^2 \left(E\left\{R_{c_1 c_k}(p, \delta_k) \cos \psi_k\right\}^2\right) \\
&= SN^2 T_c^2 \sum_{k=2}^K A_k^2 \left(E\left\{\left[\left(\frac{1}{N} \sum_{i=0}^{N-1} c_{1,i} c_{k,i} (1 - \delta_k) + \frac{1}{N} \sum_{i=0}^{N-1} c_{1,i} c_{k,i+1} \delta_k\right) \cos \psi_k\right]^2\right\}\right) \\
&= SN^2 T_c^2 \sum_{k=2}^K A_k^2 \left(E\left\{\left[\frac{1}{N} \sum_{i=0}^{N-1} c_{1,i} c_{k,i} (1 - \delta_k)\right]^2\right\} + E\left\{\left[\frac{1}{N} \sum_{i=0}^{N-1} c_{1,i} c_{k,i+1} \delta_k\right]^2\right\} E[\cos^2 \psi_k]\right) \\
&= SNT_c^2 \sum_{k=2}^K \left(A_k^2 E\{(1 - \delta_k)^2\} + E\{\delta_k^2\} E[\cos^2 \psi_k]\right) \\
&= SNT_c^2 \sum_{k=2}^K \left(A_k^2 E\{(1 - 2\delta_k + 2\delta_k^2)\} E[\cos^2 \psi_k]\right) \tag{5.24}
\end{aligned}$$

Note that δ_k is uniformly distributed over $[0, 1]$ and ψ_k over $[0, 2\pi]$, therefore:

$$\begin{aligned}
\sigma_{ls-mai, H_1}^2 &= SNT_c^2 \sum_{k=2}^K \left(A_k^2 \left\{\int_0^1 (1 - 2\delta_k + 2\delta_k^2) d\delta_k\right\} \left\{\frac{1}{2\pi} \int_0^{2\pi} \cos^2 \psi_k\right\}\right) \\
&= SNT_c^2 \sum_{k=2}^K \left(A_k^2 \left[\left(\delta_k - \delta_k^2 + 2\delta_k^3/3\right)\Big|_0^1 \left[\psi_k/(4\pi)\right]_0^{2\pi}\right)\right) \\
&= \sum_{k=2}^K \frac{SNT_c^2 A_k^2}{3} = \frac{A_1^2 SNT_c^2 (K-1)}{3} \tag{5.25}
\end{aligned}$$

In (5.25), it was assumed that all the other users have the same power as the user of interest, which is user 1.

For the Rayleigh fading components of the user of interest, from (5.11a), the output of the MF is given as:

$$v_{nl} = \int_0^{NT_c} \left(\sqrt{2S} c_1(t + \hat{\tau}_1 T_c) c_1(t + \tau_1 T_c) x(t) \cos wt \right) \sqrt{2} \cos wt dt \\ + \int_0^{NT_c} \left(\sqrt{2S} c_1(t + \hat{\tau}_1 T_c) c_1(t + \tau_1 T_c) y(t) \sin wt \right) \sqrt{2} \cos wt dt \quad (5.26)$$

Neglecting double frequency terms, v_{nl} can be written as:

$$v_{nl} = \int_0^{NT_c} \sqrt{S} c_1(t + \hat{\tau}_1 T_c) c_1(t + \tau_1 T_c) x(t) dt \quad (5.27)$$

Let x_i represents the i th chip component of the fading process $x(t)$. Its mean is zero with variance given as $E[x_i^2] = \sigma^2$ and autocorrelation given from [41] as $E[x_i x_j] = \rho_{|i-j|} \sigma^2$.

Here,

$$\rho_i = J_0(2\pi t f_D T_c) \quad (5.28)$$

where J_0 is the zero order Bessel function of the first kind, and f_D takes into consideration the Doppler shift.

The mean of (5.27) is zero and the variance is given as:

$$\sigma_{nl, H_1}^2 = \text{var}[v_{nl}] = E \left\{ \left[\int_0^{NT_c} \sqrt{S} c_1(t + \hat{\tau}_1 T_c) c_1(t + \tau_1 T_c) x(t) dt \right]^2 \right\} \\ = SN^2 T_c^2 E \left\{ \left[R_{c_1 c_1}(p, \delta_1) x(t) \right]^2 \right\} \\ = SN^2 T_c^2 E \left\{ \left[\frac{1}{N} \sum_{i=0}^{N-1} c_{1,i} c_{1,i} (1 - \delta_1) x_i + \frac{1}{N} \sum_{i=0}^{N-1} c_{1,i} c_{1,i+1} \delta_1 x_i \right]^2 \right\} \\ = SN^2 T_c^2 E \left\{ \left[\frac{1}{N} \sum_{i=0}^{N-1} (1 - \delta_1) x_i + \frac{1}{N} \sum_{i=0}^{N-1} c_{1,i} c_{1,i+1} \delta_1 x_i \right]^2 \right\}$$

$$\begin{aligned}
& \times \left[\frac{1}{N} \sum_{j=0}^{N-1} (1 - \delta_1) x_j + \frac{1}{N} \sum_{i=0}^{N-1} c_{1,j} c_{1,j+1} \delta_1 x_j \right] \\
& = SN^2 T_c^2 E \left[\left[\frac{1}{N^2} \sum_{i=0}^{N-1} \sum_{j=0}^{N-1} (1 - \delta_1)^2 x_i x_j + \frac{1}{N^2} \sum_{i=0}^{N-1} \sum_{j=0}^{N-1} c_{1,i} c_{1,j} c_{1,i+1} c_{1,j+1} \delta_1^2 x_i x_j \right] \right] \\
& = ST_c^2 \sigma^2 \left[\left(N + \sum_{i=1}^{N-1} \sum_{\substack{j=1 \\ j \neq i}}^{N-1} \rho_{|i-j|} \right) (1 - \delta_1)^2 + N \delta_1^2 \right] \\
& = ST_c^2 \sigma^2 \left[\left(N + 2 \sum_{i=1}^{N-1} (N - i) \rho_i \right) (1 - \delta_1)^2 + N \delta_1^2 \right] \\
& = ST_c^2 \sigma^2 \left[G(1 - \delta_1)^2 + N \delta_1^2 \right] \tag{5.29}
\end{aligned}$$

Where $G = N + 2 \sum_{i=1}^{N-1} (N - i) \rho_i$.

The effect of the MAI term due to Rayleigh fading can be expressed as:

$$\begin{aligned}
v_{nl-mai} &= \sum_{k=2}^K \sqrt{2S} \int_0^{NT_c} c_1(t + \hat{\tau}_1 T_c) c_k(t + \tau_k T_c) x(t) \cos(\omega t + \theta_k) \sqrt{2} \cos \omega t dt \\
&+ \sum_{k=2}^K \sqrt{2S} \int_0^{NT_c} c_1(t + \hat{\tau}_1 T_c) c_k(t + \tau_k T_c) y(t) \sin(\omega t + \theta_k) \sqrt{2} \cos \omega t dt \\
&= \sqrt{S} NT_c X_x + \sqrt{S} NT_c X_y \tag{5.30}
\end{aligned}$$

where;

$$X_x = \sum_{k=2}^K \frac{1}{NT_c} \int_0^{NT_c} c_1(t + \hat{\tau}_1 T_c) c_k(t + \tau_k T_c) x(t) \cos \theta_k \tag{5.31a}$$

$$X_y = \sum_{k=2}^K \frac{1}{NT_c} \int_0^{NT_c} c_1(t + \hat{\tau}_1 T_c) c_k(t + \tau_k T_c) y(t) \sin \theta_k \quad (5.31b)$$

Since X_x and X_y are i.i.d. Gaussian random variable, uncorrelated and of zero-mean and same variance, the variance of v_{nl-mai} is therefore given as:

$$\begin{aligned} \sigma_{nl-mai, H_1}^2 &= E[(v_{nl-mai})^2] = E\left[(\sqrt{S} NT_c X_x)^2\right] + E\left[(\sqrt{S} NT_c X_y)^2\right] \\ &= 2E\left[(\sqrt{S} NT_c X_x)^2\right] \\ &= 2SN^2 T_c^2 (E[X_x^2]) \end{aligned} \quad (5.32)$$

From (5.32), $E[X_x^2]$ can be evaluated as follows:

$$\begin{aligned} E[X_x^2] &= E\left[\left(\sum_{k=2}^K \frac{1}{N} \sum_{i=0}^{N-1} c_{1,i} c_{k,i} (1 - \delta_k) x_i + \sum_{k=2}^K \frac{1}{N} \sum_{i=0}^{N-1} c_{1,i} c_{k,i+1} \delta_k x_i\right)^2 \cos^2 \theta_k\right] \\ &= \sum_{k=2}^K \frac{1}{N^2} E_{\delta_k, \theta_k} \left\{ [N\sigma^2 (1 - \delta_k)^2 + N\sigma^2 \delta_k^2] \cos^2 \theta_k \right\} \\ &= \sum_{k=2}^K \frac{\sigma^2}{N} E_{\delta_k, \theta_k} \left\{ [1 - 2\delta_k + 2\delta_k^2] \cos^2 \theta_k \right\} \end{aligned} \quad (5.33)$$

Note that since δ_k is uniformly distributed in $[0, 1]$ and θ_k is uniformly distributed in $[0, 2\pi]$, it follows that:

$$\begin{aligned} E[X_x^2] &= \sum_{k=2}^K \frac{\sigma^2}{N} \left\{ \int_0^1 (1 - 2\delta_k + 2\delta_k^2) d\delta_k \cdot \frac{1}{2\pi} \int_0^{2\pi} \cos^2 \theta_k d\theta_k \right\} \\ &= \frac{\sigma^2 (K-1)}{3N} \end{aligned} \quad (5.34)$$

Therefore, using (5.32) the variance resulting from the effect of MAI due to the NLOS signal is given as:

$$\sigma_{nl-mai,H_1}^2 = \frac{2\sigma^2 ST_c^2 N(K-1)}{3} \quad (5.35)$$

Finally, from (5.11a):

$$N_{AW} = \int_0^{NT_c} n(t)I(t)dt \quad (5.36)$$

The mean of (5.36) is zero and neglecting double frequency terms, the variance is given as:

$$\sigma_{AW,H_1}^2 = \int_0^{NT_c} \frac{N_0}{2} [c_1(t + \hat{\tau}_1 T_c)]^2 dt \quad (5.37)$$

Since $[c_1(t + \hat{\tau}_1 T_c)]^2 = 1$ for all $t + \hat{\tau}_1 T_c$, then

$$\sigma_{AW,H_1}^2 = \frac{NN_0 T_c}{2} \quad (5.38)$$

The above equations have been derived for the case of H_1 hypothesis. Under H_0 hypothesis, $p > 0$ and it means that the received signal is out-of-phase with the locally generated signal. The following results are obtained for the H_0 hypothesis.

For the LOS signal in the case of the user of interest, the mean of v_{ls} is zero since the mean is given as:

$$\mu_{ls,H_0} = E[v_{ls}] = \sqrt{S} A_1 N T_c E[X] \cos \phi_1 = 0 \quad (5.39)$$

This is due to the fact that, under H_0 ; $X = \frac{1}{N} \sum_{i=0}^{N-1} c_{1,i} c_{1,i+p} (1 - \delta_1) + \frac{1}{N} \sum_{i=0}^{N-1} c_{1,i} c_{1,i+p+1} \delta_1 \approx 0$,

by virtue of property (iii) of m -sequence.

The variance is given as:

$$\sigma_{ls,H_0}^2 = \text{var}[v_{ls}] = \text{var}[v_l] \cos^2 \phi_1 \quad (5.40)$$

The variance of v_l in (5.40) is obtained as:

$$\text{var}[v_l] = E[v_l^2] - (E[v_l])^2 \quad (5.41)$$

where,

$$\begin{aligned} E[v_l^2] &= E \left\{ \sqrt{S} A_1 T_c N \left[\frac{1}{N} \sum_{i=0}^{N-1} c_{1,i} c_{1,i+p} (1 - \delta_1) + \frac{1}{N} \sum_{i=0}^{N-1} c_{1,i} c_{1,i+p+1} \delta_1 \right] \right\}^2 \\ &= S A_1^2 T_c^2 N^2 \left\{ E \left[\left(\frac{1}{N} \sum_{i=0}^{N-1} c_{1,i} c_{1,i+p} (1 - \delta_1) \right)^2 \right] + E \left[\left(\frac{1}{N} \sum_{i=0}^{N-1} c_{1,i} c_{1,i+p+1} \delta_1 \right)^2 \right] \right\} \\ &= S A_1^2 T_c^2 N [(1 - \delta_1)^2 + \delta_1^2] \end{aligned} \quad (5.42)$$

From (5.18);

$$(E[v_l])^2 = S A_1^2 T_c^2 N (1 - \delta_1)^2 \quad (5.43)$$

Using (5.42) and (5.43) in (5.40):

$$\sigma_{ls, H_0}^2 = S A_1^2 T_c^2 N \delta_1^2 \cos^2 \phi_1 \quad (5.44)$$

For the NLOS signal, considering the output of the MF for the user of interest under H_0 , the mean is zero and the variance is given as

$$\begin{aligned} \sigma_{nl, H_0}^2 &= E \left\{ \left[\int_0^{NT_c} \sqrt{2S} c_1(t + \hat{\tau}_1 T_c) c_1(t + \tau_1 T_c) x(t) dt \right]^2 \right\} \\ &= S N^2 T_c^2 E \left\{ \left[\frac{1}{N} \sum_{i=0}^{N-1} c_{1,i} c_{1,i+p} (1 - \delta_1) x_i + \frac{1}{N} \sum_{i=0}^{N-1} c_{1,i} c_{1,i+p+1} \delta_1 x_i \right]^2 \right\} \\ &= \sigma^2 S N T_c^2 (1 - 2\delta_1 + 2\delta_1^2) \end{aligned} \quad (5.45)$$

The effect of the MAI term for the LOS signal on the circuit under H_0 is the same as under H_1 and therefore the variance under H_0 is given by (5.25). Similarly, the variance

due to MAI in the NLOS signal under H_0 is the same as under H_1 as given by (5.35). The same is true for variance due to the AWGN component.

In the analysis that follows, the step-search size, Δ is set as 1. It is also assumed that $\delta_1 \ll 1$ and thus can be set to zero [11, 54]. If this is not the case, it is easily seen from (5.17) that as $\delta_1 \rightarrow 1$, X reduces, meaning less energy available at the output of the detector. The effect of this has been analysed in [11, 54] and it was shown that the best result is obtained when $\delta_1 = 0$ for the case $\Delta = 1$. The results for other values of Δ can be studied in [54].

Using the above derived results, under H_1 , the mean of (5.11a) is given as:

$$\mu_{ls,H_1} = \sqrt{S} A_1 N T_c \cos \phi_1 \quad (5.46)$$

Similarly, the mean of (5.11b) is given as:

$$\mu_{ls,H_1} = \sqrt{S} A_1 N T_c \sin \phi_1 \quad (5.47)$$

The variance of (5.11a), which is the same as that of (5.11b) under H_1 , is given as:

$$\begin{aligned} \sigma_{H_1}^2 &= \sigma_{ls-mai,H_1}^2 + \sigma_{nl,H_1}^2 + \sigma_{nl-mai,H_1}^2 + \sigma_{AW,H_1}^2 \\ &= \frac{A_1^2 S N T_c^2 (K-1)}{3} + \sigma^2 S T_c^2 G + \frac{2\sigma^2 S T_c^2 N (K-1)}{3} + \frac{N N_0 T_c}{2} \end{aligned} \quad (5.48)$$

Under H_0 , the mean of (5.11) is zero and variance of (5.11a) which is the same as that of (5.11b), is given as:

$$\begin{aligned} \sigma_{H_0}^2 &= \sigma_{ls-mai,H_0}^2 + \sigma_{nl,H_0}^2 + \sigma_{nl-mai,H_0}^2 + \sigma_{AW,H_0}^2 \\ &= \frac{A_1^2 S N T_c^2 (K-1)}{3} + \sigma^2 S T_c^2 N + \frac{2\sigma^2 S T_c^2 N (K-1)}{3} + \frac{N N_0 T_c}{2} \end{aligned} \quad (5.49)$$

From Figure 5.1, the output of the MF after squaring and summing is given as:

$$v = v_I^2 + v_Q^2 \quad (5.50)$$

Under H_1 , (5.50) has a non-central chi-square distribution with 2 degrees of freedom [32]. Its pdf is given as:

$$P(v | H_1) = \frac{1}{2\sigma_{H_1}^2} e^{-\left(\frac{s^2+v}{2\sigma_{H_1}^2}\right)} I_0\left(\frac{s\sqrt{v}}{\sigma_{H_1}^2}\right), \quad v \geq 0 \quad (5.51)$$

where $s^2 = \left(\sqrt{S} A_1 N T_c \cos \phi_1\right)^2 + \left(\sqrt{S} A_1 N T_c \sin \phi_1\right)^2 = A_1^2 S T_c^2 N^2$ and I_0 is the zeroth-order modified Bessel function of the first kind.

However, under H_0 , (5.50) has a central chi-square distribution with 2 degrees of freedom [32] with pdf given as:

$$P(v | H_0) = \frac{1}{2\sigma_{H_0}^2} e^{-\left(\frac{v}{2\sigma_{H_0}^2}\right)}, \quad v \geq 0 \quad (5.52)$$

Equations (5.51) and (5.52) are the statistics of the detector in the first dwell. In the second dwell, PDI is used for the implementation. If the length of the PDI is L , then the decision statistics under H_1 is also a non-central chi-square distribution but with $2L$ degrees of freedom and the pdf is thus given as:

$$P(v | H_1) = \frac{1}{2\sigma_{H_1}^2} \left(\frac{v}{s^2}\right)^{(L-1)/2} e^{-\left(\frac{s^2+v}{2\sigma_{H_1}^2}\right)} I_{L-1}\left(\frac{s\sqrt{v}}{\sigma_{H_1}^2}\right), \quad v \geq 0 \quad (5.53)$$

where I_{L-1} is the $(L-1)$ th-order modified Bessel function of the first kind.

Similarly, in the second dwell under H_0 , (5.50) has a central chi-square distribution with $2L$ degrees of freedom and pdf given as:

$$P(v | H_0) = \frac{v^{L-1}}{(2\sigma_{H_0}^2)^L \Gamma(L)} e^{-\left(\frac{v}{2\sigma_{H_0}^2}\right)}, \quad v \geq 0 \quad (5.54)$$

where $\Gamma(\cdot)$ denotes the gamma function.

The operation of the CA-CFAR processor is that prior to acquisition decision, out-of-phase correlation values from the MF, which are basically H_0 values, are stored in the n registers. These are summed to give the value u , as shown in Figure 5.2. This value is scaled by a fixed factor T_r , (for $r = 1, 2$ dwells). T_r is chosen to give a constant probability of false alarm for each dwell, therefore deriving the name constant false alarm rate [15]. Therefore, in the first dwell, the decision statistics of the CA-CFAR processor is a central chi-square distribution with $2n$ degrees of freedom and pdf given as:

$$P(u | H_0) = \frac{u^{n-1}}{(2\sigma_{H_0}^2)^n \Gamma(n)} e^{-\left(\frac{u}{2\sigma_{H_0}^2}\right)}, \quad u \geq 0 \quad (5.55)$$

In the second dwell, the statistics of CA-CFAR processor is also a central chi-square distribution but with $2Ln$ degrees of freedom with pdf given as:

$$P(u | H_0) = \frac{u^{Ln-1}}{(2\sigma_{H_0}^2)^{Ln} \Gamma(Ln)} e^{-\left(\frac{u}{2\sigma_{H_0}^2}\right)}, \quad u \geq 0 \quad (5.56)$$

The probability of detection and false alarm are given by:

$$\Pr\{v > T_r u | H_i\} \quad (5.57)$$

for $i = 0, 1$ and $r = 1, 2$ dwells.

Under H_1 , (5.57) gives the probability of detection, P_{dr} . It is the false alarm probability, P_{far} under H_0 . Since CA-CFAR processing is performed prior to acquisition decision, it can be assumed that v and u are statistically independent. Thus the probability of detection and false alarm are given as:

$$P_{dr}, P_{far} = \int_0^{\infty} P(u | H_0) \int_{T_1 u}^{\infty} P(v | H_i) dv du \quad (5.58)$$

From (5.58), the detection and false alarm probabilities for each dwells ($r = 1, 2$) are obtained as follows. In the first dwell, the output of the CA-CFAR processor is scaled by T_1 . Thus the probability of detection is given as:

$$\begin{aligned} P_{d1} &= \int_0^{\infty} \frac{u^{n-1}}{(2\sigma_{H_0}^2)^n \Gamma(n)} e^{-\frac{u}{2\sigma_{H_0}^2}} \int_{T_1 u}^{\infty} \frac{1}{2\sigma_{H_1}^2} e^{-\left(\frac{s^2+v}{2\sigma_{H_1}^2}\right)} I_0\left(\frac{s\sqrt{v}}{\sigma_{H_1}^2}\right) dv du \\ &= \int_0^{\infty} \frac{u^{n-1}}{(2\sigma_{H_0}^2)^n \Gamma(n)} e^{-\frac{u}{2\sigma_{H_0}^2}} Q\left(\frac{s}{\sigma_{H_1}}, \frac{\sqrt{T_1}u}{\sigma_{H_1}}\right) du \end{aligned} \quad (5.59)$$

where,

$Q(\cdot, \cdot)$ is the first order Marcum's Q-function [52], and

$$\frac{s}{\sigma_{H_1}} = \sqrt{\frac{A_1^2 N(E_c / N_0)}{A_1^2 (K-1) (E_c / N_0) + \frac{2\sigma^2 (K-1)}{3} (E_c / N_0) + \frac{\sigma^2 G}{N} (E_c / N_0) + 1}}$$

Note that $E_c / N_0 = 2ST_c / N_o$ is defined as the SNR per chip.

The probability of false alarm is given as:

$$P_{fa1} = \int_0^{\infty} \frac{u^{n-1}}{(2\sigma_{H_0}^2)^n \Gamma(n)} e^{-\frac{u}{2\sigma_{H_0}^2}} \int_{T_1 u}^{\infty} \frac{1}{2\sigma_{H_0}^2} e^{-\frac{v}{2\sigma_{H_0}^2}} dv du \quad (5.60)$$

From appendix II,

$$P_{fa1} = \frac{1}{(1+T_1)^n} \quad (5.61)$$

In the second dwell, the output of the CA-CFAR processor is scaled by T_2 . Thus the probability of detection is given as:

$$\begin{aligned}
P_{d2} &= \int_0^{\infty} \frac{u^{Ln-1}}{(2\sigma_{H_0}^2)^{Ln} \Gamma(Ln)} e^{-\frac{u}{2\sigma_{H_0}^2}} \int_{T_2 u}^{\infty} \frac{1}{2\sigma_{H_1}^2} \left(\frac{v}{s^2}\right)^{(L-1)/2} e^{-\left(\frac{s^2+v}{2\sigma_{H_1}^2}\right)} I_{L-1}\left(\frac{s\sqrt{v}}{\sigma_{H_1}^2}\right) dv du \\
&= \int_0^{\infty} \frac{u^{Ln-1}}{(2\sigma_{H_0}^2)^{Ln} \Gamma(Ln)} e^{-\frac{u}{2\sigma_{H_0}^2}} Q_L\left(\frac{s}{\sigma_{H_1}}, \sqrt{T_2 u}\right) du
\end{aligned} \tag{5.62}$$

where $Q_L(\cdot, \cdot)$ it is the L th order Marcum's Q-function.

There is no close form solution to the integral involving the Marcum's Q-function [52], and so solutions of (5.59) and (5.62) were obtained using approximate integration method with the aid of Matlab[®].

The probability of false alarm in the second dwell is given as:

$$P_{fa2} = \int_0^{\infty} \frac{u^{Ln-1}}{(2\sigma_{H_0}^2)^{Ln} \Gamma(Ln)} e^{-\frac{u}{2\sigma_{H_0}^2}} \int_{T_2 u}^{\infty} \frac{v^{L-1}}{(2\sigma_{H_0}^2)^L \Gamma(L)} e^{-\frac{v}{2\sigma_{H_0}^2}} dv du \tag{5.63}$$

From Appendix II, the false alarm probability can be shown to be given as:

$$P_{fa2} = \sum_{q=0}^{L-1} 1/q! \frac{(Ln-1+q)!(T_2)^q}{(Ln-1)!(1+T_2)^{Ln+q}} \tag{5.64}$$

It is seen that if $L = 1$, then (5.64) reduces to (5.61), as it should be. Also, (5.61) and (5.64) do not depend on E_c / N_0 and therefore P_{fa} does not depend on the SNR of the environment.

5.3.1.2. Frequency Selective Rayleigh Fading Channel

In order to fully understand the performance of the circuit under this channel condition, it is necessary to fully derive the statistics at the output of the MF. The transmitted signal for the user of interest from (5.1) is given as:

$$s(t) = \sqrt{2S} c(t) \cos(\omega t + \theta) \tag{5.65}$$

The signal is assumed to pass through a frequency selective Rayleigh fading channel whose channel model is represented by a tapped delay line as explained in Section 3.3.4. The total number of paths is given as L_p . The impulse response of the channel for the l th path can be given as:

$$\tilde{h}(t, \tau_l(t)) = \alpha_l(t) e^{-j\varphi_l(t)} \delta(t - \tau_l(t)) \quad (5.66)$$

It is assumed that the magnitude of each tap coefficients, α_l , for $l = 1, 2, \dots, L_p$ is Rayleigh distributed and their respective phases, $\varphi_l(t)$ are uniformly distributed over $[0, 2\pi]$. From (5.66):

$$\alpha_l(t) e^{-j\varphi_l(t)} = x_l(t) + jy_l(t) \quad (5.67)$$

It is seen that (5.67) is similar to (5.3) and therefore the received signal in DS-CDMA system with K asynchronous users can be expressed as:

$$\begin{aligned} r(t) = & \sqrt{2S} \sum_{k=1}^K \sum_{l=1}^{L_p} c_k(t - [l-1]T_c + \tau'_{kl}T_c) x_{kl}(t) \cos(\omega t + \theta_{kl}) \\ & + \sqrt{2S} \sum_{k=1}^K \sum_{l=1}^{L_p} c_k(t - [l-1]T_c + \tau'_{kl}T_c) y_{kl}(t) \sin(\omega t + \theta_{kl}) + n(t) \end{aligned} \quad (5.68)$$

τ'_{kl} is the k th user delay in the received PN signal for the l th resolvable path normalised to the chip duration T_c . θ_{kl} is the k th user overall phase in the received signal for the l th path. The phases θ_{kl} are uniformly distributed over $[0, 2\pi]$. $n(t)$ is the AWGN of double-sided power spectral density given as $N_0 / 2$ Watts/Hertz.

Writing $\tau_{kl} = \tau'_{kl} - [l-1]$, then (5.68) is given as:

$$\begin{aligned} r(t) = & \sqrt{2S} \sum_{k=1}^K \sum_{l=1}^{L_p} c_k(t + \tau_{kl}T_c) x_{kl}(t) \cos(\omega t + \theta_{kl}) \\ & + \sqrt{2S} \sum_{k=1}^K \sum_{l=1}^{L_p} c_k(t + \tau_{kl}T_c) y_{kl}(t) \sin(\omega t + \theta_{kl}) + n(t) \end{aligned} \quad (5.69)$$

After down-conversion and matched filtering, the received signal with I and Q components using (5.11) are given as:

$$v_I = v_{nl} + v_{nl-mai} + N_{AW} \quad (5.70a)$$

$$v_Q = v_{nl} + v_{nl-mai} + N_{AW} \quad (5.70b)$$

For the desired user, the phase θ_{1l} is taken as the reference and set to zero, and neglecting double frequency terms, v_{nl} is given as:

$$v_{nl} = \sum_{l=1}^{L_p} \int_0^{NT_c} \sqrt{S} c_1(t + \hat{\tau}_l T_c) c_1(t + \tau_{1l} T_c) x_{1l}(t) dt \quad (5.71)$$

Under H_1 , the mean of (5.71) is zero and it can be shown that the variance of (5.71) is similar to (5.29) but modified by the power in each path, σ_l^2 to give:

$$\sigma_{nl,H_1}^2 = \sum_{l=1}^{L_p} ST_c^2 \sigma_l^2 [G(1 - \delta_1)^2 + N\delta_1^2] \quad (5.72)$$

Similarly, under H_0 , the variance is given as:

$$\sigma_{nl,H_0}^2 = \sum_{l=1}^{L_p} ST_c^2 \sigma_l^2 N(1 - 2\delta_1 + 2\delta_1^2) \quad (5.73)$$

For the effect of MAI, the mean is zero and the variance is similar to (5.35) but modified by the power in each path σ_l^2 to give:

$$\sigma_{nl-mai,H_1}^2 = \sigma_{nl-mai,H_0}^2 = \sum_{l=1}^{L_p} \frac{2\sigma_l^2 ST_c^2 N(K-1)}{3} \quad (5.74)$$

The variance due to AWGN is still the same as in (5.38).

By assuming a zero residual code offset, the total variance at the output of the MF under H_1 is given as:

$$\begin{aligned}
\sigma_{H_1}^2 &= \sigma_{nl,H_1}^2 + \sigma_{nl-mai,H_1}^2 + \sigma_{n,H_1}^2 \\
&= ST_c^2 \sum_{l=1}^{L_p} \sigma_l^2 G + \sum_{l=1}^{L_p} \frac{\sigma_l^2 ST_c^2 N(K-1)}{3} + NN_0 T_c / 2 \\
&= \frac{NN_0 T_c}{2} \left(\sum_{l=1}^{L_p} \frac{\sigma_l^2 E_c}{N_0} \frac{G}{N} + \sum_{l=1}^{L_p} \frac{\sigma_l^2 E_c (K-1)}{3N_0} + 1 \right)
\end{aligned} \tag{5.75}$$

Under H_0 , the variance is given as:

$$\begin{aligned}
\sigma_{H_0}^2 &= \sigma_{nl,H_0}^2 + \sigma_{nl-mai,H_0}^2 + \sigma_{n,H_0}^2 \\
\sigma_{H_0}^2 &= ST_c^2 \sum_{l=1}^{L_p} \sigma_l^2 N + \sum_{l=1}^{L_p} \frac{\sigma_l^2 ST_c^2 N(K-1)}{3} + NN_0 T_c / 2 \\
&= \frac{NN_0 T_c}{2} \left(\sum_{l=1}^{L_p} \frac{\sigma_l^2 E_c}{N_0} + \sum_{l=1}^{L_p} \frac{\sigma_l^2 E_c (K-1)}{3N_0} + 1 \right)
\end{aligned} \tag{5.76}$$

Define σ_s^2 as:

$$\sigma_s^2 = \sigma_{H_0}^2 / \sigma_{H_1}^2 \tag{5.77}$$

Therefore using (5.75) and (5.76), (5.77) can be written as:

$$\sigma_s^2 = \frac{\sum_{l=1}^{L_p} \frac{\sigma_l^2 E_c}{N_0} + \sum_{l=1}^{L_p} \frac{\sigma_l^2 E_c (K-1)}{3N_0} + 1}{\sum_{l=1}^{L_p} \frac{\sigma_l^2 E_c}{N_0} \frac{G}{N} + \sum_{l=1}^{L_p} \frac{\sigma_l^2 E_c (K-1)}{3N_0} + 1} \tag{5.78}$$

From equation (3.33), the overall power in each path is normalised to unity through σ_l^2 .

Thus for a frequency non-selective fading channel, $\sigma_l^2 = 1$ as it should be, from (3.33)

since $l = L_p = 1$.

From the derived results in this section, it is seen that the mean of the signal at the output of the MF is zero but with variances given by (5.75) and (5.76). Therefore, the

statistics of the output of the MF under H_1 is chi-square distributed with 2 degrees of freedom and its pdf is given as:

$$P(v | H_1) = \frac{1}{2\sigma_{H_1}^2} e^{-\left(\frac{v}{2\sigma_{H_1}^2}\right)}, \quad v \geq 0 \quad (5.79)$$

However, under H_0 , the pdf is the same as (5.52).

After PDI in the second dwell, and under H_1 , v is chi-square distributed with $2L$ degrees of freedom and its pdf is given as:

$$P(v | H_1) = \frac{v^{L-1}}{(2\sigma_{H_1}^2)^L \Gamma(L)} e^{-\left(\frac{v}{2\sigma_{H_1}^2}\right)}, \quad v \geq 0 \quad (5.80)$$

Also in the second dwell, under H_0 , the pdf is the same as (5.54). The pdf after CA-CFAR processing is still the same as in (5.55) and (5.56).

The P_d and P_{fa} for a CA-CFAR detection technique are given as follows.

In the first dwell, using (5.79) and (5.55) in (5.58) yields:

$$P_{d1} = \int_0^\infty \frac{u^{n-1}}{(2\sigma_{H_0}^2)^n \Gamma(n)} e^{-\frac{u}{2\sigma_{H_0}^2}} \int_{T_1 u}^\infty \frac{1}{2\sigma_{H_1}^2} e^{-\frac{v}{2\sigma_{H_1}^2}} dv du \quad (5.81)$$

From Appendix II, (5.81) is given as:

$$P_{d1} = \left(\frac{1}{1 + T_1 \sigma_s^2} \right)^n \quad (5.82)$$

The false alarm probability, P_{fa1} in the first dwell is the same as in (5.61).

For the second dwell, substitution of (5.80) and (5.56) into (5.58) results in:

$$P_{d2} = \int_0^\infty \frac{u^{Ln-1}}{(2\sigma_{H_0}^2)^{Ln} \Gamma(Ln)} e^{-\frac{u}{2\sigma_{H_0}^2}} \int_{T_1 u}^\infty \frac{v^{L-1}}{(2\sigma_{H_1}^2)^L \Gamma(L)} e^{-\frac{v}{2\sigma_{H_1}^2}} dv du \quad (5.83)$$

From appendix II, (5.83) is given as:

$$P_{d2} = \sum_{q=0}^{L-1} 1/q! \frac{(Ln-1+q)!(T_2\sigma_s^2)^q}{(Ln-1)!(1+T_2\sigma_s^2)^{Ln+q}} \quad (5.84)$$

The false alarm probability in the second dwell is the same as in (5.64).

5.3.2. Mean Acquisition Time

The performance of a code acquisition circuit is usually measured by the mean acquisition time denoted here as $E\{T_{acq}\}$. It is the average time that elapsed while searching the code phases before the declaration of acquisition. After this time, the tracking loop is enabled. A successful tracking loop operation is now followed by data transmission. Therefore, the time taken to complete the acquisition process is an important parameter measure of the circuit performance. $E\{T_{acq}\}$ depends on P_{fa} and P_d (and P_d is a function of the SNR of the environment in which the circuit is operating). The uncertainty region is divided into a number of discrete PN chip positions known as cells, as explained in Chapter 4. Since the step-search size, Δ is 1; it is assumed that there is only one synchro cell. Once this cell is identified, the acquisition process is completed and tracking enabled. In doing the search, the probability distribution of the circuit making a decision that the present cell is the synchro cell, is assumed to be a Markov process [55]. A Markov process [22] is a random process whose past has no influence on the future if its present is specified. Therefore, in carrying out the analysis of the acquisition process, it will be assumed that the test done on the present cell is independent from the previous tests. It is also assumed that the circuit has no prior knowledge of the position of the correct cell and thus the search can start in any of the cells. This is known as uniform serial search [10]. If there is some information about the

position of the correct cell, then other search techniques could be used [10]. A state transition diagram technique used in the analysis of Markov processes was first utilised in [55] to derive the $E\{T_{acq}\}$. The technique in [55] is difficult to analyse especially for multiple dwell systems. In [11, 54], a simple state transition diagram of the acquisition process based on uniform serial search was presented. This was a unified flow graph that can easily be applied to any acquisition system. This is the technique that will be used in the analysis of this proposed circuit. If the uncertainty region is made up of W cells and it is assumed that acquisition is achieved in the W th cell, and then from [11, 54], a reduced state transition diagram for the search process is shown in Figure 5.4 where i indicates the position of the i th cell.

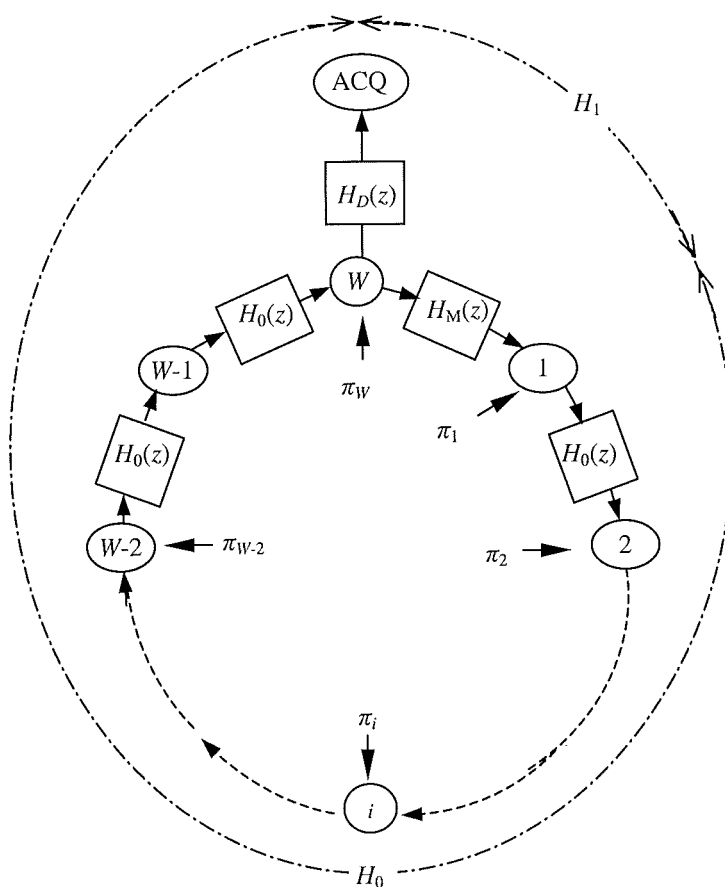


Figure 5.4. Reduced flow-graph of the state transition diagram

From Figure 5.4, $H_D(z)$ is the gain of the branch connecting the synchro cell to the acquisition state (ACQ), $H_M(z)$ is the gain of the branch connecting the missed cell to the first non-synchro cell, $H_0(z)$ is the gain of the branch connecting one non-synchro cell to another (non-synchro or the synchro) cell. $H_D(z)$ and $H_M(z)$ fall under the H_1 hypothesis and $H_0(z)$ under the H_0 hypothesis. As already explained, the synchro cell is located in the H_1 region. This is where true acquisition can occur while the rest non-synchro cells are located in the H_0 region where no true acquisition can occur.

Before using Figure 5.4 to derive the $E\{T_{acq}\}$, it is necessary to look in detail the expanded H_1 and H_0 regions. Figure 5.5 shows the expanded H_1 region for a double dwell acquisition system. It is seen that each branch is labelled with the product of the transition probability (P_d) and z raised to a power, t_{dr} ($r = 1, 2$ dwells). T_{dr} is equal to the duration of time (dwell time) associated with the transition. z is a unit delay operator.

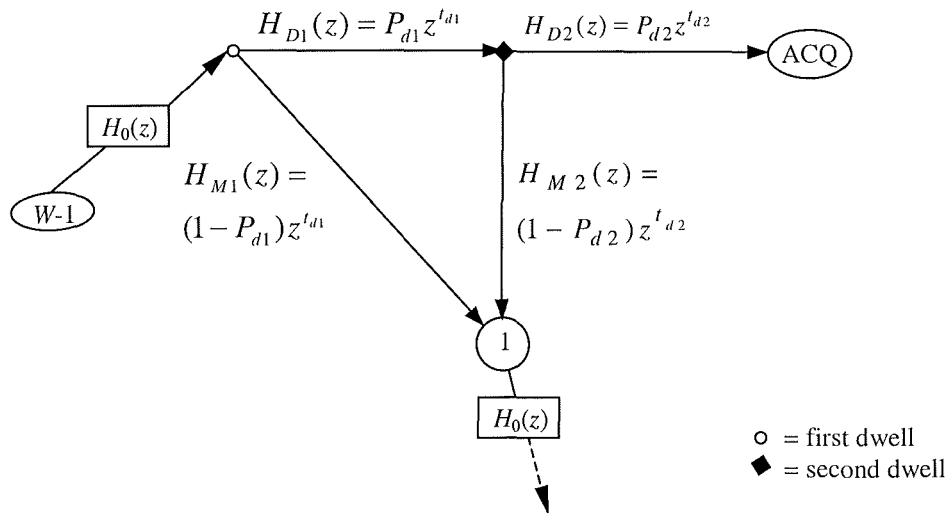


Figure 5.5. The expanded H_1 region for the double dwell acquisition system

$H_{D1}(z)$ is the gain of the branch connecting the first dwell to the second dwell for the

synchro cell. $H_{D2}(z)$ is the gain of the branch connecting the second dwell to ACQ. That is, the ACQ state is reached only on successful detection in the first and second dwell. $H_D(z)$ in Figure 5.4 is thus the product of $H_{D1}(z)$ and $H_{D2}(z)$ in Figure 5.5. Using signal flow diagrams reduction rules [56], $H_D(z)$ is given by:

$$H_D(z) = H_{D1}(z)H_{D2}(z) = P_{d1}z^{t_{d1}}P_{d2}z^{t_{d2}} = P_{d1}P_{d2}z^{(t_{d1}+t_{d2})} \quad (5.85)$$

P_{d1} means probability of detection in the first dwell and P_{d2} means probability of detection in the second dwell. t_{d1} and t_{d2} are the dwell times.

$H_M(z)$ in Figure 5.4 is made up of $H_{M1}(z)$ and $H_{M2}(z)$ as shown in Figure 5.5. $H_{M1}(z)$ is a miss of the synchro cell in the first dwell, which is equal to $(1-H_{D1}(z))$. $H_{M2}(z)$ is a miss of the synchro cell in the second dwell, which is equal to $(1-H_{D2}(z))$. Therefore, the H_M region can be described by the following equations:

$$\begin{aligned} H_M(z) &= 1 - H_{D1}(z) + H_{D1}(z)(1 - H_{D2}(z)) \\ &= (1 - P_{d1})z^{t_{d1}} + P_{d1}(1 - P_{d2})z^{(t_{d1}+t_{d2})} \end{aligned} \quad (5.86)$$

Similarly, the expanded $H_0(z)$ for i th cell in the H_0 region is shown in Figure 5.6. $H_{nfa1}(z)$ is the gain of the branch indicating that a non-synchro cell is correctly identified in the first dwell and the next cell is searched. $H_{fa1}(z)$ is the gain of the branch indicating that a non-synchro cell is falsely accepted as the synchro cell in the first dwell and the second dwell is enabled. $H_{nfa2}(z)$ is the gain of the branch indicating that a non-synchro cell is correctly identified in the second dwell and the next cell is searched. $H_{fa2}(z)$ is the gain of the branch indicating that a non-synchro cell is falsely accepted as the synchro cell in the second dwell, thus enabling the tracking circuit. This will put the circuit in a false alarm state, fa . Once this false cell is detected, the circuit returns to the search

stage with a false alarm penalty time, $T_{fa}T_c$ (T_{fa} is taken as an integer number of code chips) with a branch gain of $H_p(z) = z^{T_{fa}T_c}$.

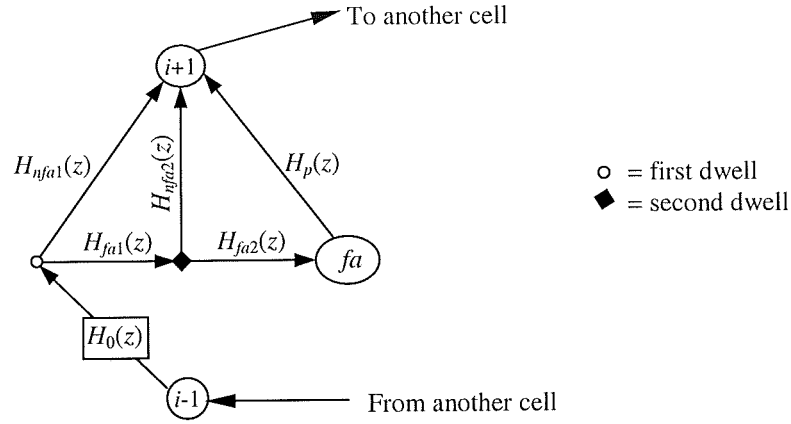


Figure 5.6. An expanded $H_0(z)$ for the i th cell in the H_0 region

From Figure 5.6, the following are defined:

$$H_{fa1}(z) = P_{fa1}z^{t_{d1}}, H_{nfa1}(z) = (1 - P_{fa1})z^{t_{d1}}, H_{fa2}(z) = P_{fa2}z^{t_{d2}} \text{ and } H_{nfa2}(z) = (1 - P_{fa2})z^{t_{d2}}.$$

P_{fa1} means probability of false alarm in the first dwell and P_{fa2} means probability of false alarm in the second dwell. Thus:

$$\begin{aligned} H_0(z) &= H_{nfa1}(z) + H_{fa1}(z)H_{nfa2}(z) + H_{fa1}(z)H_{fa2}(z)H_p(z) \\ &= (1 - P_{fa1})z^{t_{d1}} + P_{fa1}(1 - P_{fa2})z^{(t_{d1}+t_{d2})} + P_{fa1}P_{fa2}z^{(t_{d1}+t_{d2}+T_{fa}T_c)} \end{aligned} \quad (5.87)$$

The above analysis showed the different probabilities associated with each cell in the uncertainty region. Therefore, using Figure 5.4, the probability of the search starting in the i th cell is given by $\pi_i = 1/W$. The acquisition generating function, $H(z)$ can be defined to represent the sum of the transition probabilities and dwell times for each cell as:

$$H(z) = \sum_{i=1}^W H_i(z) \quad (5.88)$$

where each sub-function, $H_i(z)$ represents the product of the transition probabilities and dwell times for each cell.

In the first instance, assume that the search started from cell i and acquisition is achieved at cell W . The product of the transition probabilities and associated dwell times from the i th H_0 cell to the acquisition state is given as:

$$H_{i0}(z) = \pi_i [H_0(z)]^{W-i} H_D(z) \quad (5.89)$$

If there is a miss of the correct code phase, it is seen from Figure 5.4 that the search will continue round the circular diagram until it reaches the W th cell again. The product of this path for a missed detection is given by:

$$H_{i1}(z) = \pi_i [H_0(z)]^{W-i} H_D(z) \{H_M(z) [H_0(z)]^{W-1}\}^1 \quad (5.90)$$

Therefore, for k missed detections, (5.90) can be written as:

$$\begin{aligned} H_{ik}(z) &= \pi_i [H_0(z)]^{W-i} H_D(z) \{H_M(z) [H_0(z)]^{W-1}\}^k \\ &= \pi_i [H_0(z)]^{W(k+1)-i-k} [H_M(z)]^k H_D(z) \end{aligned} \quad (5.91)$$

It is also possible that there could be an infinite miss of the correct cell, therefore:

$$\begin{aligned} H_i(z) &= \sum_{k=0}^{\infty} H_{ik}(z) \\ &= \pi_i H_D(z) [H_0(z)]^{W-i} \sum_{k=0}^{\infty} [H_0(z)]^{(W-1)k} [H_M(z)]^k \\ &= \pi_i H_D(z) [H_0(z)]^{W-i} \frac{1}{1 - H_M(z) H_0^{(W-1)}(z)} \end{aligned} \quad (5.92)$$

Therefore, substituting (5.92) into (5.88) gives:

$$\begin{aligned} H(z) &= H_D(z) \frac{1}{1 - H_M(z)H_0^{(W-1)}(z)} \sum_{i=1}^W \pi_i [H_0(z)]^{W-i} \\ &= \frac{1}{W} \frac{H_D(z)(1 - H_0^W(z))}{(1 - H_M(z)H_0^{(W-1)}(z))(1 - H_0(z))} \end{aligned} \quad (5.93)$$

The $E\{T_{acq}\}$ is calculated as:

$$\begin{aligned} E\{T_{acq}\} &= \left[\frac{d}{dz} H(z) \right]_{z=1} \\ &= \frac{1}{H_D(1)} \left\{ H_D'(1) + H_M'(1) + (W-1)H_0'(1) \left(1 - \frac{H_D(1)}{2} \right) \right\} \end{aligned} \quad (5.94)$$

where, $H(1) = H(z)|_{z=1}$ and $H'(1) = \frac{d}{dz} H(z)|_{z=1}$.

Therefore,

$$H_D(1) = P_{d1}P_{d2} \quad (5.95a)$$

$$H_D'(1) = (t_{d1} + t_{d2})P_{d1}P_{d2} \quad (5.95b)$$

$$H_M'(1) = t_{d1} + P_{d1}t_{d2} - P_{d1}P_{d2}t_{d1} - P_{d1}P_{d2}t_{d2} \quad (5.95c)$$

$$H_0'(1) = t_{d1} + P_{fa1}t_{d2} + P_{fa1}P_{fa2}T_{fa}T_c \quad (5.95d)$$

For the proposed circuit, $t_{d1} = T_c$ and $t_{d2} = LT_c$. That is for the first dwell, the output of the MF is observed at the sampling instant, T_c . In the second dwell, the time to perform the L PDI is given as LT_c . The time taken to fill the MF prior to the first sampling instant is NT_c . The time used to perform the adaptive threshold processing prior to acquisition decision in the first and second dwells are given as nT_c and LnT_c respectively. By substituting (5.95) into (5.94) and taking these additional times into consideration, $E\{T_{acq}\}$ for the proposed circuit is given as:

$$E\{T_{acq}\} = \frac{T_c}{P_{d1}P_{d2}} \left(1 + P_{d1}L + (W-1)[1 + P_{fa1}L + T_{fa}P_{fa1}P_{fa2}](1 - P_{d1}P_{d2}/2) \right) + NT_c + nT_c + LnT_c \quad (5.96)$$

In the results, $E\{T_{acq}\}$ is normalised by dividing it with the product of the uncertainty region, W and the chip duration, T_c . That is, the normalised mean acquisition time is given as $E\{T_{acq}\} / WT_c$.

5.3.3. Numerical Results

In the numerical results that now follow, unless otherwise stated, the following parameters are used for the analysis. The PN code is m -sequence of length is 32,767 chips. The search step-size is ΔT_c with $\Delta=1$ and so $W = 32,767$ chips. The MF is of length, $N = 64$. $L = 4$ is used for the PDI. The penalty time, $T_{fa} = 10^3$ chips. It is also assumed that the channel is slowly fading with normalised Doppler shift $f_D T_c = 1 \times 10^{-4}$. Results are presented using the equations already derived for the cases of Ricean, frequency non-selective and frequency selective Rayleigh fading channels. The initial part of the results assumes that there is only one user and so MAI is not considered. Also, the effects of jamming and frequency error are not considered. Irrespective of the channel model, these interferences have the same effect on the circuit performance and hence they are treated separately for ease of understanding.

A. Ricean Fading Channel

5.3.3.1. Choice of P_{fa}

It is always desired for the circuit to have a low P_{fa} and a high P_d ^{5.2}. However, the same threshold, $T_r u$ as can be deduced from Figure 5.2 determines the values of P_{fa} and P_d . If T_r is high, $T_r u$ will be high, and vice versa. To achieve a low P_{fa} , it means that a high T_r has to be used (note the relationship between T_r and P_{fa} in (5.61) and (5.64)). The consequence as expected is that the P_d will also be low. Therefore, once the SNR in which the circuit is expected to operate is chosen, a threshold should be determined that will give the minimum $E\{T_{acq}\}$. In Figure 5.7, a plot of the normalised $E\{T_{acq}\}$ versus P_{fa} for different values of SNR is shown.

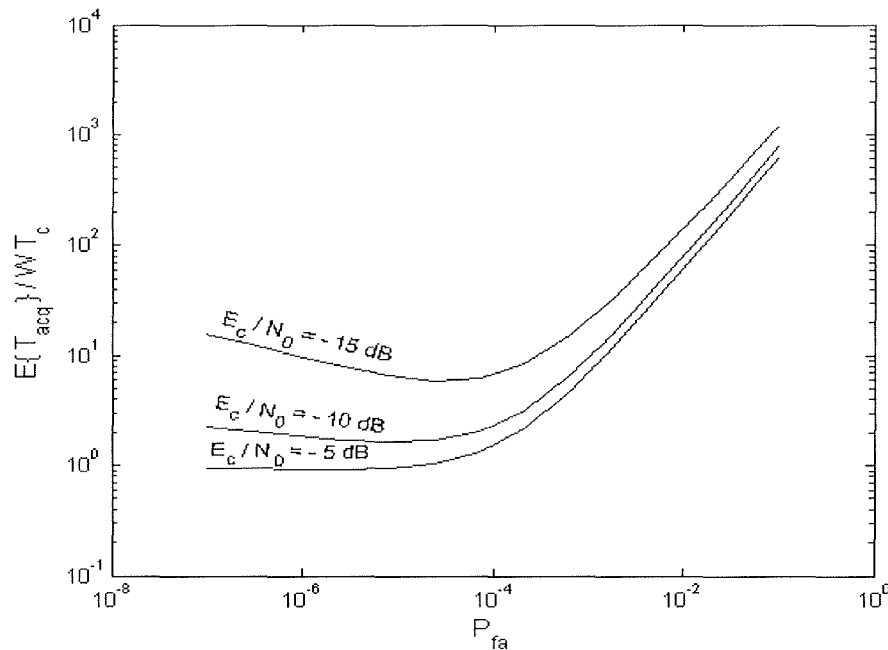


Figure 5.7. Choosing a P_{fa} (Ricean factor, $k_R = 0$ dB)

From the figure, if the circuit is expected to operate with $E_c / N_0 = -15$ dB, then a T_r that

^{5.2} $P_{fa} = P_{fa1}P_{fa2}$ and $P_d = P_{d1}P_{d2}$

gives $P_{fa} \approx 0.8 \times 10^{-5}$ is appropriate. In this analysis, a T_r that gives $P_{fa} = 10^{-5}$ at $E_c / N_0 = -5$ dB is used. Once T_r is chosen, variation of the noise power, u will lead to the variation of the threshold, $T_r u$ as already explained in Section 5.1. Thus the circuit will adaptively select the threshold for a constant value of P_{fa} . Though the P_{fa} is constant, the P_d will vary as the threshold adaptively varies, leading to a corresponding variation in the $E\{T_{acq}\}$.

Figure 5.8 is a plot of P_{fa} as a function of SNR for the adaptive and non-adaptive circuits. While the adaptive circuit maintains a constant false alarm rate, the non-adaptive circuit's false alarm rate varies according to the SNR. This means that it cannot detect the desired code phase position as fast as the adaptive circuit. For the non-adaptive circuit, a threshold that gives $P_{fa} = 10^{-5}$ at $E_c / N_0 = -5$ dB was used.

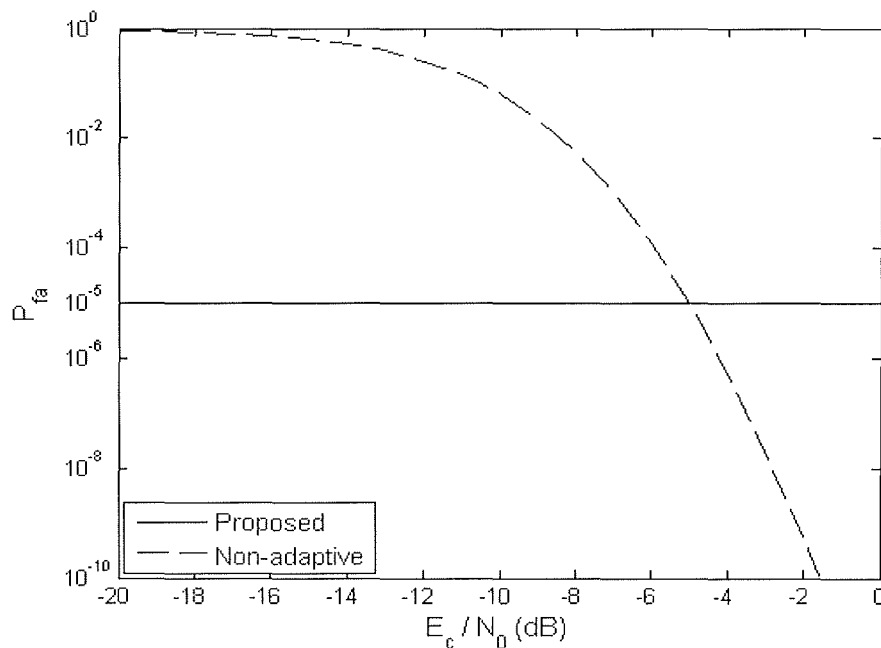


Figure 5.8. Plot showing the effect of SNR on P_{fa} (Ricean factor, $k_R = 0$ dB)

5.3.3.2. Effect of Ricean Factor

The effects of the Ricean factor, k_R on the circuit performance are shown in Figures 5.9 and 5.10. It is seen that as k_R increases, the channel tends toward an AWGN channel. This is reflected in the increasing P_d , resulting in reducing $E\{T_{acq}\}$. This is because as k_R increases, the signal strength of the LOS path increases and becomes the dominant signal. The reverse is the case when k_R decreases, tending towards Rayleigh fading channel when $k_R = -\infty$ dB. Also, as SNR improves, it is observed that the curves tend to converge. This results from the fact that at high SNR, the probability of detecting the synchro cell is also high as the effect of noise on the circuit performance is being mitigated. In the rural areas, due to the sparse locations of buildings, the LOS signal is present most of the time and there are also some Rayleigh faded multipath components. The channel condition in a rural area is therefore Ricean fading channel [16].

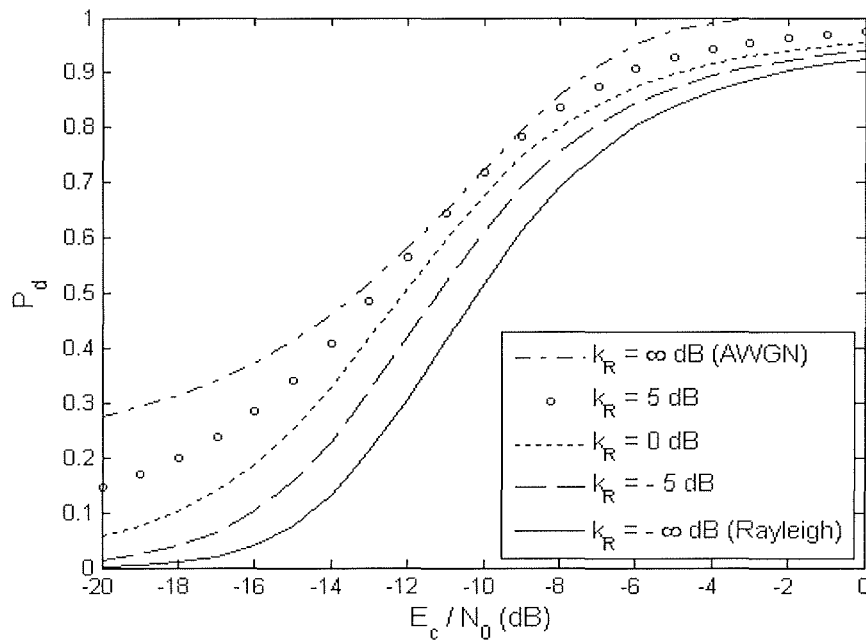


Figure 5.9. Plot showing the effect of k_R on P_d

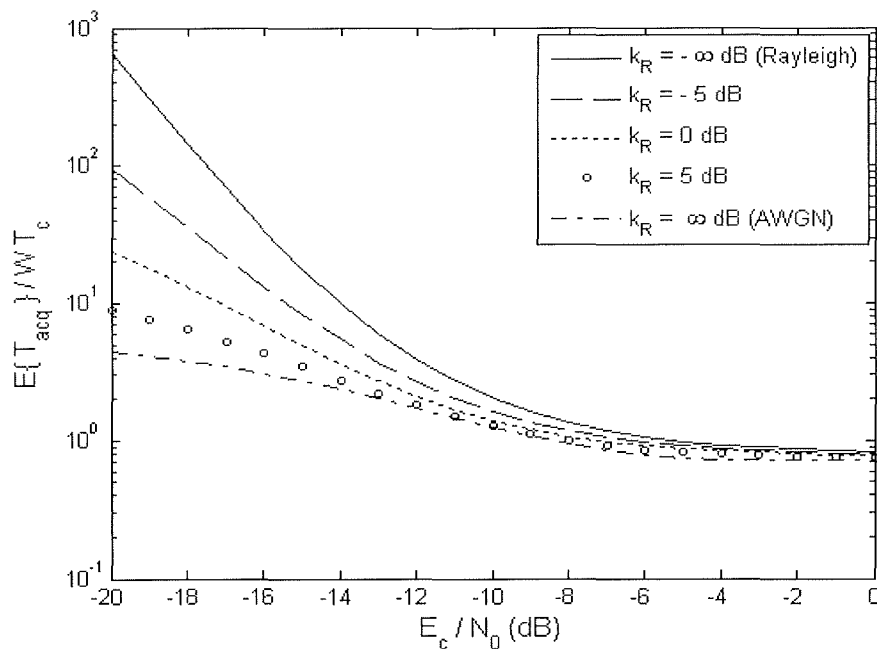


Figure 5.10. Plot showing the effect of k_R on $E\{T_{acq}\}$

A similar technique using CA-CFAR adaptive technique was analysed in [14] for an AWGN channel only. In [14], the second dwell was implemented by using another MF of longer length (let this method be denoted as MF-LL technique) with length $N/2$. This is compared to the proposed circuit where the second dwell was implemented with a PDI of $L = 4$. The results are shown in Figure 5.11 for $k_R = \infty$ dB. It can be seen that as $N/2$ increases, the performance of the method of MF-LL improves and becomes much better than the proposed circuit. This is as a result of the direct relationship between SNR and correlation length (i.e. number of correlated chips), N – since E_c/N_0 is defined as the SNR per chip. This means that SNR can be improved by correlating more number of chips. This brings about improvement in the MF-LL method as $N/2$ increases. For the proposed circuit, PDI was used to improve the SNR in the second dwell. With reference to Figure 5.11, the MF-LL method performs better than the proposed circuit in an AWGN channel. However, for a fair comparison of the proposed and MF-LL

methods, it is important to consider other channel conditions and some practical implementation issues. First and foremost, the effect of frequency offset (to be considered in Section E) was ignored in the results shown in Figure 5.11. Frequency offset is always a problem in non-coherent detectors that are used in realising these circuits [9, 11]. Secondly, the result in Figure 5.11 was considered in an AWGN channel only. Also to be noted is the fact that the proposed circuit was implemented by using just one MF of length $N = 64$ in the first dwell and the second dwell implemented by PDI. For the MF-LL method, each of such circuit as in Figure 5.1 was used for each dwell. In the first dwell, MF length of $N_1 = 64$ was used and for the second dwell circuit, MF length of N_2 ($N_2 > N_1$) was used. Thus, the proposed method is less complex.

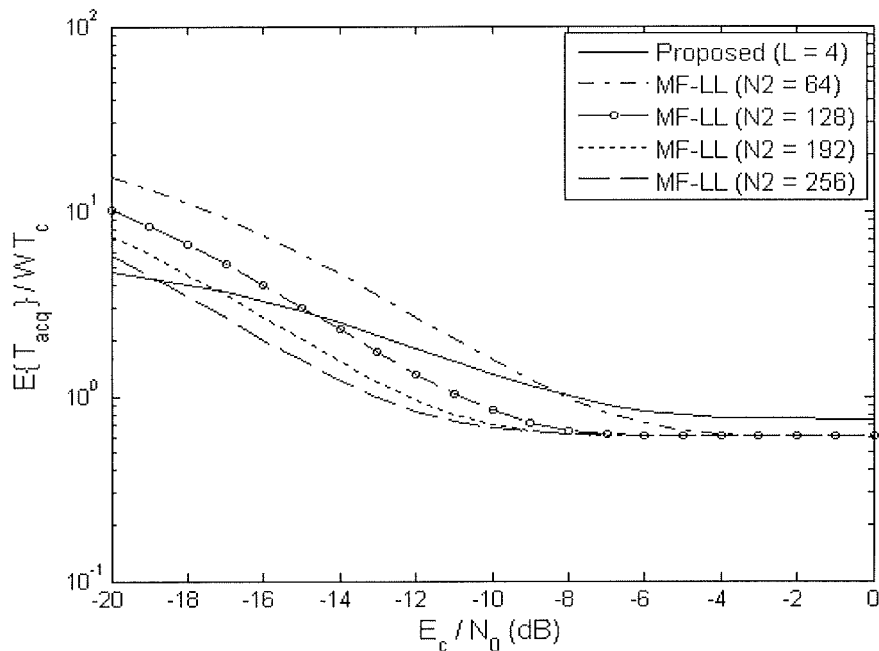


Figure 5.11. Performance comparison of the proposed and the MF-LL methods

Figure 5.12 compares the performance of the two circuits in AWGN and Rayleigh

fading channels (i.e. $k_R = \infty$ and $-\infty$ dB respectively). In the case of Rayleigh fading channel, normalised Doppler shifts of $f_D T_c = 1 \times 10^{-4}$ and $f_D T_c = 5 \times 10^{-3}$ were used. $N_2 = 256$ was used for the correlation length in the second dwell of the MF-LL method. When the channel is purely AWGN, as already explained in Figure 5.11, the MF-LL method performed better than the proposed circuit. However, as the fading in the channel increases, characterised by the increasing Doppler shift, the MF-LL performance degrades rapidly due to the use of a longer length of MF in the second dwell. Further details of how the relationship between Doppler shift and length of MF affects the circuit performance are given in Section 5.3.3.3. For the proposed circuit, even though fading results in reduction in the signal power, PDI improves the SNR by rebuilding up the amplitude of the signal attenuated by fading.

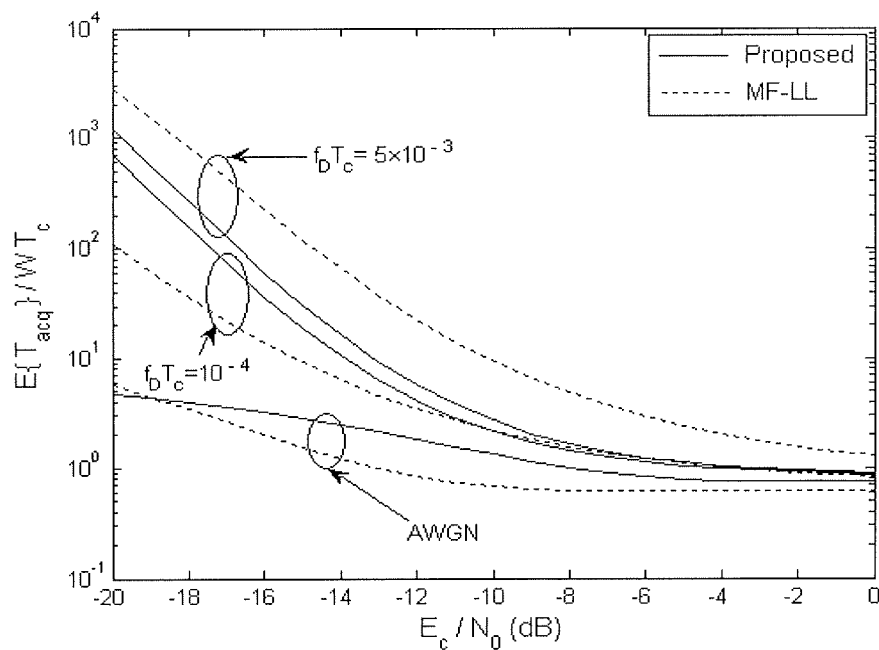


Figure 5.12. Comparison of the proposed and the MF-LL methods in AWGN and Rayleigh fading channel

This is the PDI technique mostly used in radar [15], where a number of reflected pulses are integrated to improve the SNR. In mobile environments, fading cannot be avoided, and thus the proposed circuit can achieve a reasonable acquisition time performance in the fading channel.

B. Frequency Non-selective Rayleigh Fading Channel

In this section, the performance of the circuit in a frequency non-selective Rayleigh fading channel is considered. A frequency non-selective fading channel, commonly called Rayleigh fading channel, is mostly encountered in urban mobile environment where there is no LOS signal path between the transmitter and receiver and the received signal is composed of a continuum of multiple paths that cannot be resolved into distinct paths.

5.3.3.3. Effect of N and Doppler Shift on P_d

From the mathematical equations relating P_{fa} and P_d , it is seen that P_{fa} is independent of the correlation length or SNR but P_d depends heavily on these parameters. Figure 5.13 shows the effect of N on P_d . As N increases, P_d increases. This is due to the fact that E_c / N_0 is defined as the SNR per chip and so as the number, N of correlated chips increases, the overall SNR increases. This was done using a normalised Doppler shift of $f_D T_c = 1 \times 10^{-4}$. It is necessary to see the effect of the rate of Doppler shift on the circuit performance as N increases.

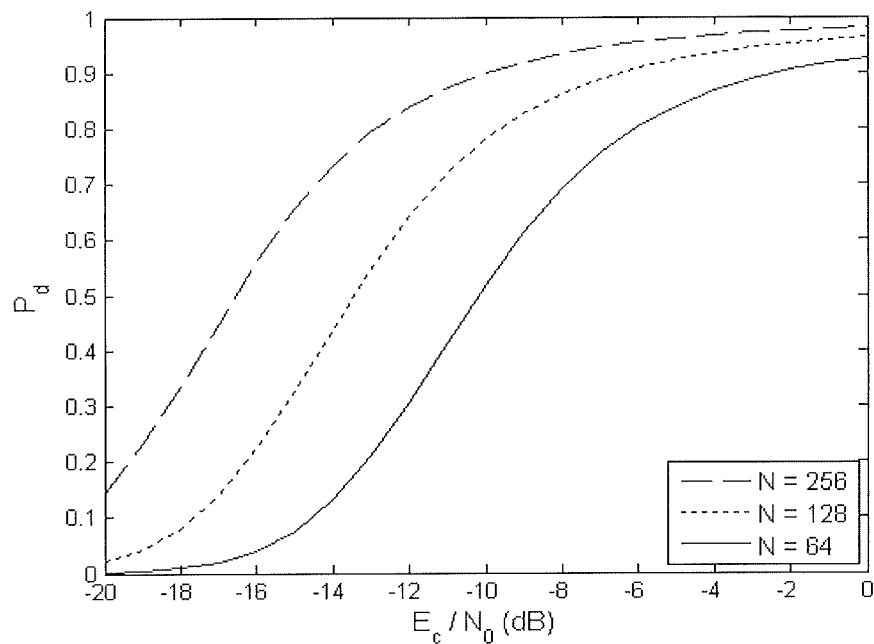


Figure 5.13. Effect of N on P_d ($f_D T_c = 10^{-4}$)

Figure 4.14 shows the detection probability as a function of the SNR for different values of normalised Doppler shift, $f_D T_c$. From (5.28), as long as $1/f_D$ is much greater than T_c or $f_D T_c \ll 1$, the fading can be assumed to be constant over each successive correlation interval, which is T_c . This is usually the case in practice (a slowly fading channel). However, as f_D increases, successive chips become highly correlated. This leads to a reduction in the available SNR, which results in a reduced P_d . Thus as the f_D increases, the fading in the channel increases.

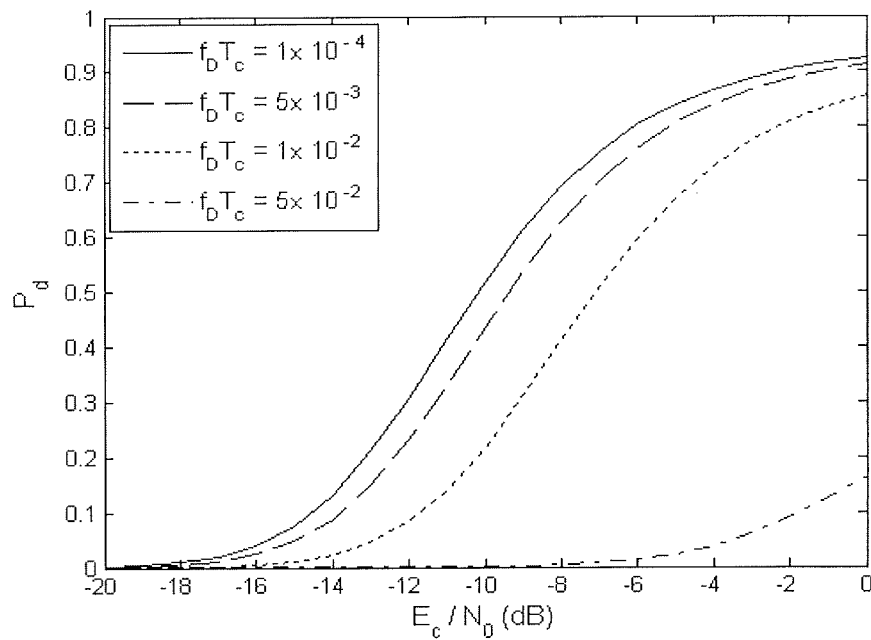


Figure 5.14. Effect of Doppler shift on P_d ($N = 64$)

Figure 5.15 shows the effect of increasing N as $f_D T_c$ increases. From (5.78), G / N (where $G = N + 2 \sum_{\iota=1}^{N-1} (N - \iota) \rho_{\iota}$) is the only parameter that is not common to the numerator and denominator. Increasing G will increase P_d . But the second term in G is a function of the channel autocorrelation function, $\rho_{\iota} = J_0(2\pi \iota f_D T_c)$. Figure 5.15 shows that as $f_D T_c$ increases, a point is reached whereby increasing the correlation length will no longer be useful in increasing the P_d , contrary to its effect as shown in Figure 5.13. In fact, the longer the correlation length, N the worse the circuit performance. Specifically, when $f_D T_c > 10^{-3}$ then G / N begins to decrease.

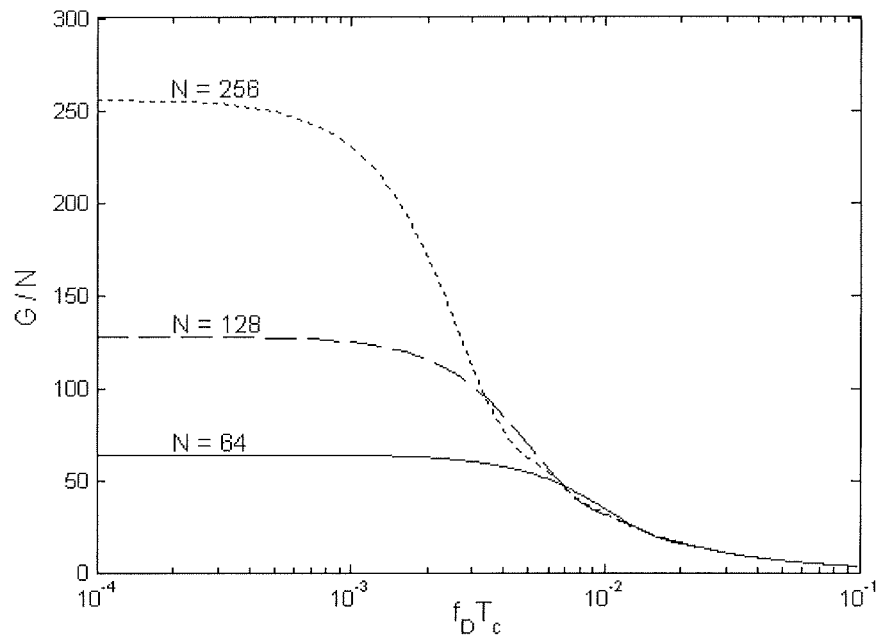


Figure 5.15. Effect of Doppler shift on G/N

At $f_D T_c > 5 \times 10^{-3}$, G/N rapidly decreases for $N = 256$ while it is only slight for $N = 64$. The use of PDI to improve the performance of the circuit instead of increasing the correlation length becomes a more feasible option in this situation. Though the technique used in [14] is quite useful in an AWGN channel, it is clear that for a fading channel, that method will not give a reliable performance. Thus, the proposed circuit can give a good measure of robustness to the fading channel. This further explains the results in Figure 5.12.

5.3.3.4. Effect of N and PDI on $E\{T_{acq}\}$

The effect of N on the circuit performance in terms of $E\{T_{acq}\}$ is shown in Figure 5.16. From (5.96), $E\{T_{acq}\}$ depends heavily on P_d and P_{fa} . However, P_d depends on E_c/N_0 , N and $f_D T_c$ for a given threshold. If E_c/N_0 and N are increased with $f_D T_c < 10^{-3}$, the P_d will

increase. This will result in reduced $E\{T_{acq}\}$. Again, it is also important to mention at this point that in non-coherent detectors, increasing N does not necessarily lead to increase in P_d (even though $f_D T_c < 10^{-3}$) as this might even lead to further degradation in SNR due to frequency offset, a topic for discussion later in Section E. However, ignoring the effect of frequency offset, it can be concluded that as the N increases, the circuit performance improves accordingly.

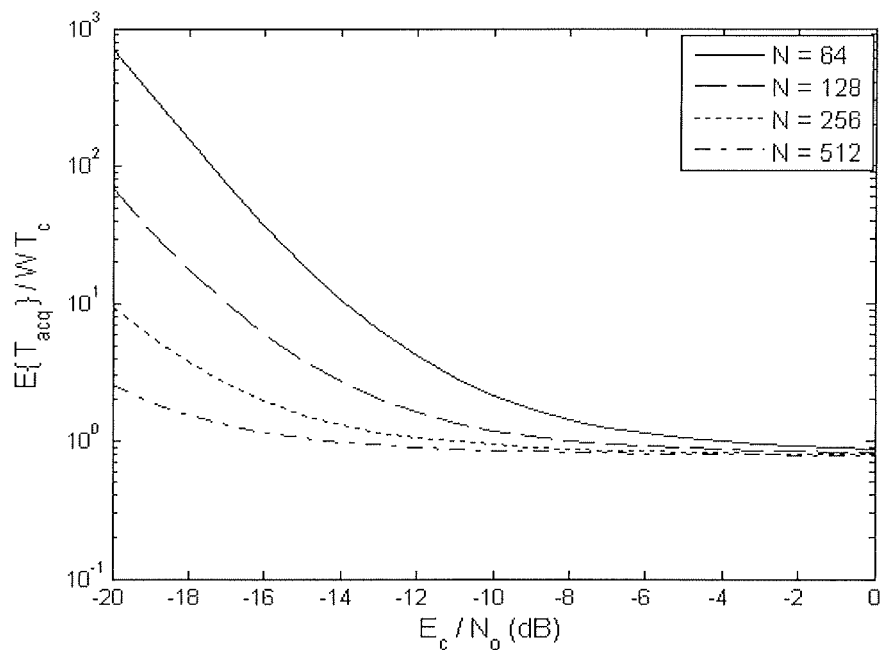


Figure 5.16. Plot of normalised $E\{T_{acq}\}$ for different values of N

Figure 5.17 shows the effect of PDI on $E\{T_{acq}\}$ for the proposed circuit in a slowly fading channel. As expected, the performance of the circuit is improved when the length, L of the PDI is increased. In this thesis however, $L = 4$ is used. In practical implementation, technical issues such power consumption, available memory space and associated components will determine the choice of L .

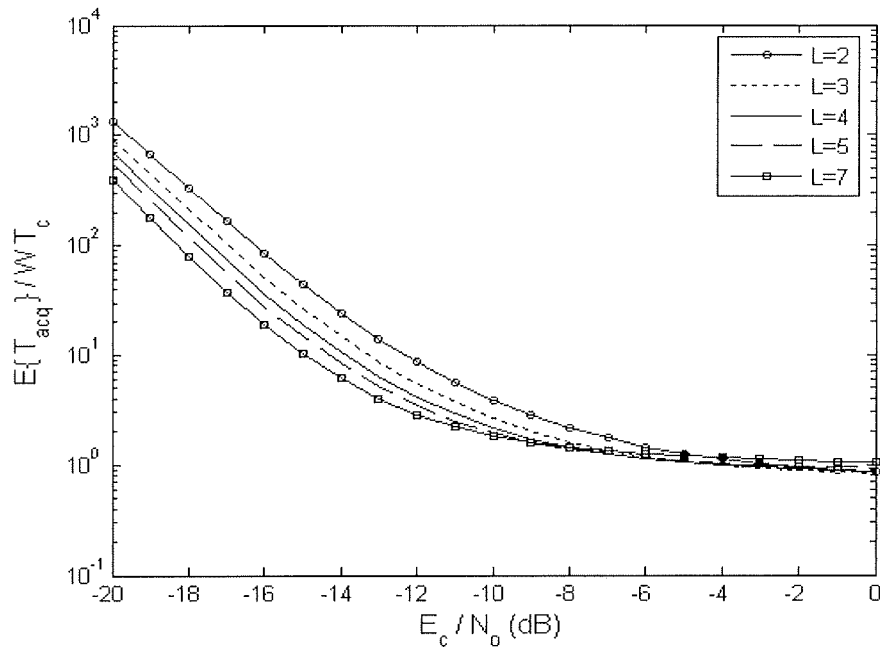


Figure 5.17. Plot of normalised $E\{T_{acq}\}$ for different length of PDI

5.3.3.5. Verification of P_{fa} , P_d and $E\{T_{acq}\}$ by Simulation

Having shown the numerical results of the proposed circuit, the theoretical analysis was verified by simulation using Matlab[®]. The results are shown in Figures 5.18 – 5.20. Monte Carlo simulation with no less than 10^6 runs was used to compute the P_{fa} and P_d ; and using these results, $E\{T_{acq}\}$ was determined. In the simulation, a frequency non-selective Rayleigh fading simulator based on Jakes method (Section 3.3.3.2) was used. The results obtained from the simulation were compared to the theoretical results and the strong agreement between theory and simulation validates the theoretical results in terms of derived equations for the proposed circuit. Figures 5.18 and 5.19 were obtained by pure Monte Carlo simulation. Figure 5.20 was by semi-analytical simulation as the simulation results of P_{fa} and P_d were used in the equation of $E\{T_{acq}\}$.

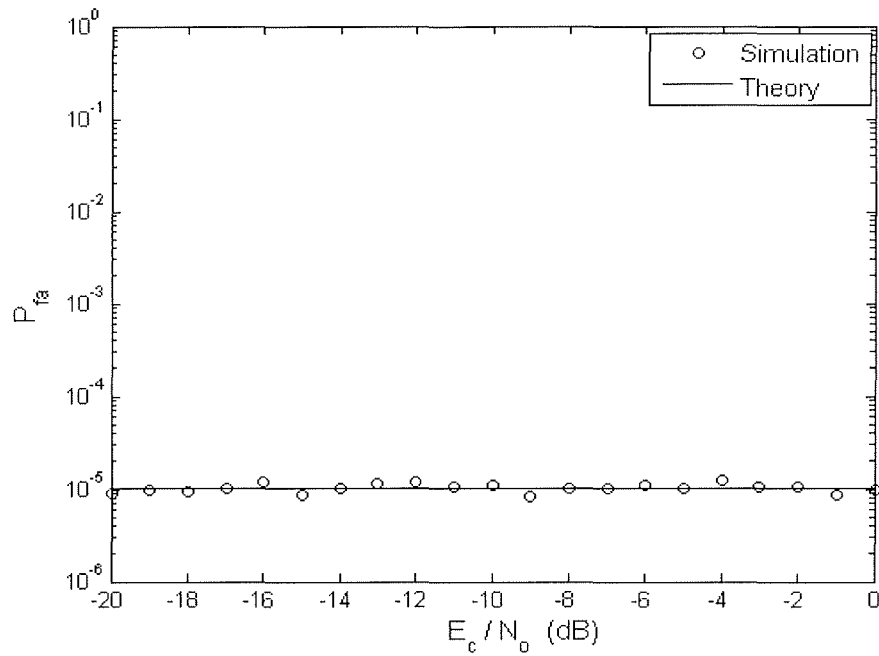


Figure 5.18. Theoretical and simulation results of the proposed circuit in terms of P_{fa}

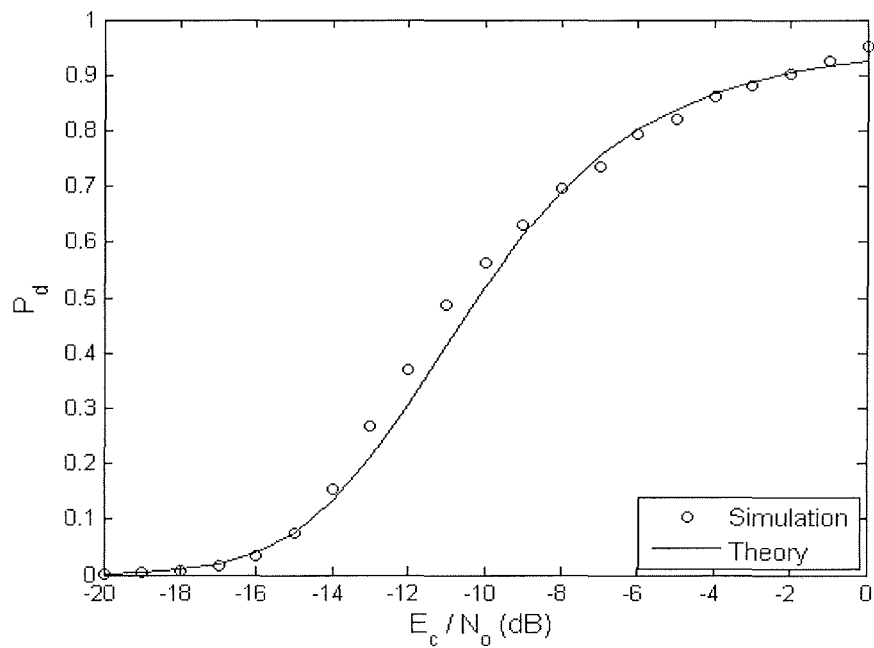


Figure 5.19. Theoretical and simulation results of the proposed circuit in terms of P_d

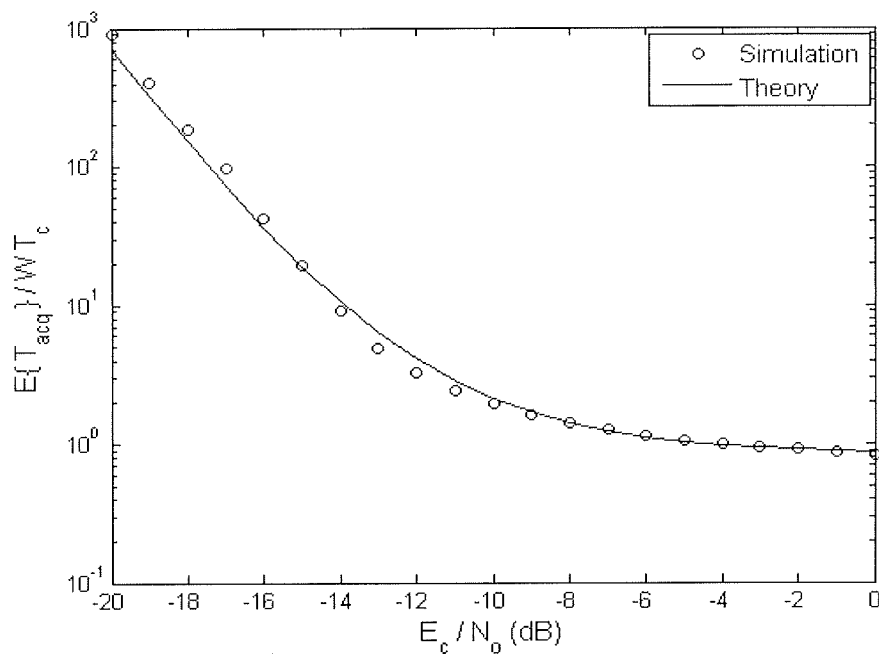


Figure 5.20. Theoretical and simulation results of the proposed circuit in terms of $E\{T_{acq}\}$

5.3.3.6. Performance Comparison

In this section, the proposed circuit is compared with a non-adaptive circuit, the MF-LL method and another circuit using a reference MF (denoted here as R-MF method). The R-MF method uses a reference circuit for the purpose of setting up the threshold adaptively. An acquisition circuit using the R-MF method was studied in [57] but in the verification stage, a coincidence detector (CD) was used instead of PDI. For a fair comparison (it has also been shown in [58] that the use of PDI performs better than the use of CD), the verification stage of the R-MF method used here is implemented by PDI of $L = 4$ as with the proposed circuit. Figure 5.21 shows the results. In the first dwell, the MF length for all the circuits is 64. For the second dwell, $L = 4$ is used for the PDI for the non-adaptive, the proposed and the R-MF circuits. Also for the non-adaptive

method, a threshold that gives a $P_{fa} = 10^{-5}$ at $E_c / N_0 = -5$ dB is used. For the MF-LL, $N_2 = 256$.

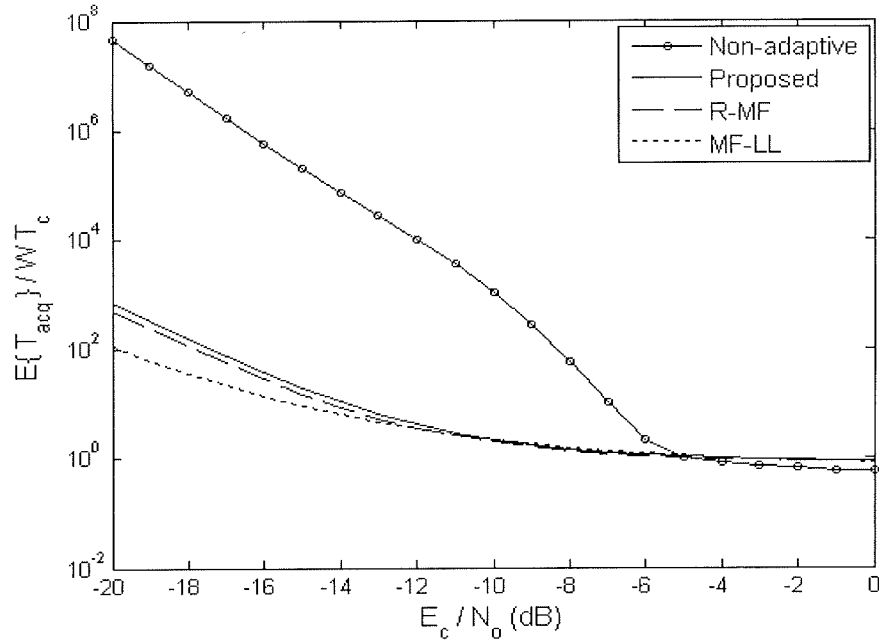


Figure 5.21. Comparison of the normalized $E\{T_{acq}\}$ of the adaptive and non-adaptive methods

It is seen that the proposed scheme gives a better performance than the non-adaptive method. For a SNR value above -5 dB, the non-adaptive method seems to perform better than the proposed method and the other adaptive circuits. This is expected since from Figure 4.8, the P_{fa} of the non-adaptive scheme begins to decrease with increase in SNR whereas all the adaptive schemes maintain a constant P_{fa} of 10^{-5} . In short, the proposed scheme gives a performance improvement of more than 9 dB than the non-adaptive method at SNR value of -7 dB. The only additional complexity of the proposed scheme is the CA-CFAR processor, which is not needed in the non-adaptive

circuit. However, a performance improvement greater than 9 dB compensate for this additional complexity.

When compared to the MF-LL method, it is seen that the performance of the proposed scheme approximates this method at high SNR ($E_c / N_o > -10$ dB). At lower SNR, the MF-LL performs better. In terms of complexity, the MF-LL is more complex than the proposed scheme. Even though the MF-LL performs better than the proposed scheme at low SNR, it should be noted that the effect of frequency offset is ignored.

When compared to the R-MF method, the performance of the proposed scheme approximates this method. The R-MF method just gives a little over 1 dB performance improvement. In terms of complexity, the proposed scheme is less complex. To implement the R-MF, a reference circuit similar to the proposed circuit, excluding the CA-CFAR processor is needed in addition to the main detecting MF circuit.

C. Frequency Selective Rayleigh Fading Channel

In the past sections, the performance of the proposed circuit in Ricean and frequency non-selective Rayleigh fading channels has been considered. In this section, the performance of the circuit in a frequency selective Rayleigh fading channel will be considered. A frequency selective fading channel is characterised by resolvable multipath. This multipath means that the circuit can declare acquisition once it is synchronised to any of these paths. Thus, the H_1 region has more than one synchro cell as shown in Figure 5.22.

$$\sigma_l^2 = \frac{1}{L_p}, \text{ (uniform)} \quad (5.100)$$

Assuming only one user, for the frequency selective Rayleigh fading channel, (5.75) and (5.76) are respectively given as:

$$\sigma_{H_1}^2 = \frac{NN_0T_c}{2} \left(\sum_{l=1}^{L_p} \frac{\sigma_l^2 E_c}{N_0} \frac{G}{N} + 1 \right), \quad (5.101)$$

$$\sigma_{H_0}^2 = \frac{NN_0T_c}{2} \left(\sum_{l=1}^{L_p} \frac{\sigma_l^2 E_c}{N_0} + 1 \right) \quad (5.102)$$

Equations (5.101) and (5.102) are substituted into (5.77) and are used in (5.82) and (5.84) for the purpose of computing the P_d of the proposed circuit.

5.3.3.7. Exponential MIP

The exponential MIP is characterised by a decaying rate η . The value of the power in each path, σ_l^2 is easily computed using (5.99). As the value of η is increased, so does the decaying rate and vice versa. Figure 5.23 is plot of the normalised mean acquisition time for a 4-path channel with $\eta = 0.6$. As the number of paths increases, the performance of the circuit deteriorates. Even though there are more paths that can lead to acquisition, it can be deduced from (5.99) that as the number of paths increases, the power in each path decreases. Thus there is less reliability of detection as compared to the frequency non-selective case ($L_p = 1$) where all the power is concentrated in one path. It can also be seen from the figure that as SNR increases, i.e. when $E_c / N_0 > -6$ dB, the performance seems to improve as the number of paths increases. This is due to the fact that the threshold is low enough to improve the probability of detection as all the paths have power values above the threshold.

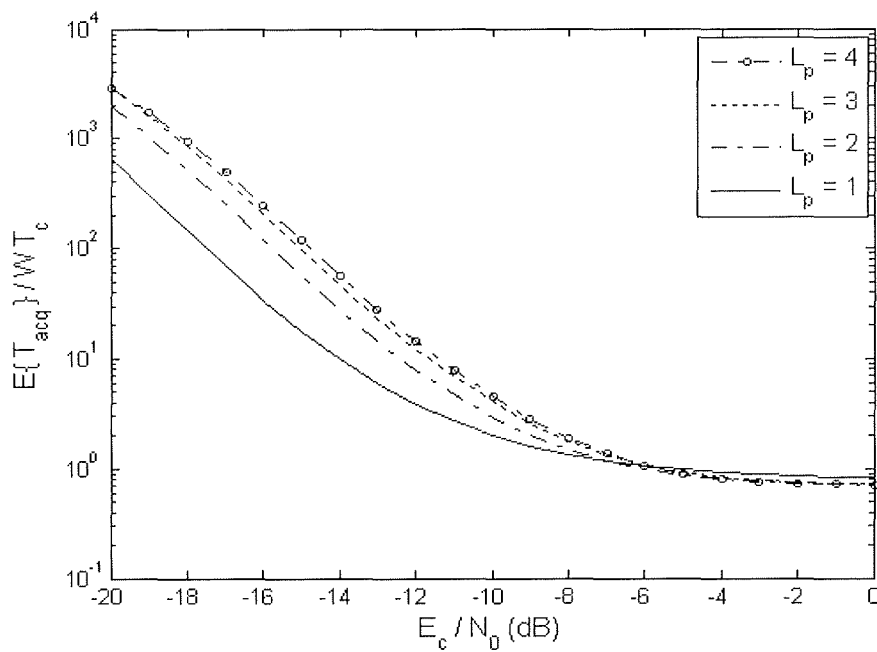


Figure 5.23. Plot of $E\{T_{acq}\}$ for a frequency selective Rayleigh fading channel using an exponential MIP with $\eta = 0.6$

5.3.3.8. Uniform MIP

For a uniform MIP, the power in each path is given by (5.100). This means that as the number of paths increases, the power per path decreases uniformly. The normalised mean acquisition time is shown in Figure 5.24. Similar to the exponential MIP case, the performance of the circuit also degrades as the number of paths increases. Comparing Figures 5.23 and 5.24, it can be observed that the exponential MIP model performs better than the uniform MIP model. This actually depends on the decaying rate, η . As $\eta \rightarrow 0$, the exponential MIP channel model approximates the uniform MIP model. Similar to the case of exponential MIP model, when $E_c / N_0 > -6$ dB, the performance of the circuit using the uniform MIP model begins to improve as the number of paths increases. Therefore, either model can be used in the analysis of a frequency selective Rayleigh fading channel as they lead to almost the same performance.

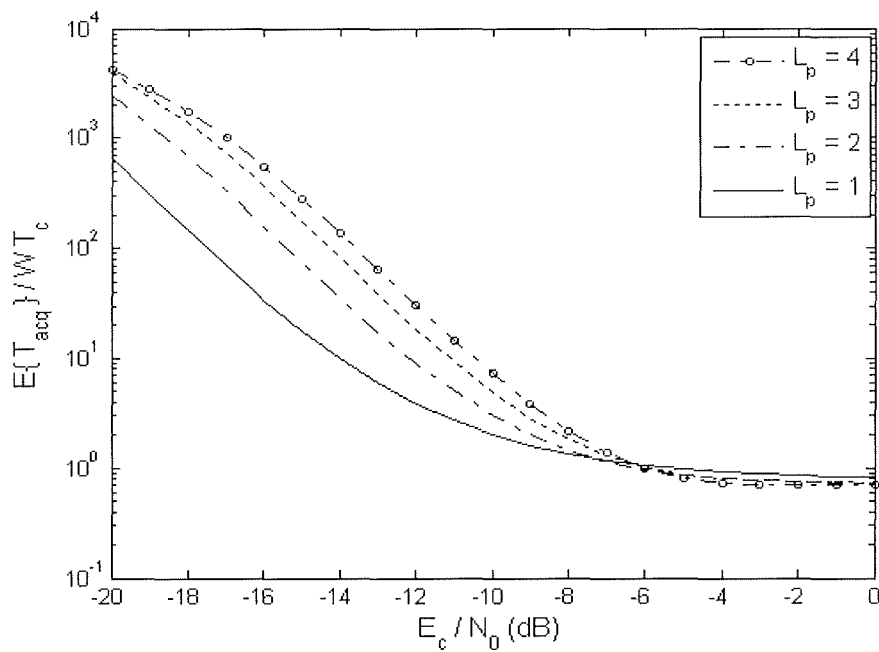


Figure 5.24. Plot of $E\{T_{acq}\}$ for a frequency selective Rayleigh fading channel using a uniform MIP

D. Effect of MAI

All the plots generated so far assumed that there is only one user, i.e. $K = 1$. In DS-SS systems, all users occupy the same spectrum. The resulting interference due to the other users on the desired user is modelled by the MAI term. Further motivation to determine the effect of MAI stems from the soft capacity of CDMA systems. Figure 5.25 shows the effect of MAI on the circuit performance. This plot was generated using equations (5.59), (5.61), (5.62) and (5.64) in (5.96). As the number of users increases, $E\{T_{acq}\}$ also increases. As expected, the performance of the circuit varies as k_R changes. It is assumed that all users are properly power-controlled to the same power with the aid of a closed loop power control algorithm administered by the BS.

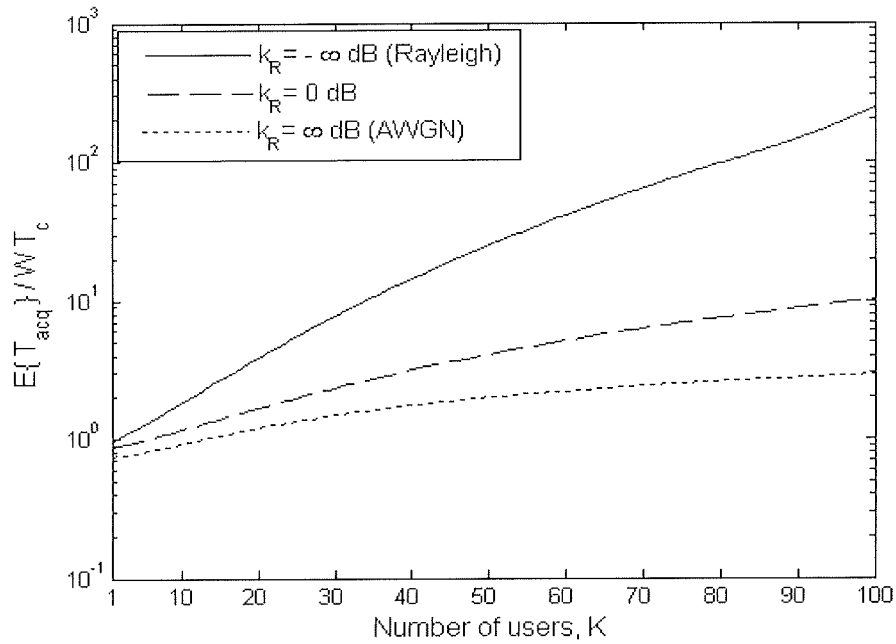


Figure 5.25. Plot showing the effect of MAI ($P_{fa} = 10^{-5}$ and $E_c / N_0 = -5$ dB are parameters)

However, since the user of interest is yet to be synchronised, it can only rely on open loop power control [59]. The implication of this, as discussed in Section 2.3 is that its power may not necessarily be the same with the other synchronised users that are already engaged in data transmission. If the average received power of the user of interest is given as S_a and that of the other users as S_o , then a new ratio t' can be defined as:

$$t' = S_o / S_a, \quad (5.103)$$

Equation (5.103) can be written as $S_o = t'S_a$. If $t' = 1$, then $S_o = S_a = S$.

Since $E_c / N_0 = 2ST_c / N_0$, it follows that:

$$t'E_c / N_0 = 2t'S_a T_c / N_0 \quad (5.104)$$

For the purpose of computing P_d , $t'E_c/N_0$ is substituted in place of E_c/N_0 in equations for the variances of the MAI terms while E_c/N_0 still remains the same for the user of interest. The effect of the variation of t' on the circuit performance is shown in Figure 5.26. A higher value of t' means the average power of the other users is greater than that of the user of interest and vice versa. It can be concluded from this analysis that by allocating more power to the user of interest to aid synchronisation, the acquisition time performance of the circuit can be improved in the presence of MAI.

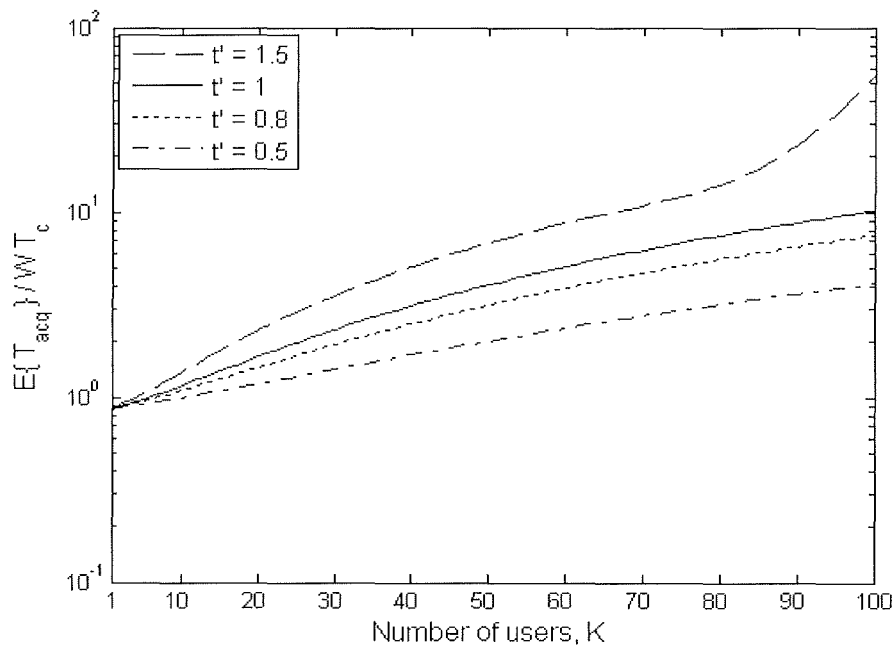


Figure 5.26. Normalised $E\{T_{acq}\}$ versus K showing the effect of t' ($k_R = 0$ dB)

E. Effect of CW Jammer

Interferences, intentional or unintentional, are a major problem in mobile networks [10, 38]. In military warfare, intentional interference or jamming is usually encountered. However, for civilian mobile communication systems, most of the interferences encountered are unintentional. Such sources include improperly configured transmitters,

cell overlap, inter-modulation, and harmonics from broadcast stations, as already discussed in Chapter 3.

It is assumed that the interference is a continuous wave (CW) jamming signal, with power denoted as J . A CW jamming signal is given from [60] as $\sqrt{2J} \cos(w_c t + \theta_j)$. Therefore, the received signal in the presence of the jammer, denoted as $r_j(t)$, can be given as

$$r_j(t) = r(t) + \sqrt{2J} \cos(w_c t + \theta_j) \quad (5.105)$$

where $r(t)$ is from (5.5), θ_j is the phase of the jamming signal. The jamming signal is uncorrelated with $r(t)$ and therefore after matched filtering, its contribution will be to increase the total noise power. Therefore the variance (for the I and Q components of the circuit) of the jammer alone is given from [60] as:

$$\sigma_{J,I}^2 = \sigma_{J,Q}^2 = JNT_c^2 \quad (5.106)$$

This is combined with equations (5.75) and (5.76) (assuming a frequency non-selective fading channel, number of users is 1 and no frequency offset) to give:

$$\sigma_{H_1}^2 = \frac{NN_0 T_c E_c}{2N_0} \left(\frac{G}{N} + \frac{1}{E_c / N_0} + \frac{J}{S} \right) \quad (5.107a)$$

$$\sigma_{H_0}^2 = \frac{NN_0 T_c E_c}{2N_0} \left(1 + \frac{1}{E_c / N_0} + \frac{J}{S} \right) \quad (5.107b)$$

where J/S is the jamming power to signal power ratio in dB.

Therefore using (5.77):

$$\sigma_s^2 = \frac{1 + 1/(E_c / N_0) + J/S}{G/N + 1/(E_c / N_0) + J/S} \quad (5.108)$$

Equation (5.108) is substituted into (5.82) and (5.84) for the purpose of computing the value of P_d . The plot of the normalised $E\{T_{acq}\}$ for different values of J/S is shown in Figure 5.27. As J/S increases, $E\{T_{acq}\}$ increases. However, $E\{T_{acq}\}$ approaches a floor at high values of J/S . This is because as J/S increases, P_d decreases, tending towards the constant P_{fa} (10^{-5}). Thus, $E\{T_{acq}\}$ is equal to the reciprocal of P_{fa} at this point. That is why $E\{T_{acq}\}$ is constant at 10^5 . From [60] it was stated that for a single dwell system, $P_{fa} = 1$ minimises $E\{T_{acq}\}$ for a non-adaptive circuit in the presence of a CW jammer.

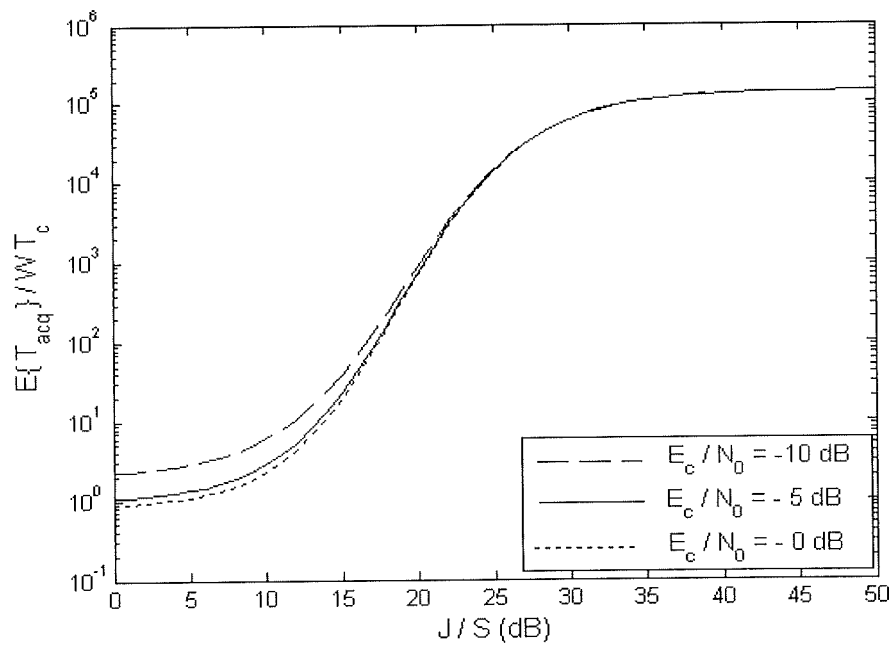


Figure 5.27. Plot showing the effect of CW jammer on $E\{T_{acq}\}$ ($P_{fa}=10^{-5}$, $E_c / N_0 = -5\text{dB}$)

Figure 5.28 is a plot showing the effect of jammer power on P_d for the proposed circuit. From the plot, the maximum value of $E\{T_{acq}\}$ is obtained when P_d equals P_{fa} . This value corresponds to the point in Figure 5.27 where the curve of the proposed circuit flattens out. At this point, $E\{T_{acq}\}$ is minimised. It can then be stated that for an adaptive

acquisition circuit, the point where P_d equals P_{fa} , a small value is where $E\{T_{acq}\}$ is minimised.

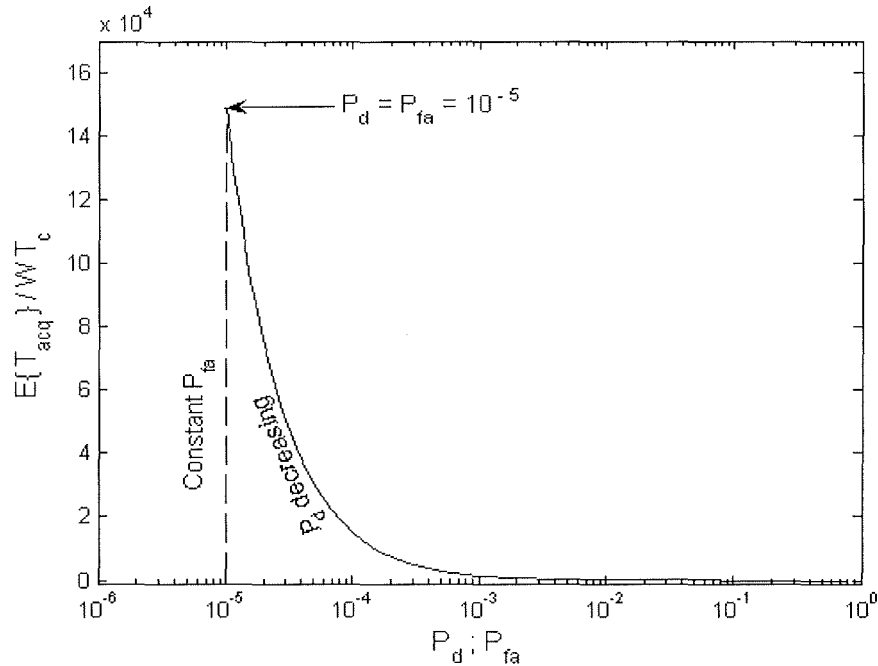


Figure 5.28. Plot of $E\{T_{acq}\}$ vs. P_{fa} and P_d (J / S varying from 0 – 50 dB and $E_c / N_0 = -5$ dB)

From the study of the effect of the CW jammer on the circuit performance, it is seen that one possible way to mitigate the effect of the jammer is to increase the transmitter power. But increasing the transmitter power will reduce the capacity in a DS-CDMA system. In Section 5.3.1.3, it was shown that increasing N can lead to improved circuit performance. This is the approach used here as shown in Figure 5.29. It is seen that the performance of the circuit improves as N increases. However, a point is reached where any further increase in N will have no effect on the jammer. At this point, the circuit performance is minimised for reasons already discussed.

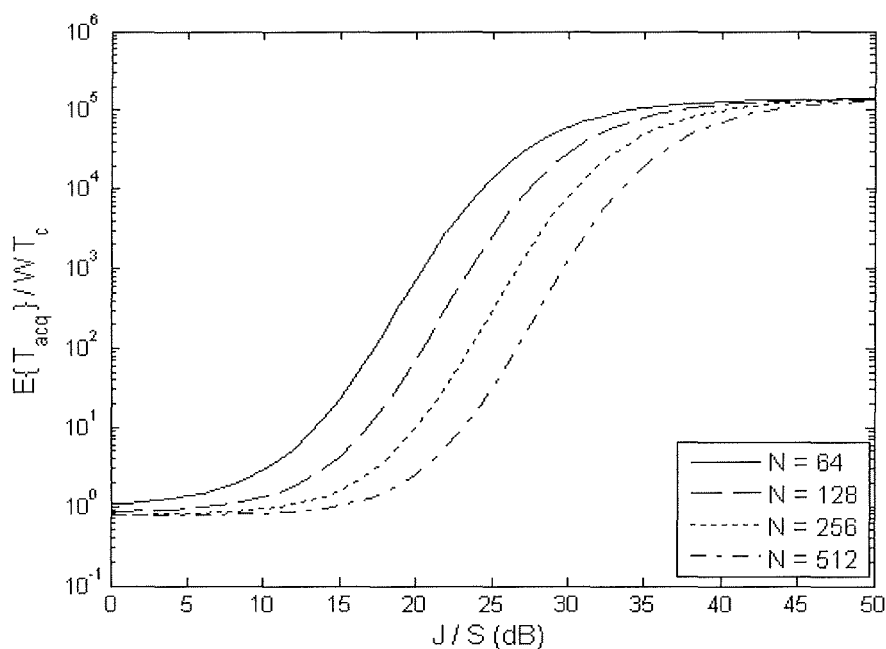


Figure 5.29. Mitigating the effect of a CW jammer by increasing N ($E_c / N_0 = -5$ dB and no frequency offset)

F. Effect of Frequency Offset

Assumption: Oscillator instability specification is ± 1 to ± 5 ppm corresponding to 1.6 to 8 kHz frequency offset in IS-95 DS-CDMA system.

All the results obtained so far assumed that in the down-conversion process of the proposed circuit in Figure 5.1, the received carrier frequency is exactly the same as the carrier frequency in the circuit and thus no frequency uncertainty. Using the assumed oscillator instability specifications, it is apparent that the oscillator frequency at the transmitter might not be exactly the same with that at the receiver. This results in what is called *frequency error* or *offset* between transmitter and receiver. This frequency offset leads to degradation in SNR and the amount of degradation, denoted here as μ is given by [9]:

$$\mu = \text{sinc}^2(2\Delta f N T_c) \quad (5.109)$$

where Δf is the frequency offset in Hz, N is the length of the MF and T_c is the chip duration in sec. Therefore, the SNR per chip, E_c / N_0 is now modified by μ as:

$$\text{SNR}_{\text{per chip}} = \mu E_c / N_0 \quad (5.110)$$

From (5.109) and (5.110), for a given Δf , increasing N will lead to degradation in SNR and thus performance degradation, contrary to what was explained in section 5.3.1.3, where it was assumed that there was no frequency offset. Figure 5.30 shows the effect of frequency offset on the SNR as N increases.

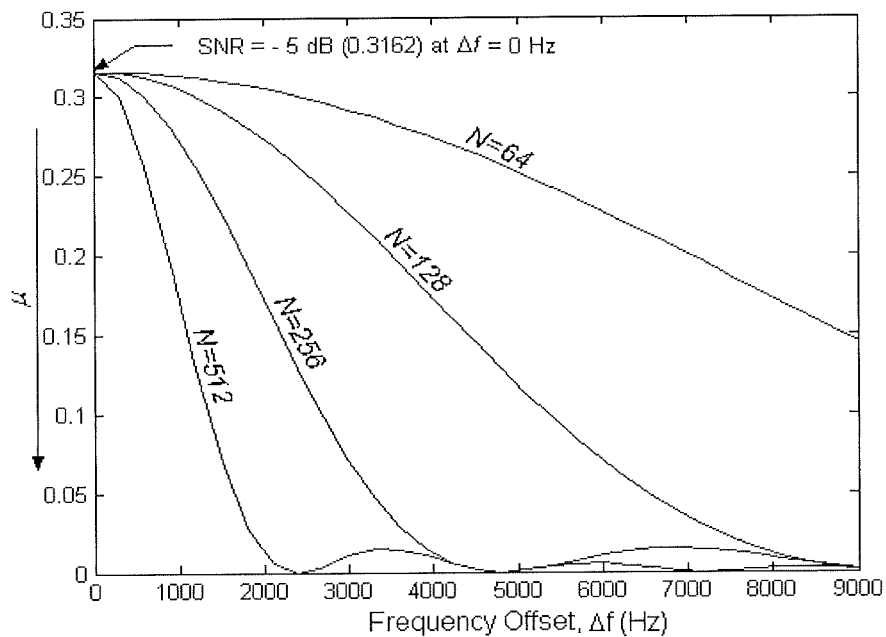


Figure 5.30. Degradation in SNR due to Δf for different values of N

Figure 5.31 shows the acquisition time performances of the adaptive schemes and the non-adaptive scheme for different values of frequency offset in a Rayleigh fading channel. From the figure, the proposed and the RF-M methods provide a good measure of robustness to frequency offset while the MF-LL method is heavily degraded

especially as the value of frequency offset increases beyond 2 kHz. Initially, when $\Delta f = 0$ Hz, and using $E_c/N_0 = -5$ dB, all the circuits gives approximately the same performance. However, as the Δf increases, the performance of the MF-LL degrades rapidly as expected (see Figures 5.30). The proposed and R-MF methods, showed a good measure of robustness to frequency offset within this frequency interval. This is because the length of the MF is 64. However, since $N = 64$, the available SNR is also small. This was why PDI was used to improve the SNR in the second dwell.

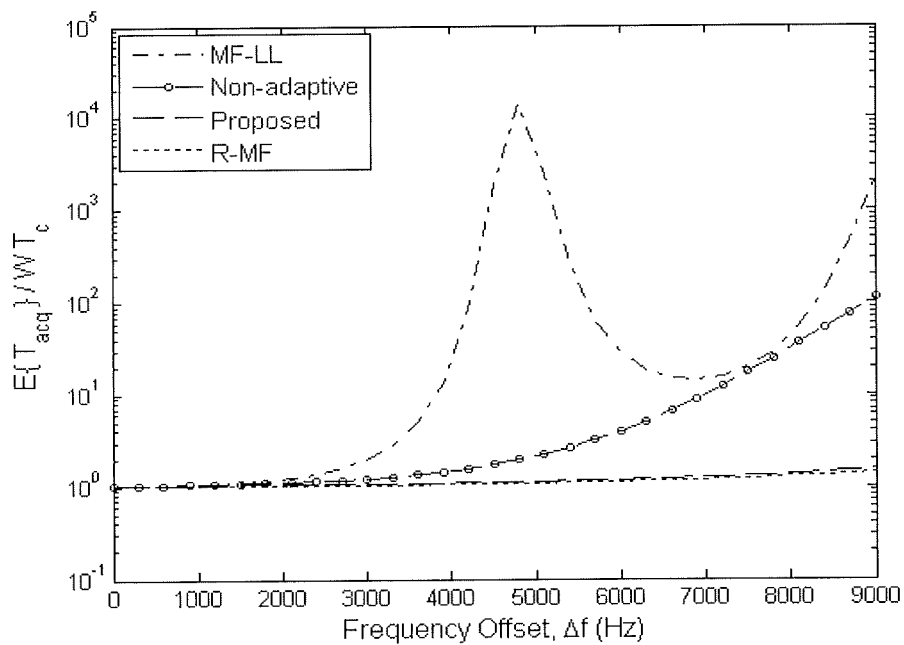


Figure 5.31. Effect of Δf on normalized $E\{T_{acq}\}$

Therefore, in situations where the value of frequency offset cannot be known for certain, such as aging of equipment coupled with the instability specifications of electronic components, especially oscillators, the proposed circuit would be an appropriate choice.

Though the second dwell of the non-adaptive method was implemented by PDI, the fact that the threshold is fixed for a SNR of -5 dB means that degradation in SNR leads to increase in P_{fa} (see Figure 5.8). This together with the corresponding decrease in P_d brought about the increase in the mean acquisition time.

5.4. Summary

An adaptive double dwell PN code acquisition circuit suitable for use in DS-CDMA systems has been proposed and analysed in Ricean, frequency selective and frequency non-selective Rayleigh fading channels. The adaptive nature of the circuit was derived from the CA-CFAR technique that is very popular in the field of radar technology. The second dwell was implemented using PDI. The equations for P_d and P_{fa} for the proposed circuit were derived. Thereafter, $E\{T_{acq}\}$ was derived. Theoretical results were presented to show the effects of the different types of channel model on the circuit performance. From the results, it was observed that the best performance is achieved in a Ricean fading channel. It was also observed that frequency selectivity degrades the circuit performance. Monte Carlo simulation was used to verify the theoretical results and the strong agreement between theory and simulation confirms the accuracy of the derived equations for the proposed circuit. The circuit was also analysed taking the effect of MAI and CW jammer into consideration. In all, the proposed scheme was shown to be adaptive to noise power variation in mobile environment. When the scheme was compared to an acquisition circuit that uses an R-MF for noise power estimation, it was seen that the performance of the proposed scheme compares favourably even though it is less complex. Its robustness to frequency offset was demonstrated when it was compared to an adaptive circuit that uses a longer MF length (MF-LL method) in

the second dwell. When compared to a non-adaptive scheme, a considerable reduction in mean acquisition time showed that the scheme could provide more robustness to the varying noise in mobile environment. It will also be useful in areas where the CDMA network may be subjected to intentional or unintentional interference. It was shown that, in the presence of MAI, the performance of the circuit could be improved by allocating more power to the user of interest compared to the other users. However the effect of this practice on the capacity of the CDMA system is worth considering. The proposed circuit can be applied to forward link of the IS-95 and CDMA2000 systems.

CHAPTER 6

PN Code Tracking

6.1. Introduction

The purpose of PN code acquisition is to bring the received PN signal into a coarse or rough alignment with the local PN signal. At this stage, data demodulation can actually take place. However, due to mobility of the user and other channel conditions, this estimate of the delay in the received signal will change and in most cases, data demodulation may not be possible. This means that with only coarse synchronisation, effective communication between the transmitter and the receiver cannot be guaranteed. Therefore, to keep track of this estimated delay and to ensure that the two PN signals (received and local) are properly aligned, the *tracking* circuit is used. This is known as *fine synchronisation*. Thus PN code tracking is done after a successful PN code acquisition. A study of some literature [7, 8, 9, 10, 17, 19, 61, 62] on PN code tracking techniques showed that the tracking is realised based on one basic operation. This operation involves correlating the received signal with two versions of the local PN signal. These are the *early* and *late* versions and it is generally referred to, in all tracking literature, as the *early-late gate* tracking loop. The difference between the output of the early and late correlators gives the timing error correction that is used to drive a voltage-controlled oscillator (VCO). Depending on this value, the VCO increases or

decreases the clocking frequency used in the local PN code generator, thereby keeping track of the changes of the phase already acquired with the acquisition circuit.

Recall from Chapter 2 that a DS-SS signal, $c(t)$ is given as:

$$c(t) = \sum_i c_i p_{T_c}(t - iT_c) \quad (6.1)$$

where $p_{T_c}(t)$ is a rectangular pulse of duration $[0, T_c]$ and $|c_n| = 1$ represents the i th chip of the PN sequence. The time autocorrelation of $p_{T_c}(t)$ is given from [9] as:

$$R(\tau_\epsilon) = \begin{cases} 1 - |\tau_\epsilon|/T_c & \tau_\epsilon \leq T_c \\ 0 & \text{otherwise} \end{cases} \quad (6.2)$$

A plot of the autocorrelation function $R(\tau_\epsilon)$ is shown in Figure 6.1.

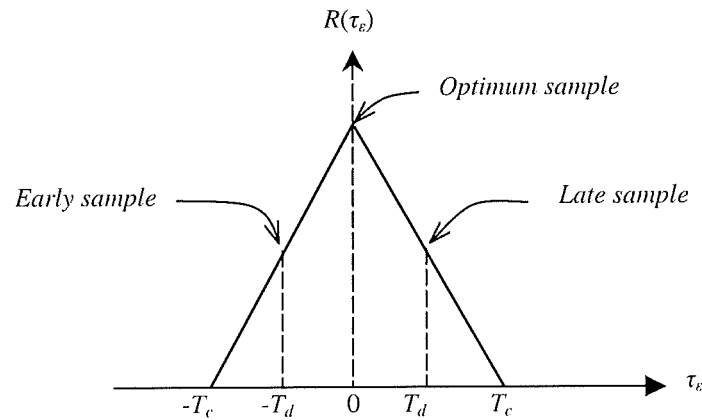


Figure 6.1. The autocorrelation function of a rectangular pulse

In Chapter 5, the received PN signal, $c_1(t + \tau_1 T_c)$ was correlated with its local version given as $c_1(t + \hat{\tau}_1 T_c)$ and it was assumed that the output, $R(\tau)$ was obtained at $\tau = 0$ (assumption of zero residual code offset, i.e. $\delta_1 = 0$), where the energy of the received

signal was maximum. At this optimum sampling point, $\hat{\tau}_1 \approx \tau_1$. But an optimum sampling position cannot be guaranteed in the acquisition circuit for reasons already stated. From Figure 6.1, a deviation from the optimum sampling position either to the left or right will lead to a low value at the output of the detector and so insufficient energy for data demodulation. In order to keep track of the optimum sampling position, the received signal is cross-correlated simultaneously or alternately with two versions of the local PN signal. One version is advanced by T_d and the other delayed by T_d . Therefore, the early local PN signal is given by $c(t + \hat{\tau}T_c - T_d)$ and the late signal by $c(t + \hat{\tau}T_c + T_d)$. From Figure 6.1, it is seen that the autocorrelation function is symmetric with respect to $\tau_e = 0$ and therefore the sampling at $\tau_e = -T_d$ and $\tau_e = T_d$ are equal. Hence the proper sampling time is at the midpoint between $\tau_e = -T_d$ and $\tau_e = T_d$.

The two main types of tracking circuits available in the literature are the *delay-locked loop* (DLL) and the *tau-dither loop* (TDL) [10]. Unlike PN code acquisition that is normally based on non-coherent implementation, tracking circuits can be operated in either the coherent or non-coherent mode [10]. The coherent operation is based on the fact that after PN code acquisition, carrier phase acquisition is now possible as there is sufficient SNR available for this operation. However, in this chapter, only the non-coherent tracking loop will be considered. This is still the most commonly used technique in CDMA systems as PN acquisition and tracking are usually done prior to carrier synchronisation [8, 19]. The non-coherent DLL is implemented by simultaneously correlating the received signal with the advanced and delayed version of the local PN signal. For the non-coherent TDL, the received signal is correlated alternately with the advanced and delayed versions of the locally generated PN signal.

The major advantage of the TDL over the DLL is that it is less sensitive to channel imbalance as the early and late signals are not correlated at the same time. For the DLL, the correlations are done at the same time and thus the early and late signals must be precisely balanced. However, the DLL is widely used in SS systems [8] and thus analysed here. In particular, the performance of a non-coherent DLL circuit in a frequency non-selective Rayleigh fading channel is considered. This analysis can be utilised in a multipath fading channel, especially when it is combined with a RAKE receiver [63] – where each finger of the RAKE receiver is used to acquire the respective multipath. Code tracking in a multipath channel with the aid of RAKE receiver has been considered in [64, 65].

6.2. The Non-Coherent Delay-Locked Loop

Figure 6.2 is a non-coherent DLL showing the basic components. The received PN signal $r(t)$ is simultaneously cross-correlated with an advance version of the local PN code $c_1(t + \hat{\tau}_1 T_c - T_d)$ and a delayed version $c_1(t + \hat{\tau}_1 T_c + T_d)$. If the output at the optimum sampling position is given as $R(\tau_\epsilon)$, then the respective outputs of the cross-correlation operations can be denoted as $R_- = R(\tau_\epsilon - T_d)$ and $R_+ = R(\tau_\epsilon + T_d)$ (the subscripts – and + indicate advance and delay respectively). The mean of Z_- and Z_+ are proportional to $R^2(\tau_\epsilon - T_d)$ and $R^2(\tau_\epsilon + T_d)$ respectively. From (6.2) and Figure 6.1, $R(\tau_\epsilon)$ is an even function monotonically decreasing in τ_ϵ within the main lobe. Therefore the difference of the measurements Z_- and Z_+ will have a mean proportional to $R_-^2 - R_+^2$. This will be positive for $\tau_\epsilon > 0$ (late estimate) and negative for $\tau_\epsilon < 0$ (early estimate). This difference is the error correcting signal $e(t)$ given as:

$$e(t) = Z_- - Z_+ \quad (6.3)$$

The signal $e(t)$ is used to drive a VCO, which corrects (increase or decrease) the clocking frequency of the PN code generator. In essence, the tracking circuit maintains $\hat{\tau}_1$ so that the generated PN signal is finely synchronised with the received signal.

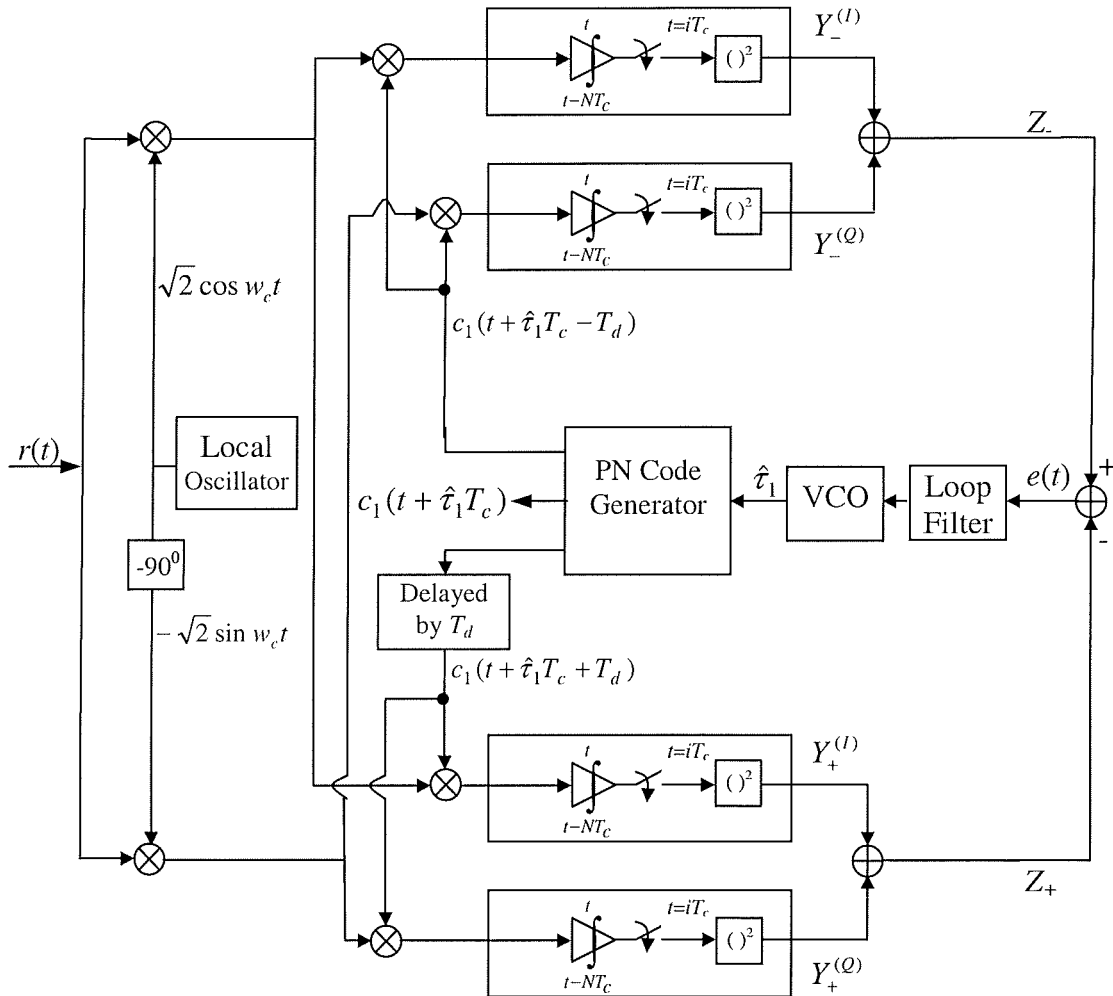


Figure 6.2. A non-coherent DLL tracking circuit

6.2.1. Statistics of the DLL in Rayleigh Fading Channel

In the following analysis, it is assumed that both signal arms (early and late) of the DLL circuit are balanced.

Let the received BPSK signal in a frequency non-selective Rayleigh fading channel with K asynchronous users be given as:

$$r(t) = \sum_{k=1}^K \sqrt{2S_k} c_k(t + \tau_k T_c) [x_k(t) \cos(w_c t + \theta_k) + y_k(t) \sin(w_c t + \theta_k)] + n(t) \quad (6.4)$$

where S_k is the k th user signal power, $c_k(t) = \sum_{i=-\infty}^{\infty} c_i p_{T_c}(t - iT_c)$ is the k th user PN signal with $|c_i|=1$ and $p_{T_c}(t)$ is a rectangular pulse of duration T_c , $x(t)$ and $y(t)$ are uncorrelated zero-mean Gaussian processes with equal variances, σ^2 . $N(t)$ represents the AWGN of double-sided power spectral density $N_0 / 2$ Watts/Hz.

The outputs of the respective detectors, neglecting double frequency terms, are given as:

$$\begin{aligned} Y_-^{(I)} &= u_-^{(I)} + v_-^{(I)} + n_-^{(I)} \\ Y_-^{(Q)} &= u_-^{(Q)} + v_-^{(Q)} + n_-^{(Q)} \end{aligned} \quad (6.5)$$

$$\begin{aligned} Y_+^{(I)} &= u_+^{(I)} + v_+^{(I)} + n_+^{(I)} \\ Y_+^{(Q)} &= u_+^{(Q)} + v_+^{(Q)} + n_+^{(Q)} \end{aligned} \quad (6.6)$$

where u_- results from correlating the received signal of the user of interest with an advanced version of the local PN code, v_- results from correlating the received signal of the other users with an advanced version of the local PN code and n_- results from correlating the AWGN noise signal with an advanced version of the local PN code. Similarly, u_+, v_+ and n_+ result from correlating the received signal with a delayed

version of the PN code. Y_- and Y_+ are analysed in the same way, the only difference is that one is advanced by T_d (indicated with a – subscript) and the other delayed by T_d (indicated with a + subscript). So it suffices to do the analysis for Y_- and use the same results for Y_+ but by taking note of the delay. Also, it should also be noted that the I and Q components are the same and so to avoid repetition, only the I component is computed.

From (6.4), the I component at the output of the MF can be defined as

$$\begin{aligned} D_k^{(I)} &= \sum_{k=1}^K \sqrt{2S} \int_0^{NT_c} c_1(t + \hat{\tau}_1 T_c) c_k(t + \tau_k T_c) x(t) \cos(\omega t + \theta_k) \sqrt{2} \cos \omega t dt \\ &\quad + \sum_{k=1}^K \sqrt{2S} \int_0^{NT_c} c_1(t + \hat{\tau}_1 T_c) c_k(t + \tau_k T_c) y(t) \sin(\omega t + \theta_k) \sqrt{2} \cos \omega t dt \\ &= \sqrt{S} NT_c X_k + \sqrt{S} NT_c Y_k \end{aligned} \quad (6.7)$$

From (6.7), neglecting double frequency terms, X_k and Y_k are written as:

$$X_k = \sum_{k=1}^K \frac{1}{NT_c} \int_0^{NT_c} c_1(t + \hat{\tau}_1 T_c) c_k(t + \tau_k T_c) x(t) \cos \theta_k \quad (6.8a)$$

$$Y_k = \sum_{k=1}^K \frac{1}{NT_c} \int_0^{NT_c} c_1(t + \hat{\tau}_1 T_c) c_k(t + \tau_k T_c) y(t) \sin \theta_k \quad (6.8b)$$

Therefore, from (6.7) and (6.8), $u_-^{(I)}$ is given by:

$$\begin{aligned} u_-^{(I)} &= \sqrt{S} NT_c X_1 + \sqrt{S} NT_c Y_1 \\ &= \sqrt{S} NT_c \left\{ \frac{1}{NT_c} \int_0^{NT_c} c_1(t + \hat{\tau}_1 T_c) c_1(t + \tau_1 T_c) x(t) \cos \theta_1 \right. \\ &\quad \left. + \frac{1}{NT_c} \int_0^{NT_c} c_1(t + \hat{\tau}_1 T_c) c_1(t + \tau_1 T_c) y(t) \sin \theta_1 \right\} \end{aligned} \quad (6.9)$$

Similarly, from (6.7) and (6.8), $v_-^{(l)}$ is given by:

$$\begin{aligned}
 v_-^{(l)} &= \sqrt{S}NT_c X_k + \sqrt{S}NT_c Y_k \\
 &= \sqrt{S}NT_c \sum_{k=2}^K \left\{ \frac{1}{NT_c} \int_0^{NT_c} c_1(t + \hat{\tau}_1 T_c) c_k(t + \tau_k T_c) x(t) \cos \theta_k \right. \\
 &\quad \left. + \frac{1}{NT_c} \int_0^{NT_c} c_1(t + \hat{\tau}_1 T_c) c_k(t + \tau_k T_c) y(t) \sin \theta_k \right\}
 \end{aligned} \tag{6.10}$$

Finally, $n_-^{(l)}$ is given by:

$$n_-^{(l)} = \int_0^{NT_c} n(t) c(t + \hat{\tau}_1 T_c - T_d) dt \tag{6.11}$$

Recall from (5.10) that:

$$\begin{aligned}
 R_{c_k c_k}(p, \tau_{\varepsilon, k}) &= \frac{1}{NT_c} \int_0^{NT_c} \sqrt{S} c_1(t + \hat{\tau}_1 T_c) c_k(t + \tau_k T_c) dt \\
 &= \frac{1}{N} \sum_{i=0}^{N-1} c_{1,i} c_{k,i+p} (1 - \delta_k) + \frac{1}{N} \sum_{i=0}^{N-1} c_{1,i} c_{k,i+p+1} \delta_k
 \end{aligned} \tag{6.12}$$

where $\delta_k = \tau_{\varepsilon, k} / T_c$ is uniformly distributed in $[-T_c, T_c]$.

Since acquisition is achieved before code tracking, then the H_0 hypothesis is not considered here. Under H_1 hypothesis, $p = 0$ and it was assumed that $\delta_1 = 0$ as explained in Chapter 5. This assumption meant that acquisition decision was made using the optimum sampling position as in Figure 6.1. The problem of code tracking will arise because δ_1 is not always fixed at zero but varies about this optimum sampling position.

It was also explained in Chapter 5 that as far as $\delta_1 \ll 1$, acquisition could take place. Therefore, for the user of interest, the last term in (6.12) will be neglected in the analysis. In most of the work on tracking, the last term is always neglected [9, 61, 62]. From (6.12) and for the user of interest, the autocorrelation function as given by (6.2) is:

$$R(\tau_\epsilon) = 1 - |\tau_\epsilon| / T_c = (1 - \delta_1) \quad (6.13)$$

If $\tau_\epsilon = 0$, then $\delta_1 = 0$ and $R(0) = 1$ corresponding to the point of optimum sampling position as shown in Figure 6.1.

For the case when the local is advanced by T_d ,

$$R(\tau_\epsilon - T_d) = (1 - |\tau_\epsilon - T_d| / T_c) = (1 - \delta_{k,-}) \quad (6.14)$$

Similarly for the case when the local code is delayed by T_d ,

$$R(\tau_\epsilon + T_d) = (1 - |\tau_\epsilon + T_d| / T_c) = (1 - \delta_{k,+}) \quad (6.15)$$

Recall from Chapter 5 that x_i and y_i represent the i th chip component of the fading processes $x(t)$ and $y(t)$ respectively. They are of zero-mean Gaussian processes with equal variances given as $E[x_i^2] = E[y_i^2] = \sigma^2$ and autocorrelation given as $E[x_i x_j] = E[y_i y_j] = \rho_{|i-j|} \sigma^2$. $\rho_i = J_0(2\pi i f_D T_c)$, where J_0 is the zero order Bessel function of the first kind, and f_D takes into consideration the Doppler shift. By using (6.12) and (6.14) in (6.9) and (6.10); and denoting $a_i = c_i c_{i+p}$, and $b_i = c_i c_{i+p+1}$, the following are obtained:

$$u_-^{(l)} = \sqrt{ST_c} \left[\sum_{i=0}^{N-1} a_{1,i} (1 - \delta_{1,-}) x_i \right] \cos \theta_1 + \sqrt{ST_c} \left[\sum_{i=0}^{N-1} a_{1,i} (1 - \delta_{1,-}) y_i \right] \sin \theta_1 \quad (6.16)$$

$$\begin{aligned}
v_-^{(l)} = & \sqrt{ST_c} \sum_{k=2}^K \left[\sum_{i=0}^{N-1} a_{k,i} (1 - \delta_{k,-}) x_i + \sum_{i=0}^{N-1} b_{k,i} (\delta_{k,-}) x_i \right] \cos \theta_k \\
& + \sqrt{ST_c} \sum_{k=2}^K \left[\sum_{i=0}^{N-1} a_{k,i} (1 - \delta_{k,-}) y_i + \sum_{i=0}^{N-1} b_{k,i} (\delta_{k,-}) y_i \right] \sin \theta_k
\end{aligned} \tag{6.17}$$

Since $p = 0$, then $a_{l,i} = 1$ for all i . Similar to the analysis in Chapter 5, the phase θ_l of the user of interest is set to zero. The variance of $u_-^{(l)}$ is given as:

$$\begin{aligned}
E\{[u_-^{(l)}]^2\} &= E\left\{\left(\sqrt{ST_c} \sum_{i=0}^{N-1} (1 - \delta_{l,-}) x_i\right)^2\right\} \\
&= E\left\{\left(\sqrt{ST_c} \sum_{i=0}^{N-1} (1 - \delta_-) x_i\right) \left(\sqrt{ST_c} \sum_{j=0}^{N-1} (1 - \delta_-) x_j\right)\right\} \\
&= ST_c^2 E\left\{\left(\sum_{i=0}^{N-1} (1 - \delta_-) x_i\right) \left(\sum_{j=0}^{N-1} (1 - \delta_-) x_j\right)\right\}
\end{aligned} \tag{6.18}$$

Comparing (6.18) to (5.27), it can be shown that $E\{[u_-^{(l)}]^2\}$ is given as:

$$E\{[u_-^{(l)}]^2\} = ST_c^2 \sigma^2 [G(1 - \delta_{l,-})^2] \tag{6.19}$$

Equation (6.17) is similar to (5.30) and it can be deduced that the variance of (6.17) is given by (5.35) as:

$$E\{[v_-^{(l)}]^2\} = 2\sigma^2 ST_c^2 N(K-1)/3 \tag{6.20}$$

For the AWGN, the variance is given as:

$$E\{[n_-^{(l)}]^2\} = NN_0 T_c / 2 \tag{6.21}$$

Using (6.19)-(6.21) in (6.5), the first moment of Z of Figure 6.2 is given as:

$$\begin{aligned} E(Z_-) &= E\{[Y_-^{(I)}]^2\} + E\{[Y_-^{(Q)}]^2\} \\ &= 2\sigma^2 ST_c^2 G(1 - \delta_{1,-})^2 + 4\sigma^2 ST_c^2 N(K-1)/3 + NN_0 T_c \end{aligned} \quad (6.22)$$

By defining the SNR per chip as $2\sigma^2 ST_c / N_0 = E_c / N_0$, (6.22) can be given as:

$$E(Z_-) = \frac{E_c G}{N_0 N} (1 - \delta_{1,-})^2 + 2 \frac{E_c}{N_0} (K-1)/3 + 1 \quad (6.23)$$

The second moment of Z is calculated thus,

$$\begin{aligned} E(Z_-^2) &= E\{([Y_-^{(I)}]^2 + [Y_-^{(Q)}]^2)^2\} \\ &= E\{[Y_-^{(I)}]^4\} + E\{[Y_-^{(Q)}]^4\} + 2E\{[Y_-^{(I)}]^2\}E\{[Y_-^{(Q)}]^2\} \end{aligned} \quad (6.24)$$

From (6.24) and using (6.5), $E\{[Y_-^{(I)}]^4\}$ is given as:

$$\begin{aligned} E\{[Y_-^{(I)}]^4\} &= E\{[u_-^{(I)}]^4\} + E\{[v_-^{(I)}]^4\} + E\{[n_-^{(I)}]^4\} + 6E\{[u_-^{(I)}]^2\}E\{[v_-^{(I)}]^2\} \\ &\quad + 6E\{[u_-^{(I)}]^2\}E\{[n_-^{(I)}]^2\} + 6E\{[v_-^{(I)}]^2\}E\{[n_-^{(I)}]^2\} \end{aligned} \quad (6.25)$$

From [9, 32], if all x variables are independent and Gaussian with zero means, then:

$$E[x^4] = 3(E[x^2])^2 \quad (6.26)$$

Therefore,

$$E\{[v_-^{(I)}]^4\} = 3(2\sigma^2 ST_c^2 N(K-1)/3)^2 \quad (6.27)$$

$$E\{[n_-^{(I)}]^4\} = 3(NN_0 T_c / 2)^2 \quad (6.28)$$

$$E\{[u_-^{(I)}]^4\} = 3(\sigma^2 ST_c^2 G(1 - \delta_{1,-})^2)^2 \quad (6.29)$$

Substituting (6.27) – (6.29) and the already derived second moments of u , v and n in (6.25), the following is obtained:

$$\begin{aligned}
E\{[Y_-^{(I)}]^4\} &= 3(\sigma^2 ST_c^2 G(1 - \delta_{1,-})^2)^2 + 3(2\sigma^2 ST_c^2 N(K-1)/3)^2 + 3(NN_0 T_c / 2)^2 \\
&\quad + 4\sigma^4 S^2 T_c^4 GN(K-1)(1 - \delta_{1,-})^2 + 3\sigma^2 ST_c^3 NN_0 G(1 - \delta_{1,-})^2 \\
&\quad + 2\sigma^2 ST_c^3 N_0 N^2 (K-1)
\end{aligned} \tag{6.30}$$

The last term in (6.24) is given as:

$$\begin{aligned}
2E\{[Y_-^{(I)}]^2\}E\{[Y_-^{(Q)}]^2\} &= 2\left[E\{[u_-^{(I)}]^2\} + E\{[v_-^{(I)}]^2\} + E\{[n_-^{(I)}]^2\}\right] \\
&\quad \times \left[E\{[u_-^{(Q)}]^2\} + E\{[v_-^{(Q)}]^2\} + E\{[n_-^{(Q)}]^2\}\right] \\
&= 2\left[\sigma^2 ST_c^2 \{G(1 - \delta_{1,-})^2\} + 2\sigma^2 ST_c^2 N(K-1)/3 + NN_0 T_c / 2\right] \\
&\quad \times \left[\sigma^2 ST_c^2 \{G(1 - \delta_{1,-})^2\} + 2\sigma^2 ST_c^2 N(K-1)/3 + NN_0 T_c / 2\right] \\
&= 2\left[\sigma^2 ST_c^2 \{G(1 - \delta_{1,-})^2\}\right]^2 + 8\sigma^4 S^2 T_c^4 N(K-1)[G(1 - \delta_{1,-})^2]/3 \\
&\quad + 2\sigma^2 ST_c^3 N_0 N [G(1 - \delta_{1,-})^2] + 2\left[2\sigma^2 ST_c^2 N(K-1)/3\right]^2 + 4\sigma^2 ST_c^3 N_0 N^2 (K-1)/3 \\
&\quad + 2[NN_0 T_c / 2]^2
\end{aligned} \tag{6.31}$$

Substituting (6.30) – (6.31) into (6.24), and noting that $E\{[Y_-^{(I)}]^4\} = E\{[Y_-^{(Q)}]^4\}$ the following is obtained:

$$\begin{aligned}
E(Z_-^2) &= 8\left[ST_c^2 \sigma^2 \{G(1 - \delta_{1,-})^2\}\right]^2 + 8\left[2\sigma^2 ST_c^2 N(K-1)/3\right]^2 + 8[NN_0 T_c / 2]^2 \\
&\quad + 32\sigma^4 S^2 T_c^4 N(K-1)[G(1 - \delta_{1,-})^2]/3 + 8\sigma^2 ST_c^3 N_0 N [G(1 - \delta_{1,-})^2] \\
&\quad + 16\sigma^2 ST_c^3 N_0 N^2 (K-1)/3
\end{aligned} \tag{6.32}$$

From (6.22),

$$\begin{aligned}
[E(Z_-)]^2 &= \left[2\sigma^2 ST_c^2 G(1 - \delta_{1,-})^2 + 4\sigma^2 ST_c^2 N(K-1)/3 + NN_0 T \right]^2 \\
&= 4 \left[\sigma^2 ST_c^2 G(1 - \delta_{1,-})^2 \right]^2 + 16\sigma^4 S^2 T_c^4 N(K-1) \left[G(1 - \delta_{1,-})^2 \right] / 3 \\
&\quad + 4\sigma^2 ST_c^3 N_0 N \left[G(1 - \delta_{1,-})^2 \right] + 8\sigma^2 ST_c^3 N_0 N^2 (K-1) / 3 \\
&\quad + 16 \left[\sigma^2 ST_c^2 N(K-1) / 3 \right]^2 + [NN_0 T]^2
\end{aligned} \tag{6.33}$$

Therefore,

$$\begin{aligned}
\text{var}(Z_-) &= E[Z_-^2] - [E(Z_-)]^2 \\
&= 4 \left\{ \sigma^2 ST_c^2 G(1 - \delta_{1,-})^2 \right\}^2 - 8 \left[2\sigma^2 ST_c^2 N(K-1) / 3 \right]^2 \\
&\quad + 16\sigma^4 S^2 T_c^4 N(K-1) \left[G(1 - \delta_{1,-})^2 \right] / 3 + 4\sigma^2 ST_c^3 N_0 N \left[G(1 - \delta_{1,-})^2 \right] \\
&\quad + 8\sigma^2 ST_c^3 N_0 N^2 (K-1) / 3 + (NN_0 T_c)^2 \\
&= \left[\frac{E_c G}{N_0 N} (1 - \delta_{1,-})^2 \right]^2 - \frac{8}{9} \left[\frac{E_c}{N_0} (K-1) \right]^2 + \frac{4}{3} \left(\frac{E_c}{N_0} \right)^2 (K-1) \left[\frac{G}{N} (1 - \delta_{1,-})^2 \right] \\
&\quad + 2 \frac{E_c G}{N_0 N} (1 - \delta_{1,-})^2 + \frac{4}{3} \frac{E_c}{N_0} (K-1) + 1
\end{aligned} \tag{6.34}$$

Using (6.23) and noting that the derived equation for $E[Z_-]$ is similar to that of $E[Z_+]$ (but for the + sign), the mean of the output signal from the circuit is given as:

$$E[Z_{T_u}] = E[Z_-] - E[Z_+]$$

$$\begin{aligned}
&= \frac{E_c G}{N_0 N} \left[(1 - \delta_{1,-})^2 - (1 + \delta_{1,+})^2 \right] \\
&= \frac{E_c G}{N_0 N} \left[(1 - |\tau_\varepsilon - T_d| / T_c)^2 - (1 - |\tau_\varepsilon + T_d| / T_c)^2 \right] \quad (6.35)
\end{aligned}$$

Using (6.34) and noting that the derived equation for $\text{var}(Z_-)$ is similar to that of $\text{var}(Z_+)$ (but for the + sign), the variance of the output signal is given as:

$$\begin{aligned}
\text{var}[Z_{T_d}] &\approx \text{var}(Z_- - Z_+) = \text{var}(Z_-) + \text{var}(Z_+) \\
&= \left(\frac{E_c G}{N_0 N} \right)^2 \left[(1 - \delta_{1,-})^4 + (1 - \delta_{1,+})^4 \right] - \frac{16}{9} \left[\frac{E_c}{N_0} (K - 1) \right]^2 \\
&\quad + \frac{4}{3} \left(\frac{E_c}{N_0} \right)^2 \frac{G}{N} (K - 1) \left[(1 - \delta_{1,-})^2 + (1 - \delta_{1,+})^2 \right] \\
&\quad + 2 \frac{E_c G}{N_0 N} \left[(1 - \delta_{1,-})^2 + (1 - \delta_{1,+})^2 \right] + \frac{8}{3} \frac{E_c}{N_0} (K - 1) + 2 \quad (6.36)
\end{aligned}$$

The reason that the variance of Z_{T_d} is approximately equal to the sum of the variances of Z_- and Z_+ is because it was assumed that both the early and late samples are based on the same received signal and so their covariance is non-zero. This is because the variance of the difference is equal to the sum of variances minus twice the covariance.

6.2.2. Time Tracking Loop Operation

Having derived the mean and variance statistics of the timing error measurement, (6.35) and (6.36) respectively, the effect of applying this error measurement as a correction to the PN code sequence clock generator is shown in this section. The error signal $e(t)$ is given as:

$$e(t) = E[Z_{T_d}] + \text{var}[Z_{T_d}] \quad (6.37)$$

The first term in (6.37) is the gain (i.e. it determines the increase or decrease in the correction signal) of the error signal and the second term the interference. The gain is given from (6.35) as:

$$E[Z_{T_d}] = \frac{E_c G}{N_0 N} D(\tau_\epsilon / T_c) \quad (6.38)$$

where, the gain function, $D(\tau_\epsilon / T_c)$ is given as:

$$D(\tau_\epsilon / T_c) = [(1 - |\tau_\epsilon - T_d| / T_c)^2 - (1 - |\tau_\epsilon + T_d| / T_c)^2] \quad (6.39)$$

Equation (6.39) is plotted in Figure 6.3 for the case T_d / T_c is 0.25, 0.5 and 0.75. If initially $\tau_\epsilon / T_c = 0$, then $D(\tau_\epsilon / T_c) = 0$ and so the gain function will be zero and the VCO will not cause any change in the frequency and so no correction to the clocking rate of the PN code generator. If $\tau_\epsilon / T_c > 0$, then $D(\tau_\epsilon / T_c) > 0$ and this will cause the frequency of the VCO to be increased and so a reduction in the clocking time of the PN code generator. If $\tau_\epsilon / T_c < 0$, then $D(\tau_\epsilon / T_c) < 0$ and this will cause the frequency of the VCO to be decreased and therefore an increase in the clocking time of the PN code generator. Figure 6.3 is also known as the *S*-curve in the literature. It is also observed from the plot that as T_d / T_c decreases, the slope at the origin increases. This is equivalent to stronger feedback signal into the loop for small change in relative timing error, τ_ϵ / T_c which is desirable. However, the drawback is reduced tracking range, which is given by $2T_d / T_c$.

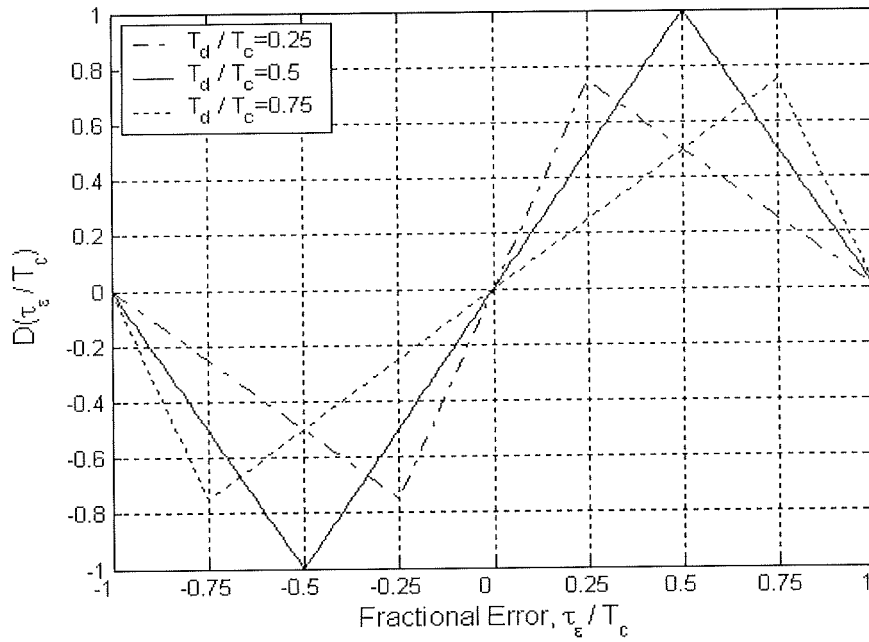


Figure 6.3. Tracking error function for different values of T_d/T_c

The effect of the second term in (6.37), that is the interference term, is to cause variation or jitter of the relative timing error τ_ϵ/T_c within the tracking range. This variation within the linear region of Figure 6.3 is given from [9] as:

$$\text{var}(\tau_\epsilon/T_c) = \frac{\text{var}(Z_{T_d})\alpha}{\frac{E_c G}{N_0 N} \left. \frac{dD(\tau_\epsilon/T_c)}{d(\tau_\epsilon/T_c)} \right|_{\tau_\epsilon=0}} \quad (6.40)$$

From appendix III,

$$\left. \frac{d(D(\tau_\epsilon/T_c))}{d(\tau_\epsilon/T_c)} \right|_{\tau_\epsilon=0} = 4(1 - T_d/T_c), \quad (6.41)$$

Therefore,

$$\text{var}(\tau_\epsilon/T_c) \approx \frac{\text{var}(Z_{T_d})\alpha}{4 \frac{E_c G}{N_0 N} (1 - T_d/T_c)} \quad (6.42)$$

In (6.42), α is a scale factor that represents the gain introduced in the voltage-to-frequency conversion. $\text{var}(\tau_e / T_c)$ can be made arbitrarily small by choosing α sufficiently small [9], thereby mitigating the effect of the interference, $\text{var}(Z_{T_d})$ on the tracking loop performance. This is equivalent to reducing the bandwidth of the loop filter in Figure 6.2. This is not an easy task as it should be noted that if the bandwidth is too small, this will also affect the desired signal that is being sensed since the loop filter actually filters $e(t)$ which is made up of the desired signal and the interference.

6.3. Summary

A brief analysis of the performance of DLL PN code tracking circuit has been carried out in this chapter. PN code tracking is not a major research area as PN code acquisition. This is partly due to the fact that once initial acquisition has been done, then tracking circuits (already well developed) in conventional communication systems can be easily applied. Therefore the purpose of this chapter was to introduce the theory of PN code tracking. However, the mathematical analysis are made simple enough for easier understanding and this will provide an insight into some important points to be noted as follows. In all, it is seen that the amount, T_d by which the local code is advanced or delayed determines the strength of the feedback signal of the tracking loop for a given change in the timing offset, τ_e in the position of the received PN code. That is, smaller T_d , stronger feedback signal but reduced tracking range and vice versa. The effect of interference may lead to variation of the relative timing error; however, from the revised literature on PN code tracking, this has not been a major problem.

CHAPTER 7

Conclusions and Future Work

7.1. Conclusions

The major aim of this thesis was to study the performance of a proposed PN code acquisition circuit in a mobile environment. The numerical results obtained showed that the circuit could lead to improved acquisition time performance of the PN code acquisition process. Overall, this thesis can provide the reader with detailed information on the theoretical and mathematical analysis of PN code synchronisation in SS systems. Each chapter of the thesis is made up of relevant and comprehensive information as is briefly summarised below.

In Chapter 1, a general overview of the present state of mobile communication was presented. It was stated that the rapid growth in the telecommunications industry were both technological and user driven. While TDMA may not be able to meet up with the growing number of users and the different types of services being demanded, CDMA was a welcome alternative to this problem. But implementation of a CDMA system is more complex than systems based on TDMA or FDMA. Two important implementation areas are power control and PN code synchronisation. This thesis was dedicated to the latter.

In Chapter 2, a review of the technology that made CDMA possible was carried out. This is SS communication. CDMA was defined as a multiple access technique based on SS principles. It was stated that an important implementation area in CDMA system is PN code synchronisation. To emphasise the importance of PN code synchronisation, a brief study of call processing in CDMA systems was presented. It was seen that the first step in the call processing operation is PN code synchronisation. SS systems are realised with the aid of PN codes. This was why a study of the different types of PN codes and their properties were carried out. The applications of these codes in CDMA systems were briefly looked at. The challenge of using these codes in CDMA system is to look for codes that have good autocorrelation and cross-correlation values. m -sequences have good autocorrelation values but their cross-correlation values are poor. They are therefore of limited use in CDMA systems. It was stated that Gold and Kasami codes have better cross-correlation values than m -sequence. However, since m -sequences have good autocorrelation values, they are used for BS identification. This autocorrelation property of m -sequence was utilised in the code acquisition process.

In Chapter 3, a brief study of the mobile channel was carried out. It was shown that the mobile channel is a filter that causes attenuation of the received signal. A Ricean fading channel that is common in rural areas was considered. In the sub-urban or urban areas, the channel could be frequency selective or frequency non-selective Rayleigh fading. Also present in the mobile environment are other type of interferences known as jamming (intentional interference), unintentional interference and MAI. The purpose of this chapter was to present an understanding of the mathematical representations of the

wireless channel. These mathematical representations were used in the performance analysis of the proposed circuit.

In Chapter 4, the theory of PN code acquisition was presented by reviewing some literature on this topic. This, though not exhaustive, is enough for the reader to understand the theory, analysis and implementation issues in the code acquisition process. It was learnt from this chapter that code acquisition has to do with techniques for obtaining a rough estimate of the delay in the received PN signal. This mainly entails correlating the received signal with a locally generated signal and looking for the delay value that gives the maximum autocorrelation. Correlation could be done using active correlator or passive MF. The MF method is preferred because it leads to fast acquisition but its implementation is more complex. To ease the search process and to make the acquisition problem mathematically tractable, the uncertainty region is quantised into discrete regions known as cells. It was stated that the cells can be searched serially or in parallel. The serial search is preferred as it is less complex. The importance of threshold setting in the implementation of the serial search was emphasised. Finally, the parameters for the acquisition circuit performance measures were stated. It was shown that the P_d , P_{fa} and $E\{T_{acq}\}$ are popularly used. Thus, the purpose of this chapter was to serve as an introduction to chapter 5, where the performance analysis of the proposed circuit was carried out.

The studies in Chapters 2, 3 and 4 were utilised in Chapter 5 in the performance analysis of the proposed PN code acquisition circuit. The circuit proposed was a double dwell adaptive PN code acquisition circuit. The adaptive nature of the circuit was based

on the CA-CFAR technique. The correlation operation of the circuit was based on the MF principle. PDI was utilised in the implementation of the double dwell acquisition circuit. The circuit analysis was carried out in Ricean and frequency selective Rayleigh fading channels. Monte Carlo simulation was carried out to verify the performance of the circuit in a frequency non-selective Rayleigh fading channel. The close agreement between theory and simulation further validated the mathematical analysis and the associated equations derived for the proposed circuit. Results presented showed that the circuit performed well in a Ricean fading channel due to the presence of deterministic LOS signal. However, its performance was degraded in a frequency selective Rayleigh fading channel. One common source of interference in CDMA systems is MAI. The effect of MAI on the proposed circuit was studied. From results obtained, MAI leads to degradation in the circuit performance. However, since the MS uses open-loop power control prior to synchronisation, it was shown that by allocating more power to the MS, the acquisition time performance could be improved. However, the effect of this practice on the CDMA network is yet to be analysed by the author. For instance, increasing the power of the MSs during the synchronisation stage may affect the capacity of the system as the interference is increased.

It was clear that one or more of the major components (correlator, PDI and CA-CFAR processor, etc) used in the realisation of the proposed circuit were common to all other acquisition circuits as can be seen from the vast literature on PN code acquisition. However, the way these components were utilised in the implementation of the proposed circuit has not been carried out elsewhere to the author's knowledge. It was for this reason that some results obtained were compared to some circuits that were

implemented using all or some of these components. It was shown that the proposed circuit performs better in certain areas. For instance, due to imperfections in the local oscillators, the resulting frequency offset usually lead to degradation in the performance of non-coherent PN code acquisition circuits. The proposed circuit performed better when compared to another adaptive circuit that was realised using the CA-CFAR technique in the presence of frequency offset. Also, its robustness to noise power variation was shown when compared to a non-adaptive circuit that was implemented using PDI. It was also compared to another adaptive circuit that uses a reference detector for noise power measure. The proposed circuit, though less complex, gave almost the same performance as this circuit. From the foregoing comparison points, it can be stated that the proposed circuit brings about improved acquisition time performance.

In Chapter 6, a study of PN code tracking was carried out to complete the analysis of the synchronisation process. Though a new implementation technique was not suggested, a mathematical analysis of a non-coherent DLL was shown. This will present the reader with an understanding of how some of the results were obtained in the cited literature. However, an important point to note is that the code tracking is only done after acquisition. This means that the failure of the tracking circuit loop to lock will most of the time indicate that a false acquisition was done in the search stage and so the circuit can return back and restart the search process. But as explained in Chapter 4, the tracking circuit can also lock with a false phase, thus enabling the data demodulation stage. The consequence of this is that no effective data demodulation will be achieved

and once this is detected, the circuit will return to the search stage to continue the search for the correct code phase.

7.2. Future Work

It was stated that the proposed circuit could be applied to any acquisition stage in the synchronisation process of SS systems. However, this work is directly applicable to CDMA IS-95 and CDMA2000. From the results shown in Chapter 5, the acquisition process was achieved by synchronising to one particular short PN sequence. This simplified the acquisition process to a single search of only the delay in the received PN sequence. In CDMA IS-95 and CDMA2000 systems, all BSs are synchronised with the aid of GPS, therefore making it possible to use the same short PN sequence for all BSs. However, each BS is identified by a unique offset of the short PN sequence. This implies that synchronisation to a BS in CDMA IS-95 and CDMA2000 systems is just a single search of the unique offset corresponding to that BS. Systems using WCDMA do not depend on GPS. The implication of this is that each BS is identified with its own unique PN code. This means that for a cluster of 512 BSs, the MS has to search 512 different PN codes. This cannot be searched by a one-step search approach, as the search time might be too long. Thus a three-step approach as suggested in [66 – 69] is currently being used. The question arises on how the proposed circuit can be applied to WCDMA. Though the proposed circuit can be applied to the first step of the of the three-step search process, its analysis has not been carried out by the author. In [67], segmented MFs were used in the first step of the 3 steps. The purpose was to avoid frequency offset and to improve the search speed. In Chapter 5, it was shown that PDI could mitigate the effect of frequency offset and improve the acquisition time

performance of the circuit. The use of PDI could be a possible alternative to the use of segmented MFs. This alternative technique has not been analysed by the author. However, the analysis of the overall search processes in WCDMA is of current interest to the author.

The proposed circuit was analysed in a slowly fading channel. It was assumed that the amplitude as well as the phase of the received signal is constant during each correlation interval and that successive correlation intervals are independent. From Figure 5.14, it was seen that for $f_D T_c > 10^{-2}$, characterising a fast fading channel, the performance of the circuit is heavily degraded. This is due to the fact that the amplitude and the phase of the received signal are not constant during each correlation interval. This therefore calls for new assumptions, techniques and mathematical analysis.

The effect of jamming on the performance of the proposed circuit was found to be very severe. Even the increase of the correlation length, N could not be considered as a feasible solution as there was still the problem of frequency offset to contend with. Investigation is currently going on to find a suitable solution so that a trade-off between frequency offset and correlation length could be used in the design of such circuits. Increasing the complexity of the proposed circuit by implementing it in a serial-parallel acquisition scheme is a possible way out. The parallel section of the circuit should be stepped in different frequency offset positions and a maximum likelihood approach could be used in the selection of the correct code phase.

Appendix I

Moments of Random Variables

Results obtained in Chapter 5 were based on some useful properties of random variables. In short the first and second moments of random variables were repeatedly used. In this section, some of the properties of random variables are stated.

Let

X be a discrete random variable with pdf $p(x)$,

a and b are real constants.

From [70], the first moment of X is called the *mean* given as:

$$E[X] = \mu_x = \sum_{i=1}^N x_i p(x) \quad (\text{I.1})$$

$$E[aX + b] = aE[X] + b = a\mu_x + b \quad (\text{I.2})$$

where $E[x]$ denotes the expectation of x .

The n th central moment is given as $E[(X - \mu_x)^n]$. The second central moment is called the *variance* defined as:

$$\begin{aligned} \text{var}(X) &= \sigma_x^2 = E[(X - \mu_x)^2] \\ &= E[X^2] - 2\mu_x E[X] + (\mu_x)^2 \\ &= E[X^2] - \mu_x^2 \end{aligned} \quad (\text{I.3})$$

If X is of zero mean, i.e. $\mu_x = 0$, then $\sigma_x^2 = E[X^2]$.

Similar to (I.2), it can be shown that $\text{var}(aX+b)$ is given as:

$$\sigma_{ax+b}^2 = a^2 \sigma_x^2 \quad (\text{I.4})$$

Also from [70],

$$\text{var}\left(\sum_{i=1}^N x_i\right) = \sum_{i=1}^N \text{var}(x_i) + \sum_{i=1}^N \sum_{\substack{j=1 \\ j \neq i}}^N \text{cov}(x_i, x_j) \quad (\text{I.5})$$

where cov denotes covariance.

It is defined as:

$$\text{cov}(x_i, x_j) = E[(x_i - \mu_{x_i})(x_j - \mu_{x_j})] \quad (\text{I.6})$$

If $\mu_{x_i} = \mu_{x_j} = 0$, then:

$$\text{cov}(x_i, x_j) = E[x_i x_j] \quad (\text{I.7})$$

Another useful property has to do with the variance of the difference or sum of two random variables. It states that the sum or difference of two i.i.d. random variables that are of zero means is given by the sum of their respective variances.

Proof:

Let X and Y be two random variables with respective means of μ_x and μ_y .

$$\begin{aligned} \text{var}(X - Y) &= E\left\{[(X - Y) - (\mu_x + \mu_y)]^2\right\} \\ &= E\left\{(X - Y)^2 - 2(X - Y)(\mu_x + \mu_y) + (\mu_x + \mu_y)^2\right\} \\ &= E[X^2] - 2E[X]E[Y] + E[Y^2] - 2E[X](\mu_x + \mu_y) \\ &\quad + 2E[Y](\mu_x + \mu_y) + (\mu_x + \mu_y)^2 \end{aligned} \quad (\text{I.8})$$

From (I.2), $E[X] = \mu_x$ and $E[Y] = \mu_y$. Since X and Y are of zero means, then (I.8)

reduces to:

$$\text{var}(X - Y) = E[X^2] + E[Y^2] \quad (\text{I.9})$$

Similarly, it is easily shown that $\text{var}(X + Y) = E[X^2] + E[Y^2]$.

Appendix II

Derivation of equations for P_d and P_{fa}

$$P_{dr}, P_{far} = \int_0^{\infty} \frac{u^{Ln-1} e^{-u/\varphi}}{\varphi^{Ln} \Gamma(Ln)} \int_{T_r, u}^{\infty} \frac{v^{L-1} e^{-v/\psi_i}}{\psi_i^L \Gamma(L)} dv du \quad (\text{II.1})$$

From table of integrals [71, pp. 310, eqn. (3.351-2)], we have,

$$P_{dr}, P_{far} = \int_0^{\infty} \frac{u^{Ln-1} e^{-u/\varphi}}{\varphi^{Ln} \Gamma(Ln)} e^{-T_r u / \psi_i} \sum_{q=0}^{L-1} 1/q! \left(\frac{T_r u}{\psi_i} \right)^q du \quad (\text{II.2})$$

$$P_{dr}, P_{far} = \int_0^{\infty} \sum_{q=0}^{L-1} 1/q! \frac{u^{Ln-1+q} e^{-u(1/\varphi + T_r/\psi_i)}}{\varphi^{Ln} \Gamma(Ln)} \left(\frac{T_r}{\psi_i} \right)^q du \quad (\text{II.3})$$

Still using the table of integrals [71, pp. 310, eqn. (3.351-3)], (II.3) reduces to:

$$\begin{aligned} P_{dr}, P_{far} &= \sum_{q=0}^{L-1} 1/q! \frac{(Ln-1+q)! (T_r \varphi)^q \psi_i^{Ln}}{(Ln-1)! (\psi_i + T_r \varphi)^{Ln+q}} \\ &= \sum_{q=0}^{L-1} 1/q! \frac{(Ln-1+q)! (T_r \sigma_s^2)^q}{(Ln-1)! (1 + T_r \sigma_s^2)^{Ln+q}} \end{aligned} \quad (\text{II.4})$$

where $\sigma_s^2 = \varphi / \psi_i$.

If $L = 1$, then (II.4) reduces to:

$$P_{dr}, P_{far} = \left(\frac{1}{1 + T_r \sigma_s^2} \right)^n \quad (\text{II.5})$$

Under H_0 , i.e. $i=0$, $\varphi = \psi_0 = 2\sigma_{H_0}^2$. Thus, $\sigma_s^2 = 1$.

Similarly, under H_1 i.e. $i=1$, $\varphi = 2\sigma_{H_0}^2$ and $\psi_1 = 2\sigma_{H_1}^2$. Thus, $\sigma_s^2 = \sigma_{H_0}^2 / \sigma_{H_1}^2$.

Appendix III

Derivation of equation (6.41)

From (5.39),

$$D(\tau_\varepsilon/T_c) = \left[\left(1 - \frac{|\tau_\varepsilon - T_d|}{T_c} \right)^2 - \left(1 - \frac{|\tau_\varepsilon + T_d|}{T_c} \right)^2 \right] \quad (\text{III.1})$$

By using the following relations [72];

$$|a| = \begin{cases} a & a \geq 0 \\ -a & a < 0 \end{cases} \quad (\text{III.2})$$

$$|a-b| = \begin{cases} a-b & a-b \geq 0 \\ -(a-b) & a-b < 0 \end{cases} \quad (\text{III.3})$$

For $-T_c \leq \tau_\varepsilon < -T_d$

$$|\tau_\varepsilon - T_d| = -(\tau_\varepsilon - T_d) \quad (\text{III.4})$$

$$|\tau_\varepsilon + T_d| = -(\tau_\varepsilon + T_d) \quad (\text{III.5})$$

Therefore,

$$\begin{aligned} D(\tau_\varepsilon/T_c) &= \left[\left(1 - \frac{(-\tau_\varepsilon + T_d)}{T_c} \right)^2 - \left(1 - \frac{(-\tau_\varepsilon - T_d)}{T_c} \right)^2 \right] \\ &= \left[\left(1 - \frac{2(-\tau_\varepsilon + T_d)}{T_c} + \left(\frac{-\tau_\varepsilon + T_d}{T_c} \right)^2 \right) - \left(1 - \frac{2(-\tau_\varepsilon - T_d)}{T_c} + \left(\frac{-\tau_\varepsilon - T_d}{T_c} \right)^2 \right) \right] \\ &= \left[-2 \left(\frac{-\tau_\varepsilon + T_d}{T_c} \right) + \left(\frac{-\tau_\varepsilon + T_d}{T_c} \right)^2 + 2 \left(\frac{-\tau_\varepsilon - T_d}{T_c} \right) - \left(\frac{-\tau_\varepsilon - T_d}{T_c} \right)^2 \right] \\ &= \left[2 \frac{\tau_\varepsilon}{T_c} - 2 \frac{T_d}{T_c} + \left(\frac{\tau_\varepsilon}{T_c} \right)^2 - 2 \frac{\tau_\varepsilon T_d}{T_c^2} + \left(\frac{T_d}{T_c} \right)^2 - 2 \frac{\tau_\varepsilon}{T_c} - 2 \frac{T_d}{T_c} - \left(\frac{\tau_\varepsilon}{T_c} \right)^2 - 2 \frac{\tau_\varepsilon T_d}{T_c^2} - \left(\frac{T_d}{T_c} \right)^2 \right] \end{aligned}$$

$$= -4 \left(1 + \frac{\tau_\varepsilon}{T_c} \right) \frac{T_d}{T_c} \quad (\text{III.6})$$

For $-T_d < \tau_\varepsilon < T_d$

$$|\tau_\varepsilon - T_d| = -(\tau_\varepsilon - T_d) \quad (\text{III.7})$$

$$|\tau_\varepsilon + T_d| = (\tau_\varepsilon + T_d) \quad (\text{III.8})$$

therefore,

$$\begin{aligned} D(\tau_\varepsilon/T_c) &= \left[\left(1 - \frac{|\tau_\varepsilon + T_d|}{T_c} \right)^2 - \left(1 - \frac{|\tau_\varepsilon - T_d|}{T_c} \right)^2 \right] \\ &= \left[\left(1 - 2 \frac{(\tau_\varepsilon + T_d)}{T_c} + \left(\frac{\tau_\varepsilon + T_d}{T_c} \right)^2 \right) - \left(1 - 2 \frac{(\tau_\varepsilon - T_d)}{T_c} + \left(\frac{\tau_\varepsilon - T_d}{T_c} \right)^2 \right) \right] \\ &= \left[-2 \frac{(\tau_\varepsilon + T_d)}{T_c} + \left(\frac{\tau_\varepsilon + T_d}{T_c} \right)^2 + 2 \frac{(\tau_\varepsilon - T_d)}{T_c} - \left(\frac{\tau_\varepsilon - T_d}{T_c} \right)^2 \right] \\ &= \left[+2 \frac{\tau_\varepsilon}{T_c} - 2 \frac{T_d}{T_c} + \left(\frac{\tau_\varepsilon}{T_c} \right)^2 - 2 \frac{\tau_\varepsilon T_d}{T_c^2} + \left(\frac{T_d}{T_c} \right)^2 + 2 \frac{\tau_\varepsilon}{T_c} + 2 \frac{T_d}{T_c} - \left(\frac{\tau_\varepsilon}{T_c} \right)^2 - 2 \frac{\tau_\varepsilon T_d}{T_c^2} - \left(\frac{T_d}{T_c} \right)^2 \right] \\ &= 4 \frac{\tau_\varepsilon}{T_c} - 4 \frac{\tau_\varepsilon T_d}{T_c^2} \\ &= 4 \left(1 - \frac{T_d}{T_c} \right) \frac{\tau_\varepsilon}{T_c} \quad (\text{III.9}) \end{aligned}$$

For $T_d \leq \tau_\varepsilon < T_c$

$$|\tau_\varepsilon - T_d| = (\tau_\varepsilon - T_d) \quad (\text{III.10})$$

$$|\tau_\varepsilon + T_d| = (\tau_\varepsilon + T_d) \quad (\text{III.11})$$

therefore

$$\begin{aligned}
D(\tau_\varepsilon / T_c) &= \left[\left(1 - \frac{(\tau_\varepsilon - T_d)}{T_c} \right)^2 - \left(1 - \frac{(\tau_\varepsilon + T_d)}{T_c} \right)^2 \right] \\
&= \left[\left(1 - \frac{2(\tau_\varepsilon - T_d)}{T_c} + \left(\frac{\tau_\varepsilon - T_d}{T_c} \right)^2 \right) - \left(1 - \frac{2(\tau_\varepsilon + T_d)}{T_c} + \left(\frac{\tau_\varepsilon + T_d}{T_c} \right)^2 \right) \right] \\
&= \left[-2 \left(\frac{\tau_\varepsilon - T_d}{T_c} \right) + \left(\frac{\tau_\varepsilon - T_d}{T_c} \right)^2 + 2 \left(\frac{\tau_\varepsilon + T_d}{T_c} \right) - \left(\frac{\tau_\varepsilon + T_d}{T_c} \right)^2 \right] \\
&= \left[-2 \frac{\tau_\varepsilon}{T_c} + 2 \frac{T_d}{T_c} + \left(\frac{\tau_\varepsilon}{T_c} \right)^2 - 2 \frac{\tau_\varepsilon T_d}{T_c^2} + \left(\frac{T_d}{T_c} \right)^2 + 2 \frac{\tau_\varepsilon}{T_c} + 2 \frac{T_d}{T_c} - \left(\frac{\tau_\varepsilon}{T_c} \right)^2 - 2 \frac{\tau_\varepsilon T_d}{T_c^2} - \left(\frac{T_d}{T_c} \right)^2 \right] \\
&= 4 \left(1 - \frac{\tau_\varepsilon}{T_c} \right) \frac{T_d}{T_c} \tag{III.12}
\end{aligned}$$

Combining (III.6), (III.9) and (III.12),

$$D\left(\frac{\tau_\varepsilon}{T_c}\right) = \begin{cases} -4 \left(1 + \frac{\tau_\varepsilon}{T_c} \right) \frac{T_d}{T_c}, & -T_c \leq \tau_\varepsilon < -T_d, \\ 4 \left(1 - \frac{T_d}{T_c} \right) \frac{\tau_\varepsilon}{T_c}, & -T_d < \tau_\varepsilon < T_d, \\ 4 \left(1 - \frac{\tau_\varepsilon}{T_c} \right) \frac{T_d}{T_c}, & T_d < \tau_\varepsilon < T_c \end{cases} \tag{III.13}$$

$\left. \frac{d(D(\tau_\varepsilon / T_c))}{d(\tau_\varepsilon / T_c)} \right|_{\tau_\varepsilon=0}$ involves differentiating the value of $D\left(\frac{\tau_\varepsilon}{T_c}\right)$ that is

within $-T_d < \tau_\varepsilon < T_d$, which is the linear region of $D\left(\frac{\tau_\varepsilon}{T_c}\right)$ from Figure 5.3. Thus,

$$\left. \frac{d(D(\tau_\varepsilon / T_c))}{d(\tau_\varepsilon / T_c)} \right|_{\tau_\varepsilon=0} = 4 \left(1 - \frac{T_d}{T_c} \right) \tag{III.14}$$

Publications

- [1] A. J. Obiebi, M. Sharif and J. Sharp, "Fast PN Code Acquisition in DS-CDMA Systems using CA-CFAR Technique", in *Proc. Postgraduate Research Conference in Electronics, Photonics, Communications & Networks, and Computing Science*. University of Hertfordshire, UK, April 5-7, 2004, pp. 119-120.
- [2] A. J. Obiebi, M. Sharif and J. Sharp, "Adaptive PN Code Acquisition in DS-CDMA Systems" in *Proc. of the 4th International symposium on Communication Systems, Networks and Digital signal Processing*, University of Newcastle, UK, July 21-22, 2004, pp 51-54.
- [3] A. J. Obiebi, M. Sharif and J. Sharp, "Efficient PN Code Acquisition in DS-CDMA Systems in the Presence of a CW Jamming Signal", in *Proc. of the Postgraduate Research Conference in Electronics, Photonics, Communications & Networks, and Computing Science*, Lancaster University, UK, March 30 - April 1, 2005, pp 1-2.

**PUBLISHED PAPER
NOT INCLUDED**

References

- [1] T. S. Rappaport, *Wireless Communications: Principles and Practice*, 2nd ed., New York: Prentice Hall, 2002.
- [2] *IEEE Personal Communications*, Special Issue on IMT-2000: Standards Efforts of the ITU. vol. 4, no. 4, August 1997.
- [3] T. Ojanpera and R. Prasad, "An Overview of Air Interface Multiple Access for IMT-2000/UMTS," *IEEE Communications Magazine*, vol. 36, no. 6 September 1998, pp. 82-95.
- [4] CDMA101: Technology and Solutions, [online]. Available from: www.qualcomm.com/technology/cdma101.html, (accessed 21/07/2005).
- [5] A. M. Viterbi and A. J. Viterbi, "Erlang capacity of a power controlled CDMA System," *IEEE Journal on Selected Areas in Communications*, vol. 11, no. 6, August 1993, pp. 892-900.
- [6] K. S. Gilhousen, I. M. Jacobs, R. Padovani, A. J. Viterbi, L. A. Weaver Jr., C. E. Wheatley III, "On the Capacity of a Cellular CDMA System," *IEEE Transactions on Vehicular Technology*, v 40, n 2, May 1991, pp 303-312.
- [7] S. Glisic and B. Vucetic, *Spread Spectrum CDMA Systems for Wireless Communications*, Artech House Publishers, 1997.
- [8] J.S. Lee and L.E. Miller, *CDMA Systems Engineering Handbook*, Artech House Publishers, 1998.
- [9] A. J. Viterbi, *CDMA: Principles of Spread Spectrum Communication*, Addison Wesley Publishing Company, 1995.
- [10] M. K. Simon, J. K. Omura, R. A. Scholtz, B.K. Levitt, *Spread Spectrum Communications Handbook*, McGraw-Hill, Inc., 2002.

-
- [11] A. Polydorus and C. L. Weber, "A Unified approach to Serial Search Spread-Spectrum Code Acquisition – Part 1& 2: General Theory & Matched Filter Receiver," *IEEE Transactions on Communications*, vol. 32, no. 5, May, 1984, pp. 542-560.
- [12] S. Bregni, *Synchronisation of Digital Telecommunications Networks*, John Wiley and Sons, Ltd. 2002.
- [13] D. M. DiCarlo and C. L. Weber, "Multiple Dwell Serial Search: Performance and Application to Direct Sequence Code Acquisition," *IEEE Transactions on Communications*, vol. 31, no. 5, May 1983, pp. 650- 659.
- [14] H. Oh, D. Han, C. Lim and K. Park, "Adaptive Double-Dwell PN Code Acquisition in Direct-Sequence Spread-Spectrum Systems," *IEEE Military Communications Conference*, no. 1, October 2000, pp. 139-143.
- [15] B. Mahafza, *Radar Systems Analysis and Design using Matlab*, Chapman and Hall/CRC, 2002.
- [16] M. Patzold, *Mobile Fading Channels*, John Wiley and Sons Ltd, 2002.
- [17] R. L. Pickholtz, D. L. Schilling and L. B. Milstein, "Theory of Spread-Spectrum Communications – A Tutorial," *IEEE Transactions on Communications*, vol. COM-30, May 1982, pp. 855-884.
- [18] H. Harada and R. Prasad, *Simulation and Software Radio for Mobile Communications*, Artech House, 2002.
- [19] K. Leonhard, *Designing CDMA2000 Systems*, John Wiley and Sons Ltd, 2004.
- [20] S. Lee, *Spread Spectrum CDMA: IS-95 and IS-2000 for RF Communications*, McGraw-Hill, 2002.
- [21] K. S. Zigangirov, *Theory of Code Division Multiple Access Communication*, IEEE, Inc., 2004.

-
- [22] J. G. Proakis and M. Salehi, *Contemporary Communication Systems using Matlab*, Brooks/Cole, 2000.
- [23] E. H. Dinan and B. Jabbari, "Spreading Codes for Direct Sequence CDMA and Wideband CDMA Cellular Networks," *IEEE Communications Magazine*, September 1998, pp. 48-54.
- [24] R. Gold, "Optimal Binary Sequences for Spread Spectrum Multiplexing," *IEEE Transactions on Information Theory*, vol. IT-13 Oct. 1967, pp 619-621.
- [25] R. Gold, "Maximal Recursive Sequences with 3-Valued Recursive Cross Correlation Functions," *IEEE Transactions on Information Theory*, vol. IT-14 January 1968, pp 154-156.
- [26] T. Kasami, "Weight Distribution Formula for Some Class of Cyclic Codes," Coordinated Science Laboratory, University of Illinois, Urban, III. Technical Report No. R-285, April 1966.
- [27] E. Ifeachor and B. Darvis, *Digital Signal Processing: A Practical Approach*, 2nd ed. Prentice Hall, 2002.
- [28] W. C. Y. Lee, *Mobile Communications Design Fundamentals*: 2nd ed. John Wiley and Sons Ltd, 1993.
- [29] J. D. Parsons, *The Mobile Radio Propagation Channel*, John Wiley and Sons Ltd, 2000
- [30] B. Sklar, *Digital Communications: Fundamentals and Applications*, 2nd edition Prentice Hall, 2001.
- [31] M. C. Jeruchin, P. Balban and K. S. Shanmugan, *Simulation of Communication Systems*, 2nd ed. New York: Kluwer Academic/Plenum Publishers, 2000.
- [32] J. G. Proakis, *Digital communications*, 4th ed., McGraw-Hill, 1995.

-
- [33] W. H. Tranter, K. S. Shanmugan, T. S. Rappaport and K. L. Kosbar, *Communication Systems Simulation with Wireless Applications*, Prentice Hall, 2004.
- [34] W. C. Jakes, *Microwave Mobile Communications*, Bell Telephone Labs, Inc., 1974.
- [35] R. R. Rick and L. B. Milstein, "Parallel Acquisition in Mobile DS-CDMA Systems," *IEEE Transactions on Communications*, vol. 45, no. 11, Nov. 1997, pp. 1466-1476.
- [36] K.A. Stroud, *Engineering Mathematics – Programmes and Problems*, 3rd ed. Macmillan Press 1990.
- [37] J. A. Obiebi, *Quality of Service Requirements for Mobility Support in CDMA Wireless Network*, MSc Dissertation, University of Plymouth, UK, 2002.
- [38] Tektronix Application Notes, *Fundamentals of Interference in Mobile Networks*, [online]. Available from: www.tektronix.com/mobile (accessed 13/06/2005).
- [39] C. E. Cook and H. S. Marsh, "An Introduction to Spread Spectrum: Reliable Detection at the Communications Receiver when Interference is present," *IEEE Communications Magazine*, March 1983, pp. 8-16.
- [40] S. S. Rappaport and D. M. Grieco, "Spread-Spectrum Signal Acquisition: Methods and Technology," *IEEE Communications Magazine*, vol. 22, No. 6, June 1984, pp. 6-21.
- [41] E. Sourour and S. C. Gupta, "Direct-Sequence Spread-Spectrum Parallel Acquisition in Nonselective and Frequency-Selective Ricean Fading Channels," *IEEE Journal on Selected Areas in Communications*, vol. 10, no. 3, April 1992, pp. 535-544.

-
- [42] R. R. Rick and L. B. Milstein, "Optimal Decision Strategies for Acquisition of Spread-Spectrum Signals in Frequency-Selective fading Channels," *IEEE Transactions on Communications*, vol. 46, no. 5, May 1998, pp. 686-694.
- [43] W. Zhuang, "Noncoherent Hybrid Parallel PN Code Acquisition for CDMA Mobile Communications," *IEEE Transactions on Vehicular Technology*, vol. 45, no. 4, Nov. 1996, pp. 643- 656.
- [44] R. B. Ward, "Acquisition of Pseudonoise Signals by Sequential Estimation," *IEEE Transactions on Communications*, COM-13, December 1965, pp. 475-483.
- [45] R. B. Ward and K. P. Yiu, "Acquisition of Pseudonoise Signals by Recursion Aided Sequential Estimation," *IEEE Transactions on Communications*, COM-25, August 1977, pp. 784-794
- [46] G. L. Turin, "An Introduction to Matched Filters," *IRE Transactions on Information Theory*, vol. IT-6, June 1960, pp. 311-329.
- [47] R. C. Dixon, *Spread Spectrum Systems: with Commercial Applications*, John Wiley and Sons Ltd, 1994.
- [48] D.M. Grieco, "The application of Charged-Coupled devices in Spread-Spectrum Communications," *IEEE Transactions on Communications*, COM-28, September 1980, pp. 1693-1705.
- [49] L.B. Milstein, J. Gevargiz and P. K. Das, "Rapid Acquisition for Direct Sequence Spread Spectrum Communications using Parallel SAW Convolver," *IEEE Transactions on Communications*, COM-33, No. 7, July 1985, pp 593-599.
- [50] J. Iinatti, "On the Threshold Setting Principles in Code acquisition of DS-SS Signals," *IEEE Journal on Selected Areas in Communications*, vol. 18, no. 1, January 2000, pp. 62-72.

-
- [51] E. K. Al-Hussaini and B. M. Ibrahim, "Comparison of Adaptive Cell-Averaging Detectors for Multiple Targets Situations," *IEE Proceedings-F: Communications, Radar and Signal Processing*, vol. 133, Part F, no. 3, June 1986, pp. 217-223.
- [52] M. K. Simon and M. Alouini, *Digital Communications over Fading Channels*, New York: John Wiley & Sons, 2000.
- [53] R. E. Ziemer and R.L Peterson, *Digital Communications and Spread Spectrum Systems*, New York, N.Y. Macmillan Canada Collier Macmillan, 1985.
- [54] A. Polydoros, *On the Synchronisation Aspects in Direct-Sequence Spread Spectrum Systems*, PhD Dissertation, University of Southern California, Los Angeles, CA, USA, 1982.
- [55] J. K. Holmes and C. C. Chen, "Acquisition Time Performance of PN Spread-Spectrum Systems," *IEEE Transactions on Communications*, vol. COM-25, no. 8, August 1977, pp. 778- 783.
- [56] S. S. Haykin, *Active Network Theory*, Addison-Wesley Publishing Company, Inc. 1970.
- [57] B. Ibrahim and H. Aghvami, "Direct Sequence Spread Spectrum Matched Filter Acquisition in Frequency Selective Rayleigh Fading Channels," *IEEE Journal on Selected Areas in Communications*, vol. 12, no. 5, June 1994, pp. 885-890.
- [58] H. G. Kim, I. Song; Y. Lee, S. C. Kim and Y. H. Kim, "Double-Dwell Serial-Search PN Code Acquisition using a Nonparametric Detector in DS/CDMA Systems," in *proc. IEEE Military Communications Conference*, vol. 1, 31 Oct.-3 November 1999, pp. 571 – 574.
- [59] L. Yang and L. Hanzo, "Serial Acquisition of DS-CDMA Signals in Multipath Fading Mobile Channels," *IEEE Transactions on Vehicular Technology*, vol. 50, no. 2, March 2001, pp. 617-628.

-
- [60] E.W. Siess and C.L. Weber, "Acquisition of Direct Sequence Signals with Modulation and Jamming," *IEEE Journal on Selected Areas in Communications*, vol. 4, no. 2, March 1986, pp. 254-272.
- [61] A. Polydoros and C. L. Weber, "Analysis and Optimisation of Correlative Code-Tracking Loops in Spread Spectrum Systems," *IEEE Transactions on Communications* vol. 33, no.1 January 1985 pp. 30-43.
- [62] W. R. Brawn, "PN Acquisition and Tracking Performance in DS/CDMA Systems with Symbol-Length Spreading Sequences," *IEEE Transactions on Communications*, vol. 45, no.12 December 1997 pp. 1595-1601.
- [63] R. Price and P. Green, "A Communication Technique for Multipath Channels," *Proc. IRE*, vol. 46, March 1958, pp. 555-570.
- [64] J. Lin, "A Modified PN Code Tracking Loop for Direct-Sequence Spread-Spectrum Communication over Arbitrarily Correlated Multipath Fading Channels," *IEEE Journal on Selected Areas in Communications*, vol. 19 no. 12, pp. 2381-2395, December 2001.
- [65] G. Fock, J. Baltersee, P. Rittich and H. Meyr, "Channel Tracking for RAKE Receivers in Closely Spaced Multipath Environments," *IEEE Journal on Selected Areas in Communications*, vol. 19 no. 12, pp. 2420-2431, December 2001.
- [66] K. Higuchi, M. Sawashi and F. Adachi, "Fast Cell Search Algorithm in Inter-Cell Asynchronous DS-CDMA Mobile Radio," *IEICE Transactions on Communications*, vol. E81-B, no. 7, July 1998, pp. 1527-1534.
- [67] Y. Wang and T. Ottosson, "Cell Search in W-CDMA," *IEEE Journal on Selected Areas in Communications*, vol. 18, no. 8, August 2000, pp. 1470-1482.

-
- [68] S. Sriram and S. Hosur, "An Analysis of the 3-stage Search Process in W-CDMA," in *proc. 52nd IEEE Vehicular Technology Conference*, vol. 6, September 2000, pp. 2672-2679.
- [69] V. Tripathi, A. Mantravadi and V. V. Veeravalli, "Channel Acquisition for Wideband CDMA Signals," *IEEE Journal on Selected Areas in Communications*, vol. 18, no. 8, August 2000, pp. 1483-1494.
- [70] S. M. Ross, *Introduction to Probability and Statistics for Engineers and scientists*, 3rd ed, Elsevier Inc, 2004.
- [71] I. S. Gradshteyn and I. M. Ryzhik, *Table of Integrals: Series and products*, Academic Press. Inc., 1980.
- [72] G. J. Etgen S. L. Salas, *Calculus: One and Several Variables*, John Wiley & Sons, 1990.